EFFECT OF CO_2 SEQUESTRATION ON THE MECHANICAL PROPERTIES OF CARBONATE ROCKS

BY

WAHBI ABDUL QADER AL-AMERI

A Thesis Presented to the

DEANSHIP OF GRADUATE STUDIES

KING FAHD UNIVERSITY OF PETROLEUM & MINERALS

DHAHRAN, SAUDI ARABIA

In Partial Fulfillment of the
Requirements for the Degree of

MASTER OF SCIENCE

In

PETROLEUM ENGINEERING

December, 2014

KING FAHD UNIVERSITY OF PETROLEUM & MINERALS

DHAHRAN-31261, SAUDI ARABIA

DEANSHIP OF GRADUATE STUDIES

This thesis, written by **WAHBI ABDUL QADER AL-AMERI** under the direction his thesis advisor and approved by his thesis committee, has been presented and accepted by the Dean of Graduate Studies, in partial fulfilment of the requirements for the degree of **MASTER OF SCIENCE IN PETROLEUM ENGINEERING.**

Dr. Abdulazeez Abdulraheem
(Advisor)

Dr. Abdullah S. Sultan
Department Chairman

Dr. Mohammed Mahmoud
(Member)

Prof. Salam A. Zummo
Dean of Graduate Studies

Dr. Osman Abdullatif
(Member)

24/12/14
Date

DEDICATION

This thesis is dedicated to

MY BELOVED MOTHER & FATHER,

MY BROTHERS, MY SISTERS, MY WIFE & CHILDREN

ACKNOWLEDGMENTS

In the name of Allah, Most Gracious. All praise is to Almighty Allah who gave me courage, knowledge and ability to complete this work and blessing of Allah be upon his prophet Mohammed (peace be upon him).

I wish to express my deep appreciation and thanks to Dr. Abdulazeez Abdulraheem, thesis advisor, and Dr. Mohammed Mahmoud, and Dr. Osman Abdullatif, committee members, for providing their invaluable help and guidance throughout this work.

Acknowledgment is due to King Fahd University of Petroleum & Minerals. My sincere appreciation is extended to all faculty and staff of the Centre for Petroleum and Minerals at Research Institute, and the Petroleum Engineering Department for the contribution to this work.

I am also indebted to the help provided by: Dr. Abdullah S. Sultan, Mr. Abdulrauf Adebayo, Mr. Abdurahim Mohammedeen, Mr. Syed Shujath Ali, Mr. Syed Nizamuddin, Mr. Khalid Munif, Mr. Mosa Ali Mosa, Mr. Saheed Adekunle, Mr. Panoy Deresma, and Mr. Noor during my experimental work in PETE Department, and the RI laboratories.

Special thanks are due to all my colleagues and friends who helped me in my work and made my stay at the University memorable and source of valuable experience.

Finally, I am indebted to Eng. A. A. Bugshan & Hadhramout Establishment for Human Development (HEFHD) for providing me with scholarship and for their moral support and encouragement throughout my master program.

TABLE OF CONTENTS

ACKNOWLEDGMENTS ..... **vii**

TABLE OF CONTENTS ..... **viii**

LIST OF TABLES ..... **xiii**

LIST OF FIGURES ..... **xv**

LIST OF ABBREVIATIONS ..... **xxiii**

ABSTRACT ..... **xxvi**

ملخص الرسالة ..... **xxviii**

CHAPTER 1 INTRODUCTION **1**

1.1 Introduction 1

1.2 Value to the Kingdom 3

1.3 Research Objectives 4

CHAPTER 2 LITERATURE REVIEW **6**

2.1 Geological Sequestration of CO_2 6

2.1.1 The Concept of Geological Sequestration 6

2.1.2 Sequestration Options 7

2.1.3 Deep Saline Aquifers 8

2.2 Geological Sequestration of CO_2 into Carbonate Rocks 8

2.2.1 Carbonate Rocks 8

2.2.2 Dissolution/Precipitation Mechanisms in Carbonates 9

2.3 Effect of CO_2 on the Properties of the Rocks 10

2.3.1 Effect of CO_2 on the Acoustic Properties 10

2.3.2 Effect of CO_2 on Petrophysical Properties 15

2.3.3 Effect of CO_2 on Mechanical Properties and the Strength of the Rocks .. 20

CHAPTER 3 RESEARCH METHODOLOGY 28

3.1 Introduction 28

3.2 Material 29

3.2.1 Synthetic Brine 29

3.2.2 Core Sample 29

3.2.3 Fluid Properties 32

3.3 Petrographic Description 33

3.3.1 Thin Section Petrography 33

3.3.2 X-Ray Diffraction (XRD) 34

3.3.3 Scanning Electron Microscopy (SEM) 34

3.4 Core Sequestration Apparatus 35

3.4.1 Core Holder 36

3.4.2 Syringe (ISCO) Pump 36

3.4.3 Pressure Gauges 36

3.4.4 High Temperature Oven 36

3.4.5 Carbon Dioxide Supply 36

3.4.6 Carbon Dioxide Accumulator 36

3.5 Experimental Procedure 37

3.5.1 Saturation and Porosity Measurement 37

3.5.2 Porosity Measurement Using TPI–219 Teaching Helium Porosimeter 39

3.5.3 Gas Permeability Determination Using TKA-209 Gas Permeameter 40

3.5.4 Carbon Dioxide Sequestration Procedures 41

3.6 Measurement of Mechanical Properties 41

3.6.1 Unconfined Compression Test 42

3.6.2 Indirect Tensile Strength (ITS) Test 45

3.7 Measurement of Wave Velocities 47

3.7.1 Ultrasonic Velocity Measuring System 48

3.7.2 Sample Preparation 49

3.7.3 Experimental Procedure 49

3.7.4 Data Acquisition 50

3.7.5 Calculation 52

CHAPTER 4 PETROGRAPHIC AND PETROPHYSICAL ANALYSIS 54

4.1 Petrographic Analysis 54

4.1.1 Thin Section Petrography 54

4.1.2 X-Ray Diffraction (XRD) Analysis 56

4.1.3 Scanning Electron Microscopy (SEM) Analysis 60

4.2 Petrophysical Analysis 72

4.2.1 Porosity and Permeability Measurements 72

4.2.2 Nuclear Magnetic Resonance (NMR) 73

CHAPTER 5 RESULTS AND DISCUSSION 74

5.1 Introduction 74

5.2 Effect of CO_2 Sequestration on Petrophysical Properties 74

5.3 Effect of CO_2 Sequestration on the Acoustic Properties 76

5.4 Effect of CO_2 Sequestration on Static Elastic Moduli and Unconfined Compressive Strength 90

5.5 Effect of CO_2 Sequestration on Indirect Tensile Strength 94

5.6 Concluding Remarks 96

CHAPTER 6 IMPACT OF CO_2 SEQUESTRATION ON ENGINEERING OPERATIONS 98

6.1 Borehole Instability 99

6.2 Aquifer Compaction 101

CHAPTER 7 CONCLUSION AND RECOMMENDATIONS 103

7.1 Conclusions 103

7.2 Recommendations 104

REFERENCES 105

APPENDIX-A (NMR RESULTS) 113

APPENDIX-B (UNCONFINED COMPRESSION TEST RESULTS) 117

APPENDIX-C (XRD RESULTS) 122

VITAE 129

LIST OF TABLES

Table 2.1 Estimates of the volumes of CO_2 that can be sequestered below surface (Herzog, 2001)..... 7

Table 2.2 Triaxial tests of dry Indiana limestone at room temperature (Xuejun et al., 2009).22

Table 2.3 Triaxial strength tests of Indiana limestone after flooding with CO_2 and water at 136 ºF (Xuejun et al., 2009). 22

Table 2.4 Results of drained triaxial tests for rock samples after different flooding scenarios (Xuejun et al., 2009)..... 22

Table 2.5 Average rock mechanical and petrophysical properties (Masoudi et al., 2012). 25

Table 3.1 Ionic composition of the brine. 29

Table 4.1 Quantitative analysis of the core samples using XRD. 57

Table 4.2 Chemical compositions for different core samples using SEM. 61

Table 4.3 Basic core properties. 73

Table 4.4 Liquid permeability and gas porosity of specimens. 73

Table 4.5 Porosity values by using NMR. 73

Table 5.1Gas porosity and liquid permeability before and after CO_2 sequestration for different time periods. 75

Table 5.2 Porosity by using NMR before and after CO_2 sequestration. 75

Table 5.3 Static values of Young's modulus and Poison's ratio and unconfined compressive strength values of Indiana limestone samples. 93

Table 5.4 Indirect tensile strength values of Pink Desert limestone samples. 95

Table 5.5 Indirect tensile strength values of Khuff limestone samples. 95

LIST OF FIGURES

Figure 2.1 Geological storage (Gomez, 2006). 7

Figure 2.2 Compressional and shear velocities in n-hexadecane-saturated and CO_2-flooded Berea sandstone vs. pore pressure (Wang and Nur, 1989). 11

Figure 2.3 Results of resistivity measurements on Berea sample saturated with brine and then flooded with CO_2 at 300 psi (Myer, 2001). 12

Figure 2.4 Changes in P-wave velocity for Berea sample saturated with 1.1 Ω–m brine and then flooded with CO_2 at 300 psi (Myer, 2001). 13

Figure 2.5 The changes of resistivity and P-wave velocity against CO_2 injected time (Kim et al., 2010). 14

Figure 2.6 Wave velocity-CO_2 saturation relations with Gassmann fluid-mixing laws (Kim et al., 2010). 14

Figure 2.7 Porosity and permeability variations and change after aging with carbon dioxide (Gupta, 2010). 16

Figure 2.8 Variation of permeability as a function of porosity for sandstones measured before (red dots) and after (yellow dots) alternating injection of seawater and CO_2 injection (Vanorio et al., 2011). 17

Figure 2.9 Time-lapse SEM (up panel) and CT-scan (down panel) images monitoring the permanent changes induced in the rock microstructure by calcite dissolution upon injection of CO_2-rich water (Vanorio et al., 2011). 17

Figure 2.10 A single slice extracted from a 3D volume showing the apparent enhancement of porosity in a carbonate sample (Nur et al., 2011). 18

Figure 2.11 Permeability vs. porosity computed on a digital sub-sample (Nur et al., 2011). 18

Figure 2.12 Change in cores permeability when different concentration of $CaCl_2$ brine was injected (Mohamed et al., 2011). 19

Figure 2.13 Change in cores permeability when different concentration of $MgCl_2$ brine was injected (Mohamed et al., 2011). 19

Figure 2.14 Young's modulus and Poisson ratio for several sandstones, limestones, dolomitic marble and shales (Riano, 2012). 21

Figure 2.15 Change in sample length along the main axis and porosity versus the injected volume of CO_2-rich fluid, for the carbonate sample exhibiting the highest reactivity (Vialle and Vanorio, 2010). 23

Figure 2.16 Mohr circles and failure envelope for pre- and post-CO_2 treated limestone samples (Masoudi et al., 2012). 26

Figure 2.17 Variations of Young's modulus with effective confining stress for pre- and post-CO_2 treated limestone samples (Masoudi et al., 2012). 26

Figure 2.18 Tensile strength for pre- and post-CO_2 treated limestone samples (Masoudi et al., 2012). 27

Figure 3.1 Coring machine for preparing plugs. 30

Figure 3.2 Core cutter for cutting rock samples to required size. 30

Figure 3.3 Soxhlet type extractor. 31

Figure 3.4 Vacuum oven. 32

Figure 3.5 End face grinder. 32

Figure 3.6 Thin section under a microscope. 33

Figure 3.7 X-Ray Diffraction (XRD) setup. 34

Figure 3.8 The Scanning Electron Microscopy (SEM) setup. 35

Figure 3.9 A schematic diagram of core sequestration setup..... 37

Figure 3.10 Saturation apparatus. 39

Figure 3.11 TPI–219 Helium Porosimeter. 39

Figure 3.12 TKA-209 Gas Permeameter. 40

Figure 3.13 Compression machine 300 kN. 43

Figure 3.14 Graph of a typical stress-strain relationship. 45

Figure 3.15 Indirect tensile strength machine. 47

Figure 3.16 Safety enclosure with pressurization system. 51

Figure 3.17 Ultrasonic transducer assembly. 52

Figure 3.18 Data acquisition system. 52

Figure 4.1 Microphotograph for thin section of Indiana limestone. The rock is peloidal echinoidal grainstone. 55

Figure 4.2 Microphotograph for thin section of Pink Deseret limestone. The rock is peloidal echinoderm grainstone. 55

Figure 4.3 Microphotograph for thin section of Khuff limestone. The rock is oolitic grainstone. 56

Figure 4.4 The phase identification for Indiana limestone sample before CO_2 sequestration using XRD. 57

Figure 4.5 The phase identification for Indiana limestone sample after CO_2 sequestration using XRD. 58

Figure 4.6 The phase identification for Pink Desert limestone sample before CO_2 sequestration using XRD. 58

Figure 4.7 The phase identification for Pink Desert limestone sample after CO_2 sequestration using XRD..... 59

Figure 4.8 The phase identification for Khuff limestone sample before CO_2 sequestration using XRD..... 59

Figure 4.9 The phase identification for Khuff limestone sample after CO_2 sequestration using XRD. 60

Figure 4.10 SEM microphotograph for Indiana limestone sample before CO_2 sequestration.61

Figure 4.11 SEM microphotograph for Indiana limestone sample before CO_2 sequestration.61

Figure 4.12 SEM microphotograph for Indiana limestone sample after CO_2 sequestration... 62

Figure 4.13 SEM microphotograph for Indiana limestone sample after CO_2 sequestration... 62

Figure 4.14 SEM microphotograph for Indiana limestone sample after CO_2 sequestration... 63

Figure 4.15 SEM microphotograph for Pink Desert limestone sample before CO_2 sequestration..... 63

Figure 4.16 SEM microphotograph for Pink Desert limestone sample before CO_2 sequestration..... 64

Figure 4.17 SEM microphotograph for Pink Desert limestone sample after CO_2 sequestration. 64

Figure 4.18 SEM microphotograph for Pink Desert limestone sample after CO_2 sequestration. 65

Figure 4.19 SEM microphotograph for Pink Desert limestone sample after CO_2 sequestration. 65

Figure 4.20 SEM microphotograph for Khuff limestone sample before CO_2 sequestration. . 66

Figure 4.21 SEM microphotograph for Khuff limestone sample before CO_2 sequestration. . 66

Figure 4.22 SEM microphotograph for Khuff limestone sample before CO_2 sequestration. . 67

Figure 4.23 SEM microphotograph for Khuff limestone sample after CO_2 sequestration. 67

Figure 4.24 SEM microphotograph for Khuff limestone sample after CO_2 sequestration. 68

Figure 4.25 SEM microphotograph for Khuff limestone sample after CO_2 sequestration. 68

Figure 4.26 SEM microphotograph for Khuff limestone sample after CO_2 sequestration. 69

Figure 4.27 SEM microphotograph for Khuff limestone sample after CO_2 sequestration. 69

Figure 4.28 Three different locations (spectrums 1, 3, and 4) for Indiana limestone sample before CO_2 sequestration..... 70

Figure 4.29 One location (spectrum 5) for Indiana limestone sample after CO_2 sequestration. 71

Figure 4.30 One location (spectrum 7) for Pink Desert limestone sample before CO_2 sequestration..... 71

Figure 4.31 One location (spectrum 8) for Khuff limestone sample before CO_2 sequestration. 71

Figure 4.32 One location (spectrum 9) for Khuff limestone sample after CO_2 sequestration.72

Figure 5.1 Comparison of compressional and shear wave velocities of Indiana limestone sample (IL-10-2) before and after CO_2 sequestration for 90 days. 77

Figure 5.2 Comparison of Young's modulus of Indiana limestone sample (IL-10-2) before and after CO_2 sequestration for 90 days..... 77

Figure 5.3 Comparison of Poisson's ratio of Indiana limestone sample (IL-10-2) before and after CO_2 sequestration for 90 days. 78

Figure 5.4 Comparison of compressional and shear wave velocities of Pink Desert limestone sample (PL-S-1-A) before and after CO_2 sequestration for 14 days..... 79

Figure 5.5 Comparison of Young's modulus of Pink Desert limestone sample (PL-S-1-A) before and after CO_2 sequestration for 14 days. 79

Figure 5.6 Comparison of Poisson's ratio of Pink Desert limestone sample (PL-S-1-A) before and after CO_2 sequestration for 14 days..... 80

Figure 5.7 Comparison of compressional and shear wave velocities of Khuff limestone sample (KL-S-1-A) before and after CO_2 sequestration for 90 days. 81

Figure 5.8 Comparison of Young's modulus of Khuff limestone sample (KL-S-1-A) before and after CO_2 sequestration for 90 days..... 81

Figure 5.9 Comparison of compressional and shear wave velocities of Khuff limestone sample (KL-S-1-B) before and after CO_2 sequestration for 90 days. 82

Figure 5.10 Comparison of Young's modulus of Khuff limestone sample (KL-S-1-B) before and after CO_2 sequestration for 90 days..... 82

Figure 5.11 Comparison of Young's modulus for two cap rock shale (SH) samples (SH-4-95, and SH-4-81) before and after CO_2 sequestration for 30 days..... 83

Figure 5.12 SEM microphotograph for Indiana limestone sample before and after CO_2 sequestration..... 84

Figure 5.13 SEM microphotograph for Pink Desert limestone sample before and after CO_2 sequestration..... 85

Figure 5.14 SEM microphotograph for Khuff limestone sample before and after CO_2 sequestration..... 85

Figure 5.15 Micro CT scan image for Indiana limestone sample before and after CO_2 sequestration..... 86

Figure 5.16 Micro CT scan image for Pink Desert limestone sample before and after CO_2 sequestration..... 86

Figure 5.17 Micro CT scan image for Khuff limestone sample before and after CO_2 sequestration. 87

Figure 5.18 The presence of calcite minerals in brine samples. 87

Figure 5.19 Pink Desert limestone samples before and after CO_2 sequestration. 88

Figure 5.20 Effect of sequestration time periods on Young's modulus of Pink Desert Limestone samples (PL-S-1-A, PL-S-2-A, and PL-S-3-B) at 15 MPa. 89

Figure 5.21 Reduction percentage in Young's modulus for different rock types subjected to CO_2 sequestration for 90 days. 90

Figure 5.22 Effect of sequestration time periods on Young's modulus of Pink Desert limestone samples (PL-U-2, PL-U-1-A, PL-U-2-A, and PL-U-3-B). 91

Figure 5.23 Effect of sequestration time periods on Poison's ratio of Pink Desert limestone samples (PL-U-2, PL-U-1-A, PL-U-2-A, and PL-U-3-B). 92

Figure 5.24 Effect of sequestration time periods on unconfined compressive strength of Pink Desert limestone samples (PL-U-2, PL-U-1-A, PL-U-2-A, and PL-U-3-B). 92

Figure 5.25 Reduction percentage in unconfined compressive strength for different rock types subjected to CO_2 sequestration for 90 days. 93

Figure 5.26 Indirect tensile strength (ITS) of Pink Desert limestone samples (PL-T-1-A, PL-T-1-B, PL-T-2-A, and PL-T-3-C) at different time periods. 95

Figure 5.27 Reduction percentage in indirect tensile strength for different rock types subjected to CO_2 sequestration for 90 days. 96

Figure 6.1 Mohr circles and failure envelopes for Khuff limestone samples before and after CO_2 sequestration. 99

Figure 6.2 Stresses around a vertical borehole 100

Figure 6.3 Mohr circles for stresses around the wellbore wall and failure envelopes for Khuff limestone samples before and after CO_2 sequestration. 101

Figure 6.4 Tensile fracture after CO_2 sequestration. 101

Figure 6.5 Stress-strain curve for Pink Desert limestone samples before and after CO_2 sequestration. 102

LIST OF ABBREVIATIONS

CO_2	:	Carbon dioxide
EOR	:	Enhanced Oil Recovery
ECBMR	:	Enhance Coal Bed Methane Recovery
Vp	:	Compressional wave velocity (m/s)
Vs	:	Shear wave velocity (m/s)
GtC	:	Gigatons of Carbon
K	:	Bulk Modulus (GPa)
E	:	Young's Modulus (GPa)
υ	:	Poison's ratio
ρ	:	Dry bulk density (g/cc)
LVDTs	:	Linear Variable Differential Transducers
FW	:	Formation Water
TDS	:	Total Dissolved Solids (ppm)
ρ	:	Fluid density (gm/cc)
XRD	:	X-Ray Diffraction
SEM	:	Scanning Electron Microscopy
ø	:	Porosity (%)

K	:	Permeability (md)
PV	:	Pore Volume of the core (cc)
M_{dry}	:	Weight of the dry core (gm)
$M_{sat.}$	:	Weight of the saturated core by brine (gm)
ρ_{brine}	:	Brine density (gm/cc)
V_{bulk}	:	Bulk volume of the core (cc)
D	:	Core diameter (cm)
L	:	Core length (cm)
K_a	:	Permeability to air (md)
μ_a	:	Air viscosity (cp)
Q_a	:	Flow rate of gas (cc/min)
P_a	:	Atmospheric pressure (atmospheres absolute)
P_1	:	Inlet pressure (atmospheres absolute)
P_2	:	Outlet pressure (atmospheres absolute)
A	:	Sample area (cm^2)
UCS	:	Unconfined Compressive Strength (MPa)
ε	:	Strain
σ	:	Stress (MPa)

P	:	Applied load (KN)
ITS	:	Indirect Tensile Strength (psi)
CP	:	Confining Pressure (MPa)
IL	:	Indiana Limestone
PL	:	Pink Desert Limestone
KL	:	Khuff Limestone
SH	:	Shale
σ_v	:	Vertical stress (psi)
σ_H	:	Max. Horizontal stress (psi)
σ_h	:	Min. horizontal stress (psi)
σ_r	:	Radial stress (psi)
P_w	:	Wellbore pressure (psi)
σ_θ	:	Circumferential stress (psi)

ABSTRACT

Full Name: Wahbi Abdul Qader AL-Ameri

Thesis Title: Effect of CO_2 Sequestration on the Mechanical Properties of Carbonate Rocks

Major Field: Petroleum Engineering

Date of Degree: December, 2014

Geological sequestration of carbon dioxide (CO_2) in underground formations is the most promising way to decrease the greenhouse emissions into atmosphere. The understanding of long term effects of CO_2 storage in carbonate aquifers is challenged by many uncertainties including geochemical effects of CO_2 on carbonates and the coupled chemical–mechanical effects. The carbon dioxide dissolves in water forming bicarbonate which will dissociate to carbonic acid. This acid dissolves calcites in carbonate rocks. As a result, the mechanical properties of the aquifer changes through this interaction. It is therefore necessary to study the effect of carbon dioxide sequestration on the integrity of a given formation to get safe and effective long-term storage of CO_2 sequestration in deep saline aquifers. Previous works on CO_2 sequestration have focused on the impact of CO_2 injection on the petrophysical and mechanical properties of formation rocks exposed to a short duration of exposure. This short period is not enough for carbon dioxide to react with formation brine and thus for the chemical reaction that will impact the properties of the rocks.

The main objective of this work is to investigate the effect of CO_2 storage on the mechanical properties of carbonate aquifer rocks that were exposed to soaking with CO_2 for varying durations. The effect of the duration of CO_2-brine contact time or solubility time on these

properties was investigated. CO_2 was stored in the cores at 2000 psi and 100 ºC for different time periods ranging from 14 days to 90 days. The cores were then analyzed for the mechanical properties using acoustics, unconfined compression, and indirect tensile strength testing machines.

Results showed that CO_2 sequestration affected the mechanical properties of the carbonate rocks as well as the cap rocks. Long time soaking of CO_2 in brine allowed for the formation of enough carbonic acid to react with the cores and this greatly impacted the rock mechanical and acoustic properties. The significant impact of CO_2 storage was noted on Khuff limestone and the good candidate among the carbonate rocks studied here for geological sequestration of CO_2 is found to be Indiana limestone.

ملخص الرسالة

الاسم الكامل: وهبي عبدالقادر عوض العامري

عنوان الرسالة: تأثير تخزين غاز ثاني اكسيد الكربون على الخصائص الميكانيكية للصخور الكربونية

التخصص: هندسة البترول

تاريخ الدرجة العلمية: ديسمبر 2014م

التخزين الجيولوجي لغاز ثاني أكسيد الكربون (CO_2) في التكوينات الجوفية هي الطريقة الواعدة لخفض انبعاثات الغازات الدفيئة في الغلاف الجوي. يشوب فهم التأثيرات طويلة المدى لتخزين غاز ثاني أكسيد الكربون (CO_2) في الطبقات الكربونية للمياة الجوفية كثير من الغموض بما في ذلك التأثيرات الجيوكيميائية لغاز ثاني أكسيد الكربون (CO_2)على الطبقات الكربونية بالإضافة الى التأثيرات الميكانيكية والكيميائية المقترنة. غاز ثاني أكسيد الكربون يذوب في الماء مكون بيكربونات والتي بدورها تتفكك إلى حامض الكربونيك. هذا الحامض يذيب معدن الكالسيت في الصخور الكربونية. ونتيجة لذلك، فإن الخصائص الميكانيكية لطبقات المياة الجوفية تتغير من خلال هذا التفاعل. لذا فمن الضروري دراسة تأثير تخزين غاز ثاني أكسيد الكربون على سلامة طبقة معينة للحصول على تخزين آمن وفعال على المدى الطويل لغاز ثاني أكسيد الكربون (CO_2) في طبقات المياة الجوفية المالحة والعميقة. ركزت الأعمال السابقة في مجال تخزين غازثاني أكسيد الكربون على تأثير حقن هذا الغازعلى الخصائص البتروفيزيائية والميكانيكية للصخور ، حيث إن الحقن يحدث في فترة قصيرة، والتي لم تكن كافية لغاز ثاني أكسيد الكربون لكي يتفاعل مع طبقات المياة المالحة، وبالتالي التفاعلات الكيميائية والتي من شأنها أن تؤثر على خصائص الصخور.

الهدف الرئيسي من هذا العمل هو دراسة تأثير تخزين غاز ثاني أكسيد الكربون (CO_2) على الخصائص الميكانيكية للصخور الكربونية لطبقات المياة الجوفية التي تعرضت للتمرغ والتنقع مع غاز ثاني أكسيد الكربون (CO_2). وعلاوة على ذلك، تم دراسة تأثير مدة تخزين غاز ثاني أكسيد الكربون (CO_2) او تأثير مدة التفاعل مع المحلول الملحي (فترة الذوبان) على هذه الخصائص. تم تخزين غازثاني أكسيد الكربون (CO_2) في العينات عند ضغط 2000 رطل لكل بوصة مربعة و 100 درجة مئوية لفترات زمنية مختلفة تتراوح من أسبوعين إلى ثلاثة أشهر. ثم تم تحليل العينات لدراسة

الخصائص الميكانيكية باستخدام اختبار الموجات الصوتية او المرنة ، و اختبارالضغوط غير محصورة، و اختبارقوى الشد غير المباشرة.

وأظهرت النتائج أن تخزين غاز ثاني أكسيد الكربون(CO_2) لفترات أطول غير الخصائص الميكانيكية للصخور بشكل كبير. العينات التي تم تخزينها بغاز ثاني أكسيد الكربون (CO_2) لفترات أطول أظهرت قدر أكبر من التغيير في الخصائص الميكانيكية مقارنة مع تلك التي تم تخزينها بغاز ثاني أكسيد الكربون (CO_2) لوقت أقصر. التفاعل الجيوكيميائي بين غاز ثاني أكسيد الكربون (CO_2) والمحلول الملحي والصخر يعتمد على الوقت,وبالتالي فإن التغييرات في الخصائص الميكانيكية للصخور تعتمد ايضا على الوقت. الخصائص الميكانيكية لصخور الحجر الجيري للخف تأثرت بشكل كبير مقارنة بالصخور الاخرى. من خلال هذه الدراسة وجد ان صخور الحجر الجيري للإنديانا هي الافضل لتخزين غاز ثاني أكسيد الكربون.

CHAPTER 1 INTRODUCTION

1.1 Introduction

The emissions of carbon dioxide have become the main contributing factors of a continuing increase in the temperature of the earth leading to global warming. Currently, the techniques of decreasing these emissions have been established including the capture and geological storage of carbon dioxide. There are four areas that are relevant to the geological sequestration of carbon dioxide:

- Enhanced oil recovery (EOR),
- Storage in depleted oil and gas reservoirs,
- Storage in deep saline aquifers, and
- Enhanced coal bed methane recovery (ECBMR) (Nguyen et al., 2003; Jaeger, 2005).

Among these areas, the storage of carbon dioxide into deep saline aquifers is considered to be the most effective and advanced technology for reducing the emission CO_2 when compared to other sequestration technologies.

Carbonate rocks are good candidates for CO_2 storage as they offer large capacity for sequestration. Carbonate rocks are mostly composed of calcite ($CaCO_3$) and dolomite ($CaMg(CO_3)_2$), and are bioclastic or chemical in origin, or a combination of the two. The carbon dioxide dissolves in water (brine) forming bicarbonate, which then dissociates to give a weak acid that dissolves calcites in carbonate rocks (Egermann et al., 2005). As a result, the acoustic, petrophysical and mechanical properties of rocks change.

Carbon dioxide flooding on a number of samples from West Texas carbonate caused a decrease in P-wave velocity (Vp) at all effective pressures and a decrease in S-wave velocity (Vs) in most cases. However, at high effective pressures, the result showed a slight increase in some samples (Wang et al., 1996). Myer (2001) and Kim et al. (2010) found that the displacement of brine by CO_2 caused an increase in resistivity and a reduction in seismic velocity (Vp) for sandstone rocks. Zeng et al. (2008) observed that when CO_2-saturated Indiana limestone samples were heated and cooled across the CO_2 critical temperature keeping the pore pressure constant above the CO_2 critical pressure, all three seismic velocities changed considerably in a non-linear way. On the other hand, when temperature and pressure are kept constant near the CO_2 critical point, the average seismic velocities remain almost unchanged.

CO_2 storage in carbonate aquifers showed permeability and porosity improvement as well as reduction. The carbonates (limestone aquifers) dissolving and CO_2 trapping as an ionic species were caused by the reaction of CO_2 with rocks (Rosenbauer et al., 2005). Gupta (2010) studied CO_2 storage in carbonate formations. He observed that there is dissolution in some pores (near to the end of injection), but precipitation in other pores of carbonate matrix (near to the end of production). Also, he found that the porosity and permeability of core samples were reduced. However, in another study, the injection of CO_2 caused an increase in permeability and enhancement in porosity when the carbonate rocks were used (Nur et al., 2011).

Vanorio et al. (2011) noticed that the injection of CO_2 on carbonates induced dissolution of the microcrystalline matrix leading to porosity enhancement. Mohamed et al. (2012) concluded that there is no clear effect for temperature, injection flow rate, and injection scheme on the permeability of cores. Initial core permeability is the main factor that led to

the change in core permeability when supercritical injection of CO_2 on dolomite cores for sequestration purpose was conducted. Mohamed et al. (2013) used Pink Desert limestone cores. They noticed that brine composition is the main factor that affects the chemical reactions between CO_2/brine/rock during CO_2 sequestration in carbonate aquifers.

Xuejun et al. (2009) observed that after the supercritical injection of CO_2, rock (Indiana limestone) strength was decreased considerably. However, in the second stage which was under static, no-flow conditions, there was no noticeable difference in strengths between CO_2 and water-saturated rocks. The elastic properties of carbonate rocks samples displayed a gradual loss of strength upon injection as observed by the decrease in elastic moduli (Vialle and Vanorio, 2010; Vanorio et al., 2011; Nur et al., 2011).

Alam et al. (2011) and Alam and Fabricius (2012) found that the effect of supercritical injection of CO_2 on both petrophysical and mechanical properties of chalk depend on carbonate content. Pure chalk with high carbonate content is relatively prone to mechanical weakening due to CO_2 injection, while no significant affect was observed in relatively impure chalk of Ekofisk Formation during the span of the experimental study. The impact of carbon dioxide storage on selected overburden shale and reservoir limestone was studied by Masoudi et al., 2013. The results showed that there was a reduction in Young's modulus, unconfined compressive strength, angle of internal friction, and tensile strength and an increase in Poisson's ratio for the post-CO_2 treated test samples.

1.2 Value to the Kingdom

Many countries around the world have given a big attention for one of the biggest problems that threatens the human life which is the carbon dioxide emissions. Greenhouse emissions are considered as the main cause for the global warming phenomenon. The increasing of the

CO_2 emissions sources such as the power plants and the factories consequently led to the increasing of the emissions.

The proper use of CO_2 will eliminate its bad effects on the environment. This project will help understand the effects of CO_2 sequestration on the aquifer and cap rocks. These effects could lead to CO_2 leakage or affect the cap rock seal. In this project we are going to address all these effects and try to find proper solutions to get the maximum benefits from storing CO_2 in a good quality aquifer rocks that will keep CO_2 inside for a long time. This project will help also in the site selection of the CO_2 sequestration.

1.3 Research Objectives

The main purpose of this study is to investigate the impact of storage of CO_2 on the mechanical properties of carbonate aquifers and cap rocks. Furthermore, the effect of duration of CO_2-brine contact time (solubility time) on these properties was addressed.

The objectives were achieved by injecting CO_2 into samples from carbonate aquifers (limestone) and cap rocks. CO_2 was injected and soaked with the brine with the core at high pressure (2000 psi) and high temperature (100 ºC) to simulate the actual down hole conditions.

The specific objectives of this study were as follows:

- Evaluate the effect of CO_2 sequestration on the mechanical properties of carbonate rocks by measuring the properties before and after soaking with CO_2.
- Investigate the impact of CO_2 storage on the mechanical parameters based on the sequestration time (14 days, 30 days, and 90 days).

- Study the effect of sequestration of CO_2 on rocks with different mechanical properties.
- Select good candidate carbonate rocks for geologic sequestration of CO_2.

CHAPTER 2 LITERATURE REVIEW

2.1 Geological Sequestration of CO_2

2.1.1 The Concept of Geological Sequestration

A continuing increase in the temperature of the earth is called global warming. Emissions of CO_2 are considered to be the main cause for this phenomenon. In these days, the techniques of decreasing these emissions have been developed including the capture and geological storage of carbon dioxide (Bachu, 2003; Gale, 2004; Izgec et al., 2005; Goldberg et al., 2008; Kim et al., 2010; Mohamed et al., 2011). The Department of Energy (DOE) of United States defined the carbon dioxide sequestration as the keeping of the emissions of CO_2 from emitting to the atmosphere by capturing them, separating them, and transporting them to secure storage and/or to get rid of CO_2 from the atmosphere by different technologies and store it (DOE, 1999) (Figure 2.1).

Xuejun et al. (2009) divided the geological sequestration of carbon dioxide into two steps. The first step is to inject CO_2 to underground formation and the second step is to store CO_2 in such a formation for a planned period of time, such as 1000 years.

Le Gallo et al. (2002), Jaeger (2005) and Izgec et al. (2005) defined three main mechanisms for CO_2 sequestration:

- Solubility Trapping: CO_2 is dissolved in the formation water. It is an important mechanism in deep saline aquifers.
- Hydrodynamic Trapping: CO_2 is injected in the host formation and flows according to the pressure gradient, and finally trapped as free-gas saturation in the pore spaces.

- Mineral Trapping (Geochemical Trapping): CO_2 reacts with the mineral and fluids found in the aquifer.

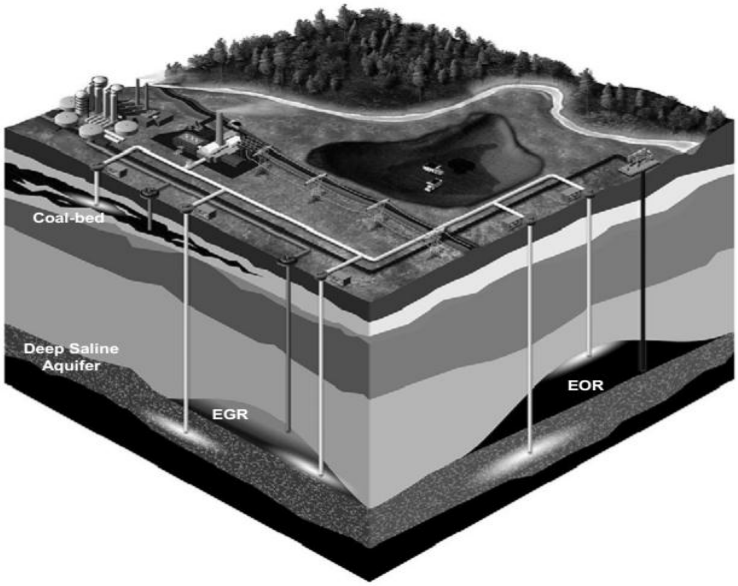

Figure 2.1 Geological storage (Gomez, 2006).

2.1.2 Sequestration Options

As mentioned earlier in 1.1, there are four options for the geological sequestration of carbon dioxide. The volumes of carbon dioxide that can be stored into these formations are considerably different (Herzog, 2001) as shown in Table 2.1.

In this study, we focused on deep saline aquifers because they are considered to be the most promising for reducing the emission CO_2 when compared to other sequestration technologies.

Table 2.1 Estimates of the volumes of CO_2 that can be sequestered below surface (Herzog, 2001).

Sequestration Option	Worldwide Capacity
Oceans	1000s GtC
Deep Saline Formations	100s-1000s GtC
Depleted Oil and Gas Reservoirs	100s GtC
Coal Seams	10s-100s GtC

2.1.3 Deep Saline Aquifers

Deep saline aquifers contain undrinkable water and are not good for agricultural water supply too.

The geological storing of carbon dioxide into deep saline aquifers has been recommended as one of best options for decreasing the emission of CO_2 when compared to other storage technologies due to the following factors:

- Deep saline aquifers have large storage capacity. Significant volumes of CO_2 can be stored within the porous space of deep saline aquifers compared to that in the other formations (Gomez, 2006; NETL, 2009; Firoozabadi and Cheng, 2010).
- Deep saline aquifers cover large areas, i.e., usually there will be one of these formations near any source of CO_2 (Bruant et al. 2002; Firoozabadi and Cheng, 2010).
- The long term duration for storage is likely in these formations (Gunter et al., 1997; Holloway, 1997; Bachu, 2000; Bruant et al., 2002).
- The sequestration in these aquifers has less environmental impact.

2.2 Geological Sequestration of CO_2 into Carbonate Rocks

2.2.1 Carbonate Rocks

Carbonate host rocks, and carbonate overburden formations into which stored CO_2 might migrate in the long term, constitute a particularly interesting case (Liteanu, 2009). Carbonate rocks are good candidates for CO_2 storage as they offer large capacity for sequestration.

Carbonate rocks are mostly composed of calcite ($CaCO_3$) and dolomite ($CaMg(CO_3)_2$). This research is focused on the sequestration of CO_2 into carbonate aquifer rocks (limestone).

Very few concrete and experimental results are available on the influence of CO_2 on the chemically coupled mechanical effects of CO_2 on carbonate rocks.

2.2.2 Dissolution/Precipitation Mechanisms in Carbonates

Carbon dioxide dissolves in water to form carbonic acid. The rate of dissolution of CO_2 in the formation water depends on the pressure and the temperature of the formation (Bahar and Liu, 2008). Calcium bicarbonate which is soluble in water is formed when carbonic acid reacts with calcite. Continuous dissolution of calcium carbonate will lower the acidity of the carbonic acid resulting in the precipitation of calcium carbonate from solution (Egermann et al., 2005; Mohamed et al., 2010).

These reactions are described by the following equations:

$$H_2O + CO_2 \leftrightarrow H_2CO_3 \tag{2.1}$$

$$CaCO_3 + H_2CO_3 \leftrightarrow Ca(HCO_3)_2 \tag{2.2}$$

A flow channel can be formed in the rock as a result of the dissolution of calcium carbonate. This flow channel then acts as the dominant flow path thereby changing the permeability and the porosity of the rock (Grigg and Svec, 2006; 2008).

The mechanical and transport properties of the reservoir and caprock may change through interaction with the injected supercritical CO_2 and the pore fluid, on both short and long time scales.

2.3 Effect of CO_2 on the Properties of the Rocks

2.3.1 Effect of CO_2 on the Acoustic Properties

Acoustic waves are divided to compressional and shear wave velocities. Compressional wave involves a periodic compression of the material and is called a longitudinal wave. It is also often termed a primary wave. Shear wave involves a periodic shearing of the material and is known as a transversal wave. It is also often called a secondary wave (Fjaer et al., 2008).

Compressional and shear waves are the only types of waves that exist for an isotropic, homogeneous solid. Compressional and shear wave velocities reflect the mechanical properties, especially the Young's modulus and Poisson's ratio as shown below.

$$K = \rho V_p^2 - \frac{4}{3}\rho V_s^2 \tag{2.3}$$

$$E = \rho V_s^2 \ \frac{3V_p^2 - 4V_s^2}{V_p^2 - V_s^2} \tag{2.4}$$

$$\upsilon = \frac{V_p^2 - 2V_s^2}{2(V_p^2 - V_s^2)} \tag{2.5}$$

This part will address the effect of CO_2 on the acoustic properties of rocks, which no significant amount of work has been done.

Wang and Nur (1989) measured both compressional and shear velocities on a number of Berea sandstones saturated with n-hexadecane ($C_{16}H_{34}$) and then flooded with CO_2 by the ultrasonic-pulse-transmission technique. They created the measurements at different pore pressure and temperature conditions. They found that CO_2 caused P-wave velocities to

considerably decrease under all conditions while S-wave velocities were decreased at high pore pressure and increased at low pore pressures (Figure 2.2). Increasing rock porosity decreases the CO_2 effect on Vp. Large decreases in P-wave velocities upon flooding are supposed to be caused by a dropped bulk modulus and increased density of the rock/hydrocarbon/CO_2.

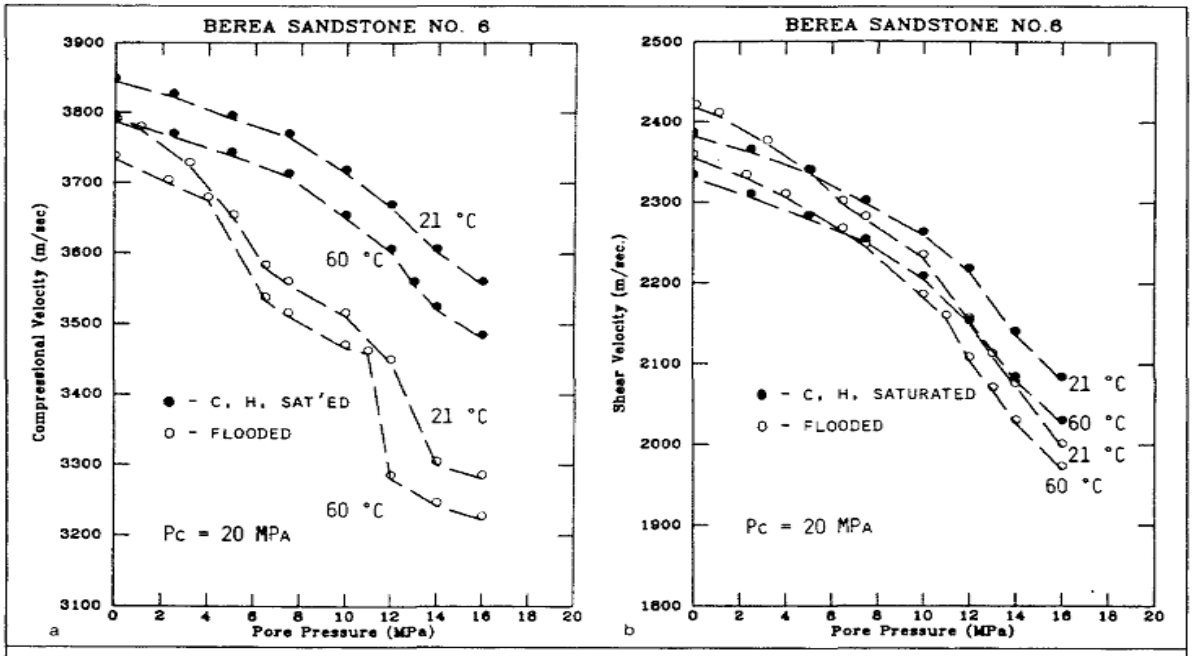

Figure 2.2 Compressional and shear velocities in n-hexadecane-saturated and CO_2-flooded Berea sandstone vs. pore pressure (Wang and Nur, 1989).

Wang et al. (1996) measured both compressional and shear velocities on a number of samples from the west Texas carbonate. They found that after CO_2 flooding; Vp decreased at all effective pressures (higher decrease at high porosity and smaller decrease at low porosity). The shear wave velocity, Vs, decreased in most cases. However, at high effective pressures (low pore pressures), the result showed a slight increase in some samples. As CO_2 displaces the original reservoir fluid, an oil/water mixture, it decreases the bulk modulus while hardly changing the bulk density of the reservoir rock.

The changes in seismic velocity, attenuation, and reflectivity associated with a miscible CO_2 injection in a west Texas carbonate reservoir were imaged by Harris et al., 1996. Using cross well tomographic images made before and after CO_2 injection, they determined that the reduction in P-wave velocity reached 20% in some formations. Differences were also observed in S-wave velocity, P-wave and S-wave reflectivity attenuation. The differences are due in part to changes in the saturating fluids and in part to changes in pressure associated with the injection process. This is confirmed experimentally. Myer (2001) conducted laboratory seismic and electrical measurements on Berea sandstone. He found that the displacement of brine by CO_2 caused an increase in resistivity and a reduction in seismic velocities and amplitudes (Figures 2.3 and 2.4). Consequently, seismic measurements and electrical properties are expected to be sensitive to the CO_2 phase changes occurring at the critical point.

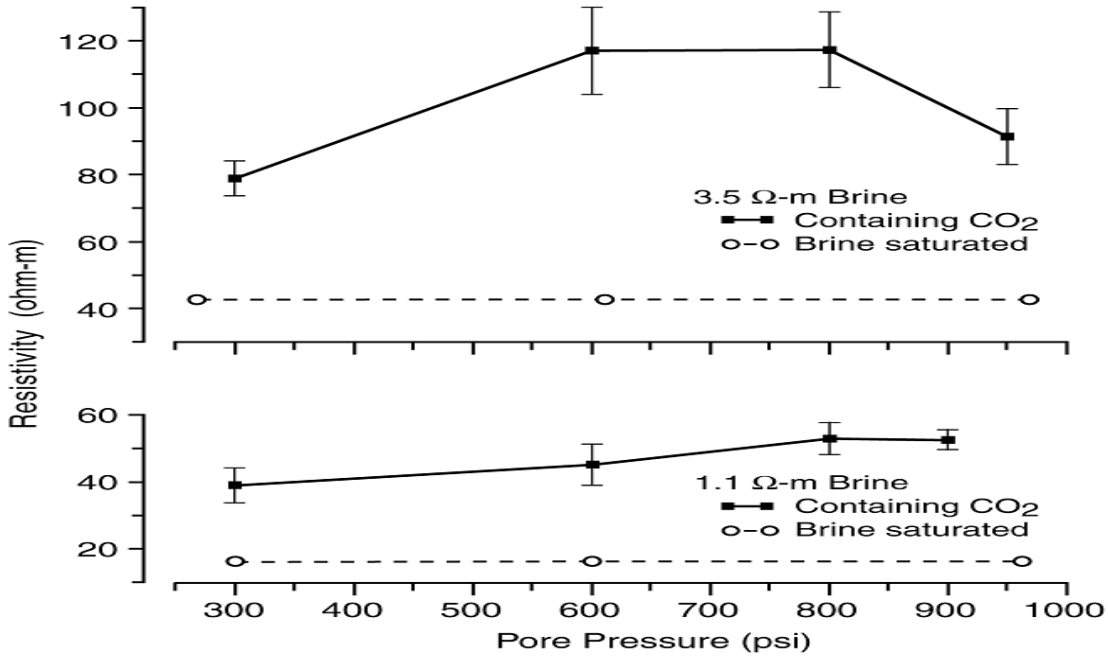

Figure 2.3 Results of resistivity measurements on Berea sample saturated with brine and then flooded with CO_2 at 300 psi (Myer, 2001).

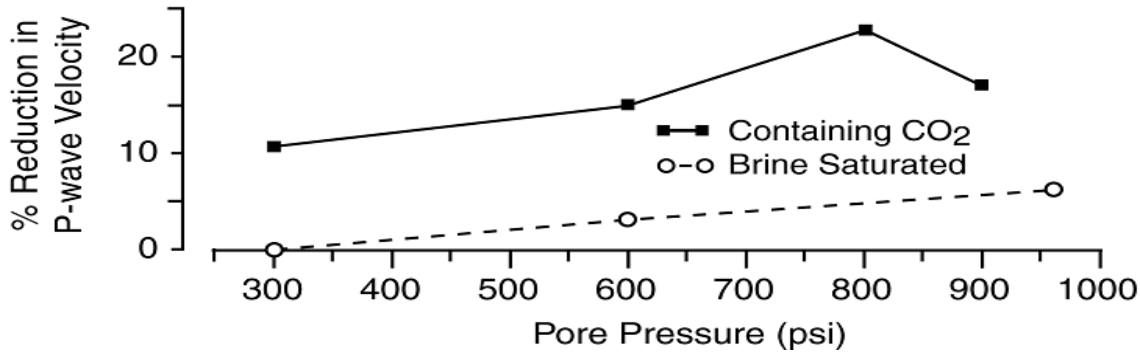

Figure 2.4 Changes in P-wave velocity for Berea sample saturated with 1.1 Ω–m brine and then flooded with CO_2 at 300 psi (Myer, 2001).

A single well and time-lapse seismic cross well experiments in a diatomite reservoir to observe the injection of CO_2 into a hydro fracture zone were conducted by Gritto, 2003. In his work, he found that before the injection of CO_2, compressional wave velocities revealed values between 1700-1900 m/s, which were reduced to 1600-1800 m/s after the injection of CO_2 (-5%). On the other hand, shear wave velocities data exhibited slow velocities (600-800 m/s), which were reduced to 500-700 m/s after the injection of CO_2 (-6%).

Kim et al. (2010) studied the effect of supercritical injection of CO_2 (10 MPa, 40 ºC) into water-saturated sandstone on compressional wave velocity and resistivity simultaneously. Experiments were conducted by simulating the reservoir condition with high temperature and high pressure in depths of about 1000 m or more. The results of this study showed that compressional wave velocity reduced drastically. However the resistivity increased monotonously during the injection duration. The Vp decreased by 5.1%, 7.1%, 8.1% when the CO_2 saturation was 10%, 20%, 30%, respectively. For CO_2 saturations above 30%, Vp did not change and increased slightly above 40% CO_2 saturation (Figures 2.5 and 2.6).

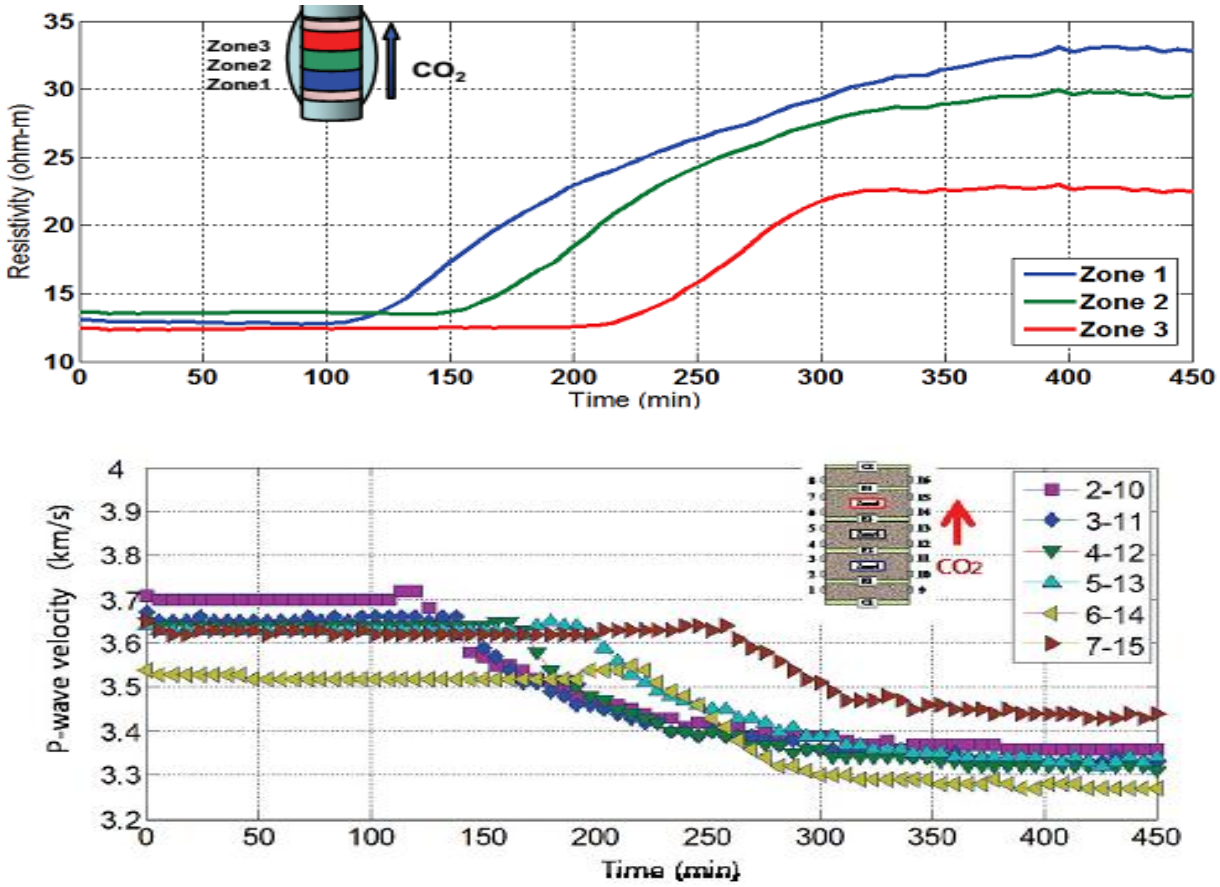

Figure 2.5 The changes of resistivity and P-wave velocity against CO_2 injected time (Kim et al., 2010).

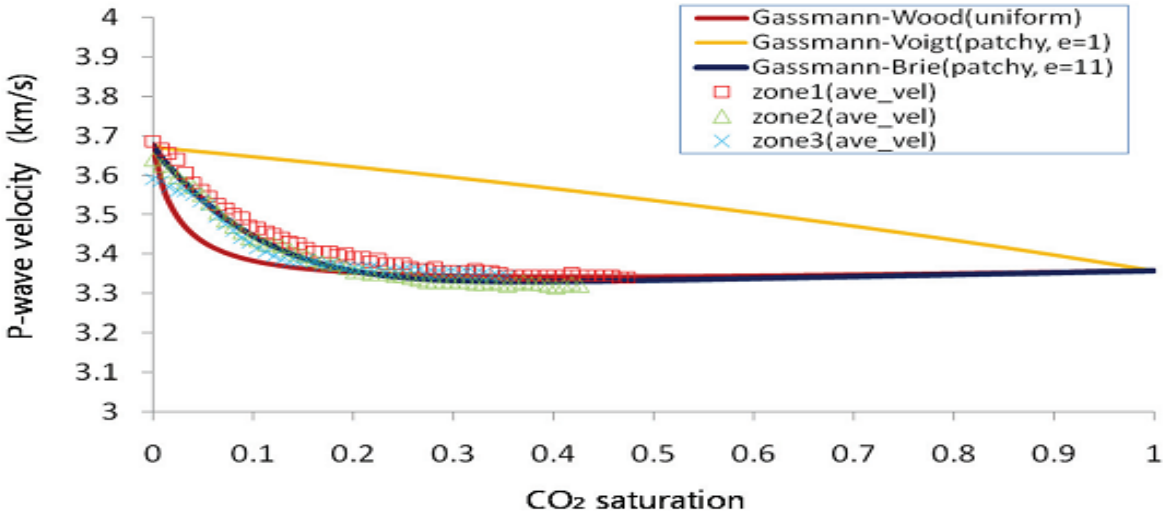

Figure 2.6 Wave velocity-CO_2 saturation relations with Gassmann fluid-mixing laws (Kim et al., 2010).

Mohapatra et al. (2012) performed experiments at in-situ pressure conditions on plugs (Tuscaloosa sandstones) to study the variation in seismic parameters (velocity and impedance) with the change in subsurface fluid type and saturation. During brine flooding on dry samples, a decrease in P-wave velocity (~2%) was observed till 95% saturation. Thereafter the velocity increased by 15% during the remaining 5% saturation. After attaining 100% brine saturation, oil was pumped to displace brine till irreducible water saturation was achieved. A linear drop of 4% in velocity was observed during this step. Liquid CO_2 was injected to displace oil-brine system and a drop of 8% in P-velocity was observed. Associated changes in P-wave impedance due to change in pore fluid saturation are 25%, -5%, and -8%, respectively, for the three flooding experiments.

2.3.2 Effect of CO_2 on Petrophysical Properties

CO_2 sequestration in carbonate aquifers showed porosity and permeability enhancement as well as reduction. CO_2 may affect the porosity and permeability positively due to carbonate rock dissolution, or negatively due to precipitation of reaction products, mainly $CaCO_3$ (Mohamed et al., 2010). Precipitation process of dissolved material can impact the permeability, while causing a small change in porosity (Grigg and Svec 2003). The trend of change in rock properties is case dependent because it is related to distribution of pores, brine composition, and thermodynamics (Izgec et al. 2006).

This section will review the impact of CO_2 on petrophysical properties of the rocks based on the previous work. Rosenbauer et al. (2005) performed series experiments of carbon dioxide sequestration into rock samples from limestone aquifers. They found that the carbonates dissolving and CO_2 trapping as an ionic species were caused by the reaction of CO_2 with rocks. On the other hand, in a particular case, the results indicated that there was no significant affect in the geochemical reactions and rock porosity when a simulated co-

injection of supercritical CO_2 with brine into limestone was conducted except for some initial dissolution of calcite. Gupta (2010) studied CO_2 storage in carbonate formations which are analogous to Arab and Khuff Formations, at simulated reservoir conditions. He observed that there is dissolution in some pores (near to the end of injection), but precipitation in other pores of carbonate matrix (near to the end of production). The porosity and permeability of core samples were reduced (Figure 2.7). He concluded that the result are applicable for evaluating the opportunities to sequester CO_2 in Qatar and Middle-East since the Khuff and Arab Formations are similar to the outcrop samples which used in this study.

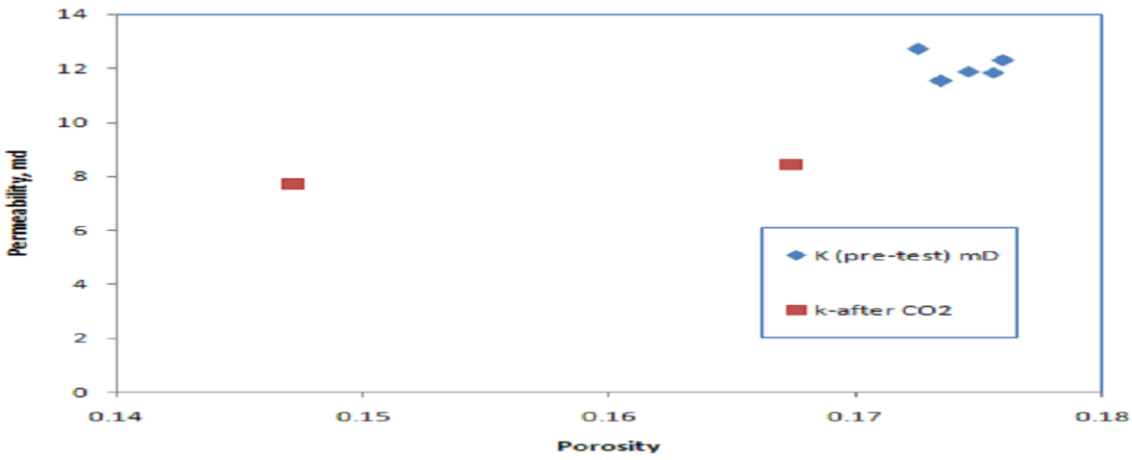

Figure 2.7 Porosity and permeability variations and change after aging with carbon dioxide (Gupta, 2010).

Vanorio et al. (2011) performed a series of laboratory experiments and high-resolution imaging techniques to study the variations in transport, microstructure, and seismic properties of brine-saturated sandstones and carbonates when injected with CO_2. The injection of CO_2 into sandstones showed salt precipitation mainly at grain contacts and/or within small pore throats. Salt precipitation decreased permeability and increased P- and S-wave velocities particularly in sandstones characterized by porosity lower than 10%. The

injection of CO_2 carbonates induced dissolution of the microcrystalline matrix leading to porosity enhancement (Figures 2.8 and 2.9).

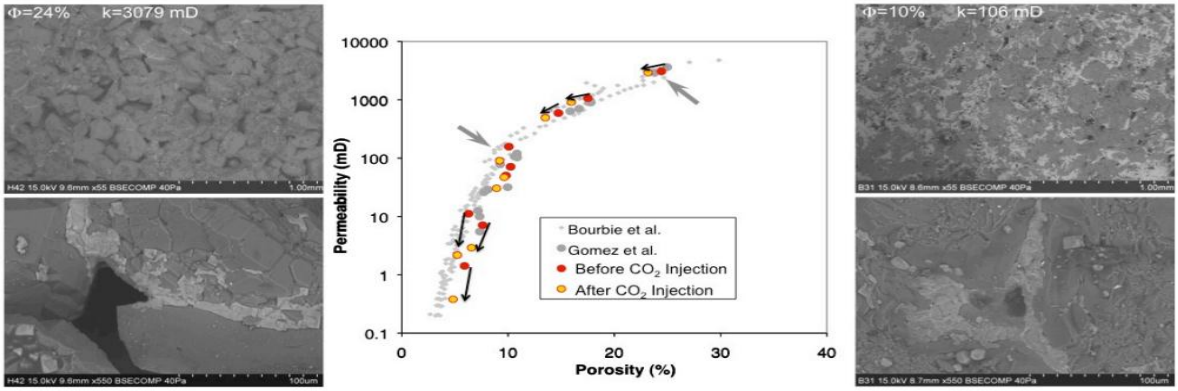

Figure 2.8 Variation of permeability as a function of porosity for sandstones measured before (red dots) and after (yellow dots) alternating injection of seawater and CO_2 injection (Vanorio et al., 2011).

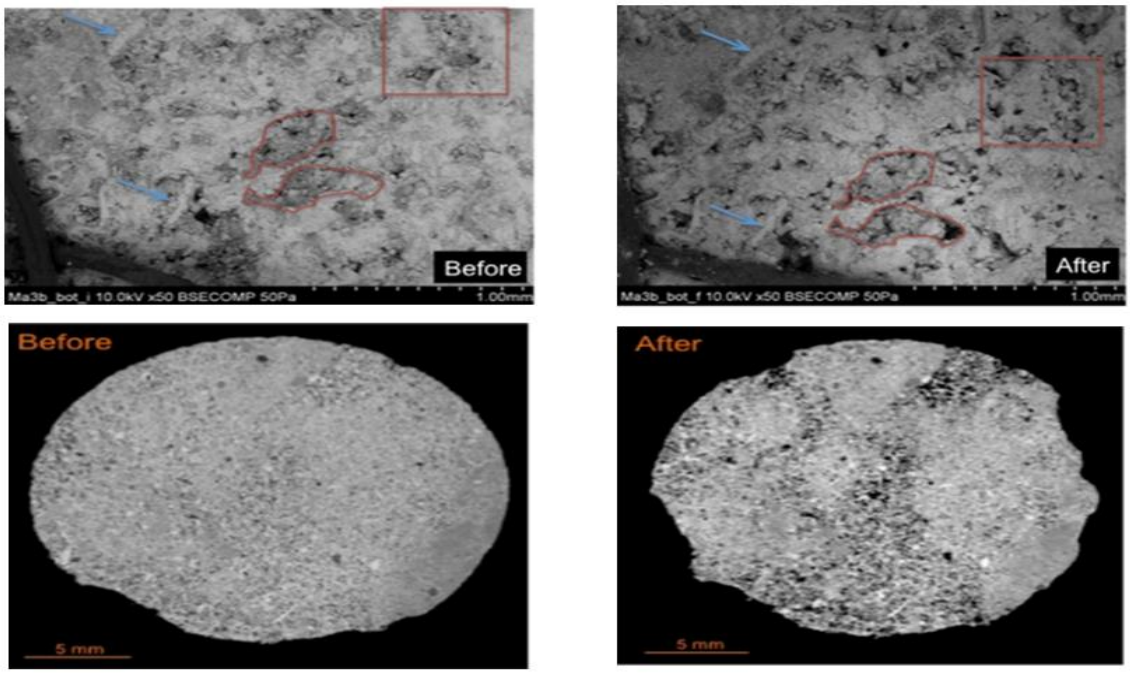

Figure 2.9 Time-lapse SEM (up panel) and CT-scan (down panel) images monitoring the permanent changes induced in the rock microstructure by calcite dissolution upon injection of CO_2-rich water (Vanorio et al., 2011).

The injection of CO_2 caused an increase in permeability and enhancement in porosity (Nur et al., 2011). This occurred because the chemical reactions related with the injection, combined with drag due to the flow, acted to dissolve and remove the fines that originally impeded the flow (Figures 2.10 and 2.11).

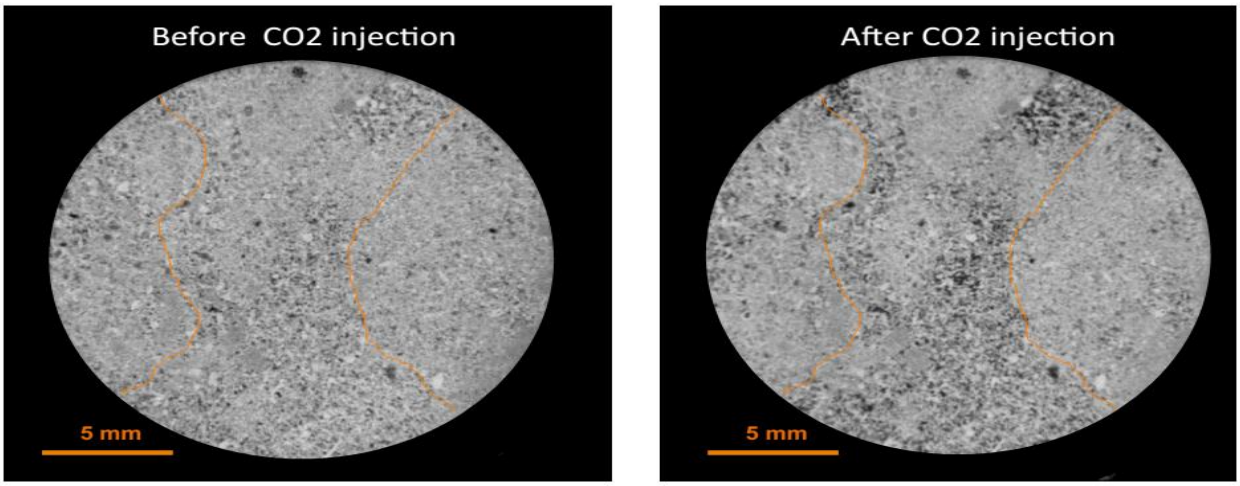

Figure 2.10 A single slice extracted from a 3D volume showing the apparent enhancement of porosity in a carbonate sample (Nur et al., 2011).

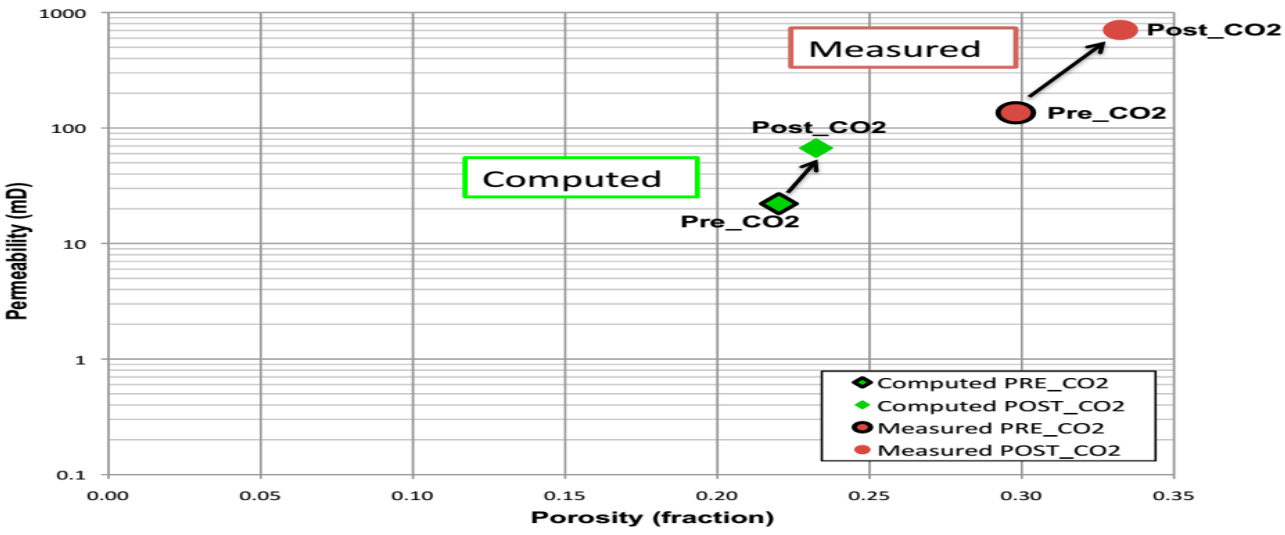

Figure 2.11 Permeability vs. porosity computed on a digital sub-sample (Nur et al., 2011).

Mohamed et al. (2011) applied CO_2 flooding experiments at the supercritical state on limestone cores. The content of calcium, magnesium, and sodium, and permeability of the limestone cores were measured before and after the injection of CO_2. They observed that the permeability of the cores remained the same when NaCl – brine was injected while injection of calcium chloride and magnesium chloride caused the damage of cores (Figures 2.12 and 2.13).

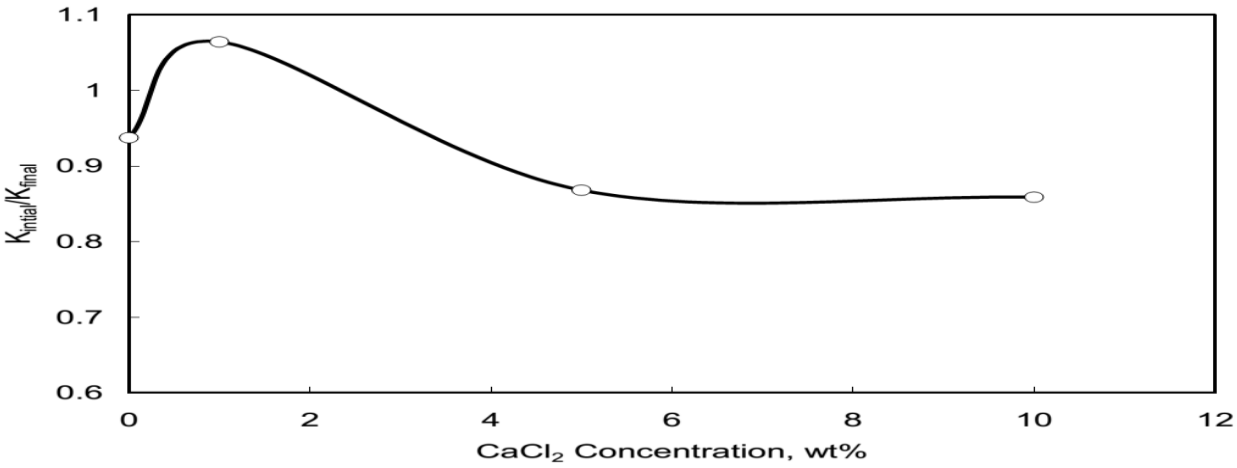

Figure 2.12 Change in cores permeability when different concentration of $CaCl_2$ brine was injected (Mohamed et al., 2011).

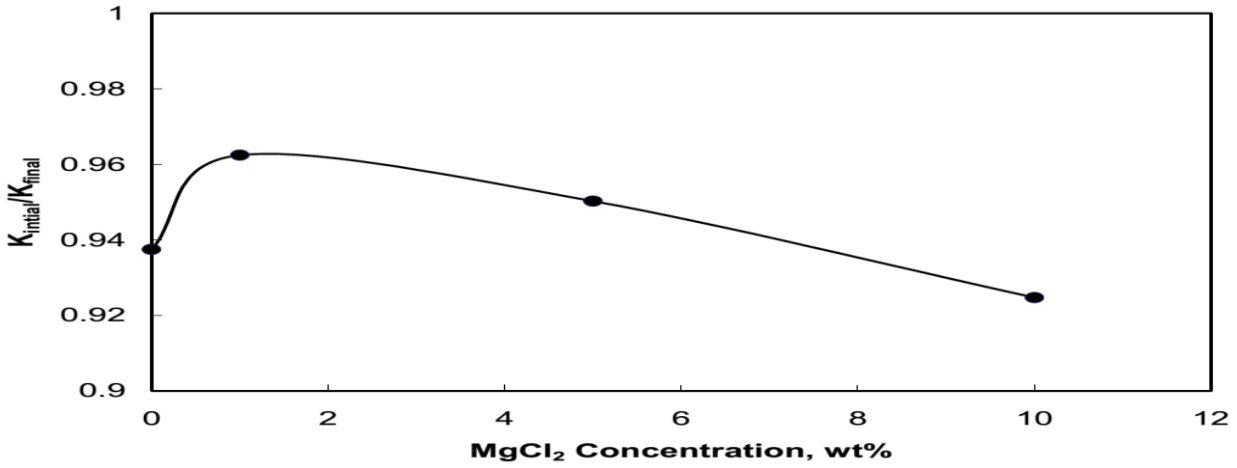

Figure 2.13 Change in cores permeability when different concentration of $MgCl_2$ brine was injected (Mohamed et al., 2011).

Mohamed et al. (2012) studied the effect of supercritical injection of CO_2 on dolomite cores for sequestration purpose in a deep saline aquifer. The parameters addressed in this study were brine composition, temperature, injection rate, and injection scheme. They concluded that there is no clear effect of temperature, injection flow rate, and injection scheme on the permeability of cores. Initial core permeability is the main factor that led to the change in core permeability. Mohamed et al. (2013) used Pink Desert limestone cores too. They noticed that brine composition is the main factor that affects the chemical reactions between CO_2/brine/rock during CO_2 sequestration in carbonate aquifers. They also concluded that there is no clear impact for the injection flow rate of CO_2 on the core permeability. However, the core permeability increased from 56.5 to 60.6 mD at a lower temperature (70 °F) and the core was damaged at a higher temperature (200 °F).

2.3.3 Effect of CO_2 on Mechanical Properties and the Strength of the Rocks

Mechanical parameters can be divided into three main groups (Abdulraheem et al., 2009): Elastic Parameters: For an isotropic medium, there are two independent elastic parameters, viz., Young's modulus and Poisson's ratio.

Strength Parameters: The strength of a material is dependent on the stress level, and that failure criteria that describe actual data normally have at least 2–3 adjustable parameters.

In Situ Stresses: The in situ stresses are given by the three principal stresses and three parameters giving the orientation of the principal stresses. The stress level determines whether a rock is critically loaded or not. Additionally, the in situ stresses influence both the elastic parameters and the strength parameters (Fjaer et al., 2008).

Sedimentary rocks (sandstone, limestone and dolomite) are potential host rocks for CO_2 storage. On the other hand, low-permeability, high-entry pressure formations, such as shale,

marl and clay stone, can form the cap rock. Mechanical properties of these rock types (Figure 2.14) can take a wide range of values (Riano, 2012).

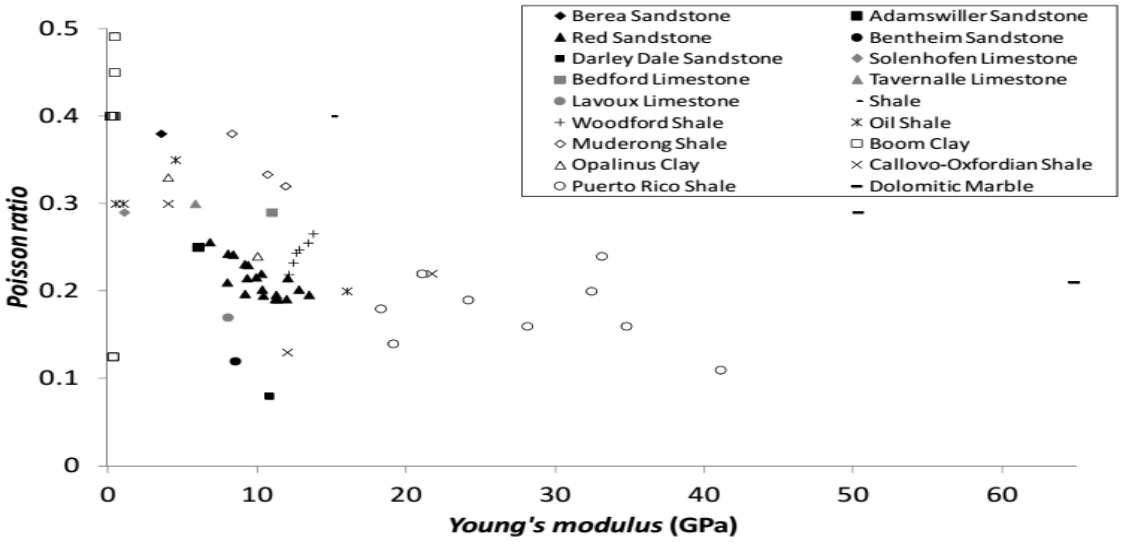

Figure 2.14 Young's modulus and Poisson ratio for several sandstones, limestones, dolomitic marble and shales (Riano, 2012).

The understanding of long term effects of CO_2 storage in carbonate reservoirs is challenged by many uncertainties including geochemical effects of CO_2 on carbonates, the coupled chemical–mechanical effects, etc. (Gledhill and Morse, 2004).

Xuejun et al. (2009) carried out a series of experiments on carbonate rocks (Indiana limestone) to study the effects of supercritical CO_2 sequestration on rock through combined water-alternative-CO_2 injection and tri-axial geomechanical tests. They observed that after the injection of CO_2, rock strength was declined considerably. Young's modulus and Poisson's ratio of the rock samples also decreased. The friction angle reduced from 42° (without flooding) to 26° (after flooding). However, in the second stage which was under static, no-flow conditions, there was no noticeable difference in strengths between CO_2- and water-saturated rocks as shown in Tables 2.2 through 2.4.

Table 2.2 Triaxial tests of dry Indiana limestone at room temperature (Xuejun et al., 2009).

Specimen ID	Confining Pressure (psi)	Ultimate Compressive Strength (psi)
08IL66	0	4338
08IL33	500	7275
08IL46	1000	9080
08IL54	1500	11183
08IL02	2000	14522

Table 2.3 Triaxial strength tests of Indiana limestone after flooding with CO_2 and water at 136 ºF (Xuejun et al., 2009).

Specimen ID	Confining Pressure (psi)	Ultimate Compressive Strength (psi)
08IL49	500	4650
08IL49	1000	6206
08IL49	1500	7435
08IL49	2000	8437
08IL49	2500	9490

Table 2.4 Results of drained triaxial tests for rock samples after different flooding scenarios (Xuejun et al., 2009).

Specimen ID	Flooding Volume and Flow Rate	Strain Ratio (lateral / Axial)	Young's Modulus ($x10^6$ psi)
08IL82	No Flooding	0.26	3.96
08IL114	3000 ml WAG 100,000ppm (0.5ml/min)	0.27	4.21
08IL106	3000 ml WAG 10,000ppm (0.5ml/min)	0.13	2.38
08IL53	3000 ml AG (0.75ml/min)	0.16	1.51
08IL61	3000 ml WAG (0.01ml/min)	0.12	2.18
08IL74	3000 ml WAG (0.1ml/m)	0.15	1.58
08IL47	3000ml WAG (1ml/min)	0.05	2.25
08IL117	Weak acid Saturated 96 hours	0.18	1.18

Vialle and Vanorio (2010) studied the elastic properties of carbonate rock samples ranging from calcite limestones containing dolomite to pure calcite mudstones during the flooding of reactive CO_2-saturated water. Their conclusion was that the elastic properties of both the saturated and dry rock display a gradual loss of strength upon injection, as appeared by the decrease in the dry P-and S-wave velocity (Figure 2.15).

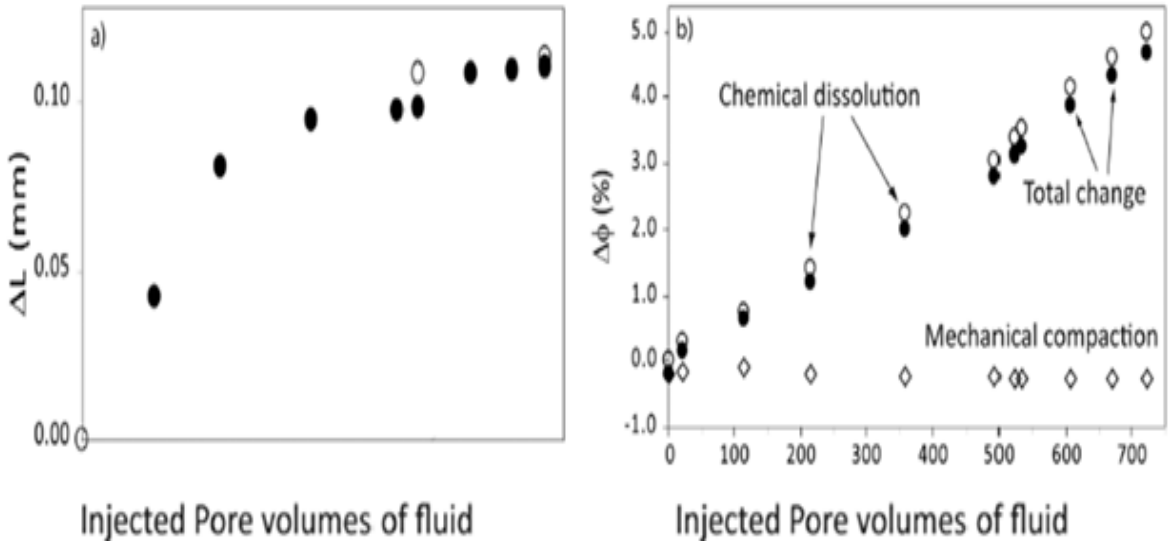

Figure 2.15 Change in sample length along the main axis and porosity versus the injected volume of CO_2-rich fluid, for the carbonate sample exhibiting the highest reactivity (Vialle and Vanorio, 2010).

Vanorio et al. (2011) found that the injection of CO_2 into brine-saturated sandstones and carbonates caused chemo-mechanical changes in the host rock. These changes altered the rock frame by decreasing the elastic moduli of the dry rock frame.

Alam et al. (2011) conducted a series of petrophysical and rock mechanics tests on Ekofisk Formation and Tor Formation chalk of the South Arne field to investigate the alterations in petrophysical and rock mechanics properties of chalk due to the injection of CO_2 at supercritical state. The non-carbonate (silica and clay) fraction forms more than 12% in Ekofisk Formation while in Tor Formation the amount of non-carbonates (silica and clay) is less than 5%. They observed an increase in porosity and permeability due to injection of supercritical CO_2. They also found that the effect of CO_2 injection on both petrophysical and mechanical properties of chalk depend on carbonate content. Pure chalk with high carbonate content is relatively prone to mechanical weakening due to CO_2 injection, while no significant affect was observed in relatively impure chalk of Ekofisk Formation during the

span of the experimental study. In general, they did not find any significant effect on mechanical strength and time dependent behavior of North Sea chalk. Also, Alam and Fabricius (2012) performed study on the same rocks with different percentage of non-carbonate minerals in Ekofisk Formation (20%). They observed a slight decrease in shear failure stress in pure Tor Formation samples. However, no significant changes were observed in Ekofisk Formation chalk where non-carbonate phase surpass 20%.

Alam et al. (2012) studied the difference in static and dynamic behavior for pure Tor Formation ($CaCO_3$> 97%) and impure Ekofisk Formation ($CaCO_3$< 85%) in South Arne field, North Sea. Furthermore, brine saturated data were compared with CO_2 injected data to reveal the effect of supercritical CO_2 injection in both static and dynamic elastic properties. They used strain gauges and LVDTs to measure static deformation. They observed lower dynamic elastic modulus for chalk with higher non-carbonate content at porosities lower than 30%. In 30% porosity chalk, dynamic compressional and bulk modulus were found significantly higher than the static modulus. Static measurements with LVDT were found lowest. The effect of CO_2 injection was notable in dynamic elastic properties, while a possible change in static elastic properties was below detection limit

Masoudi et al. (2013) performed many mechanical and petrophysical tests on selected overburden shale and reservoir limestone core materials to study the impact of carbon dioxide storage on the mechanical properties of these rocks. The results showed that there was a reduction in Young's modulus, unconfined compressive strength, angle of internal friction, and tensile strength, and is an increase in Poisson's ratio and permeability for the post-CO_2 treated test samples (Table 2.5 and Figures 2.16 through 2.18).

Table 2.5 Average rock mechanical and petrophysical properties (Masoudi et al., 2012).

Property	Shale		Limestone	
Depth Range (ft)	5779.7-5800.4		5831.5-5892.1	
Test Condition	Untreated	CO_2 Injected	Untreated	CO_2 Injected
In-Situ Porosity (Initial Conditions)	--	--	33.64%	34.93%
Porosity(Fully Depleted Conditions)	--	--	29.12%	29.00%
In-Situ Permeability to Gas (mD)	0.001161*	0.000963*	272	316
Averaged Pore-Volume Compressibility (Depletion Phase) (Cpp – Based on Reservoir Pressure)	--	--	61.5 Microsips	49.4 Microsips
Ko (Averaged Over the Entire Range of Depletion)	--	--	0.39	0.36
Critical Reservoir Pressure for Accelerated Compaction	--	--	2235	2405
Reduction in Brine Permeability (Ranging From Initial in-Situ Conditions to Abandonment)	--	--	72.4%	76.5%
Average Grain Compressibility (Cg)	--	--	Assumed to be 0.2 Microsips (10^{-6}/psi)	
Coulomb Friction Angle (Entire Range)	23.5	21.2	14.1	12.7
Coulomb Cohesion (Entire Range) (psi)	1138	1307	603	550
In-Situ Effective Compressive Strength (psi)	5932	5982	2590	2518
In-Situ Static Young's Modulus (psi)	256,500	298,850	1,190,265	1,125,765
In Situ Dynamic Young's Modulus (psi)	1,537,500	1,498,000	2,351,000	2,335,300
In-Situ Static Poisson's Ratio	0.15	0.14	0.22	0.23
In-Situ Dynamic Poisson's Ratio	0.17	0.10	0.33	0.29
Indirect Tensile Strength (psi)	--	--	87	98
Carbonate Classification	--	--	Boundstone	Boundstone
Carbonate Grain Types	--	--	Red algae, Coral, Foraminifera	Red algae, Coral, Foraminifera
Authigenic Cements	Calcite, Chert, Pyrite	Calcite, Chert, Pyrite	Sparry Calite, Monor Dolomite	Sparry Calcite Minor

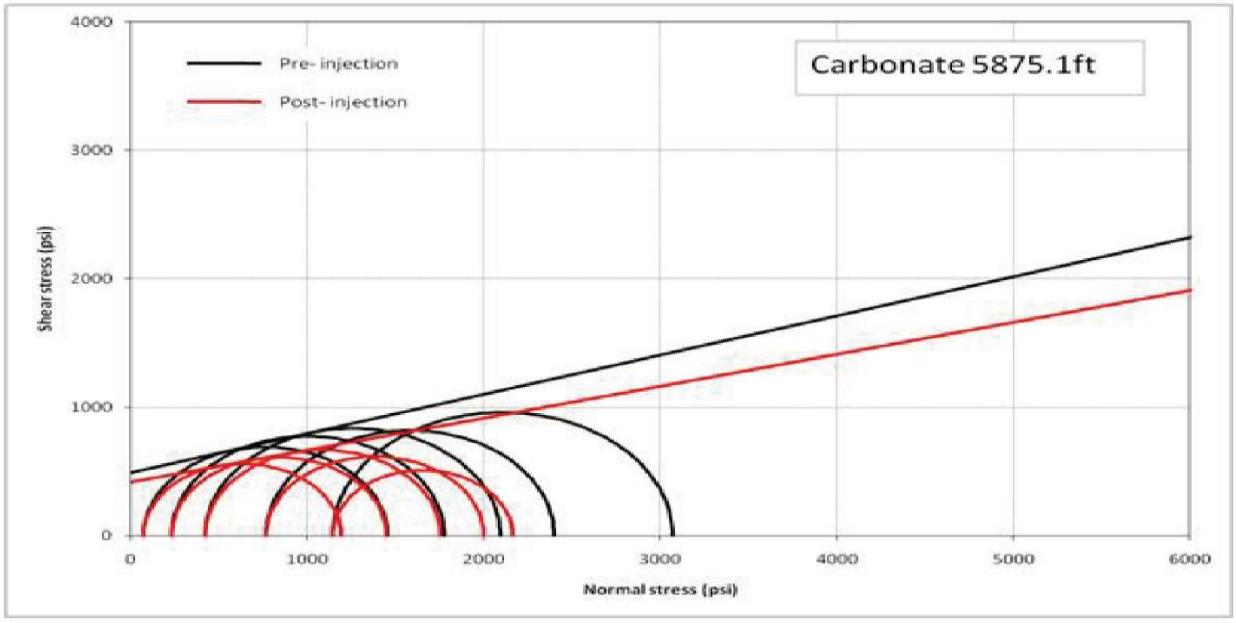

Figure 2.16 Mohr circles and failure envelope for pre- and post-CO_2 treated limestone samples (Masoudi et al., 2012).

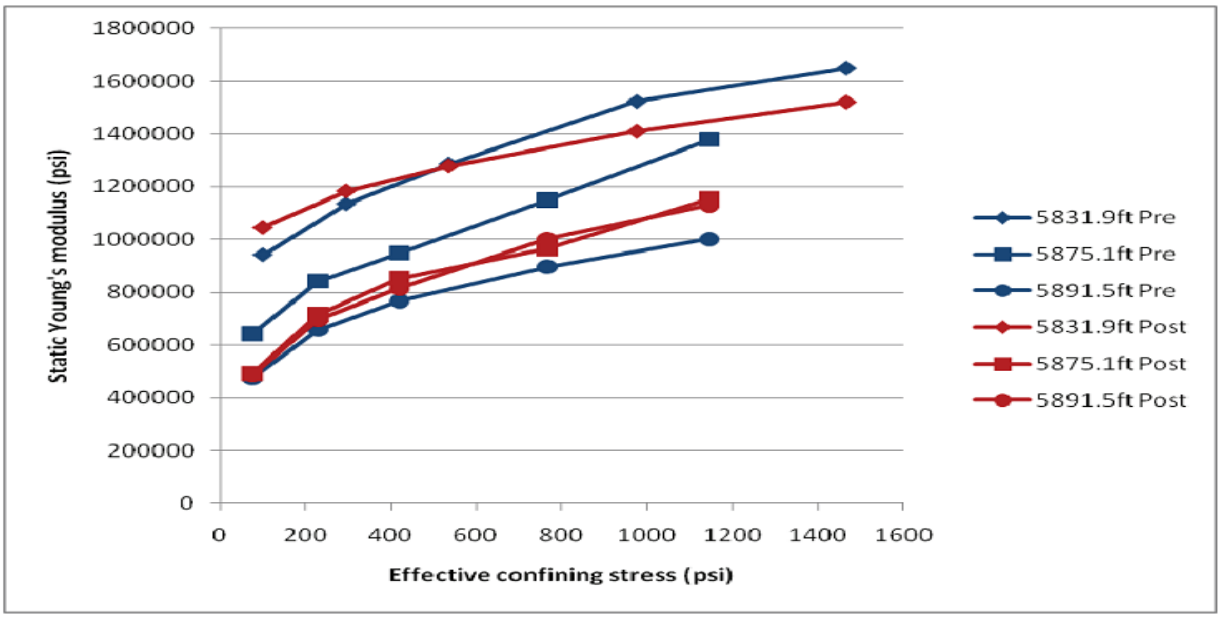

Figure 2.17 Variations of Young's modulus with effective confining stress for pre- and post-CO_2 treated limestone samples (Masoudi et al., 2012).

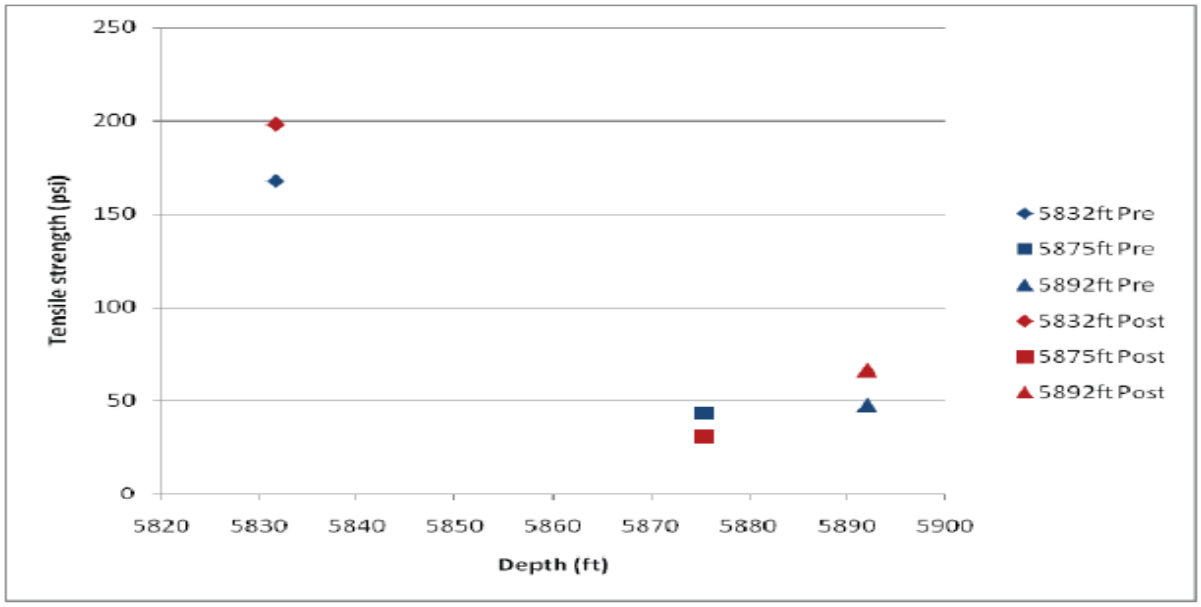

Figure 2.18 Tensile strength for pre- and post-CO_2 treated limestone samples (Masoudi et al., 2012).

Gharbi et al. (2013) studied the interactions of the pore-scale fluid-rock that occur in presence of CO_2 sequestration in saline carbonate aquifers. Brine saturated with supercritical CO_2 (9 MPa and 50 °C) is injected into two carbonate samples (Estaillades limestone and an aquifer sample). The samples were imaged before and after the injection. They noticed the formation and propagation of wormholes along the length of the samples. The generation of new connectivity in the regions away from the wormhole is evident, although the total number of pores and throats decreased as connections merge, while the distribution of coordination number remains largely unaffected. The flow field became more concentrated in the wormhole, but a very wide range distribution of local velocities, spanning more than eight orders of magnitude, is predicted.

CHAPTER 3 RESEARCH METHODOLOGY

3.1 Introduction

Carbon dioxide sequestration was performed under supercritical conditions on carbonate aquifers (limestone) and cap rocks to investigate the influence of CO_2 storage on the mechanical properties of these rocks.

To conduct the mechanical and acoustic testing, a series of tests were run on the samples before and after exposing to CO_2. These tests included the following:

- Unconfined compression test: This test provides the information about the Young's modulus, Poisson's ratio and the strength of the sample.
- Tensile strength test: Tensile strength of rocks plays an important role especially in the design, initiation and propagation of fractures.
- Test for acoustic properties: Compressional and shear wave velocities were measured in this test which reflect the mechanical properties, especially the Young's modulus and Poisson's ratio. Since this is a non-destructive test, it can be repeated on the same samples before and after exposing to CO_2.

Except for the acoustic test, the samples were divided into two groups. The first group was tested without exposing it to any saturation. The second group of samples was saturated with CO_2 for considerable amount of time so as to ensure that the rock gets enough exposure to alter its properties. However, this duration of exposure was limited by overall duration of the experimental program. Each sample in the second group was selected from the area adjacent to its number in the first group. This is to ensure that the other features and constituents of

the rock remain the same. The details of methodology to be used in this research work are described in the next section.

3.2 Material

3.2.1 Synthetic Brine

The brine used in the experiments was synthetic formation water (FW). It was prepared by adding different amounts of $NaHCO_3$, Na_2SO_4, $CaCl_2.2H_2O$, $MgCl_2.6H_2O$, and NaCl to the distilled water. The brine was filtrated through a 0.22 μm filter paper to remove suspended solid particles, and vacuumed to remove dissolved gas prior to each test. Table 3.1 shows the ionic composition of the brine.

Table 3.1 Ionic composition of the brine.

Ions	Composition (ppm)
Sodium	59,491
Calcium	19,040
Magnesium	2,439
Sulfate	350
Chloride	132,060
Carbonate	0
Bicarbonate	354
TDS	213,734
Density (g/cc)	1.1472
Viscosity (cP)	1.597

3.2.2 Core Sample

Outcrop samples from Indiana limestone, Pink Desert limestone and Khuff Limestone were used in this study. Shale samples were also used. The producers for core preparation are described below:

3.2.2.1 Rock Specimen Cutting and Coring

- Once the sections have been identified for taking core plugs, the whole core samples should be cut to desired length from each section. Plugs are then taken from the cut section using standard drill bits (Figure 3.1).
- The core plugs used for rock mechanical testing are cored vertically (along the length of the core) and are cylindrical in shape.
- During the coring process ordinary tap water is used to remove the debris and for the cooling of the drill bit.
- The cored rock plugs are then cut to desired length using high speed rotary diamond saw shown in Figure 3.2.

Figure 3.1 Coring machine for preparing plugs.

Figure 3.2 Core cutter for cutting rock samples to required size.

3.2.2.2 Rock Specimen Cleaning and Drying

- It is necessary to clean the rock specimen in order to determine their effective porosity and permeability and to measure the velocity. The Soxhlet type extractor is used for this purpose (Figure 3.3).
- To start with, sufficient quantity of ethanol is poured in the container. The core basket with the core plugs is lowered on the tripod stand and the lid of the container is closed. Then the water circulation in the condenser is started and the heater is turned on. The evaporated ethanol passes through the pores of the rock specimen and cleans them of any salts present there. This is continued for 24 hours. Then the heater is turned off and the rock specimen is allowed to cool.
- After cleaning with ethanol, the rock specimen are taken out of the container and put in a vacuum oven (Figure 3.4), where they are dried under partial vacuum at a temperature of 80 ºC for about two days.

Figure 3.3 Soxhlet type extractor.

Figure 3.4 Vacuum oven.

3.2.2.3 Grinding End Faces

It is very important that core plugs be right circular cylinders and having flat and parallel ends within 0.025 mm tolerance. The ends are made smooth, flat and parallel by grinding with fine grit diamond coated wheel rotating at high speed (Figure 3.5).

Figure 3.5 End face grinder.

3.2.3 Fluid Properties

3.2.3.1 Measurement of Density

A pycnometer is used to measure the density of the brine by using the following equation:

$$\text{Density} = \frac{\text{weigth of pycnometer filled with the fluid} - \text{weigth of pycnometer empty}}{\text{volume of the pycnometer}} \quad (3.1)$$

3.2.3.2 Measurement of Viscosity

Viscosity of the fluid (brine) was made by using an Oswald viscometer at room temperature.

3.3 Petrographic Description

3.3.1 Thin Section Petrography

Samples were cut to small size to fit them in the glass slides. These small pieces of rock were then impregnated with blue dyed epoxy to facilitate the recognition of their porosity using polarizing microscope. After impregnating, these samples were glued with glass slides using Canada balsam and then left under pressure in order to stick properly to glass slides. Following this, the rock was cut from the glass slide leaving only thin layer of sample on the glass, which was then grinded by hand using silicon carbide to finish it as a thin section of thickness around 35 microns.

Based on thin section and using polarized microscope (Figure 3.6), classification of porosity was conducted including fabric (interparticle, intraparticle, moldic, intercrystal, etc.) or non-fabric (fracture, vug, channel, etc.). In addition, assessment of mineral composition, average grain size, pore connectivity, cementation type, diagensis stages, compaction and dolomitization.

Figure 3.6 Thin section under a microscope.

3.3.2 X-Ray Diffraction (XRD)

To get qualitative and quantitative study of the mineral composition, X-Ray Diffraction (XRD) was used (Figure 3.7). The powder of sample was used to conduct this investigation at 40KV and 40 MA using a divergent slit of one degree, scatter slit of one degree and 0.2 mm nickel filter. The scanning speed used for measurements was 0.01 degree at 28 per second interval. A scanning angle of 2° to 80° has been used for general mineralogical detection. Peaks in XRD spectrum were indexed using Rigaku PDXL software while concentrations of phases were quantified using Rietveld analysis.

Figure 3.7 X-Ray Diffraction (XRD) setup.

3.3.3 Scanning Electron Microscopy (SEM)

The Scanning Electron Microscopy (Figure 3.8) gives new dimension to this study as the micro details that were difficult to be documented with the thin section study was made easy by the use of this method. The SEM is of great value in situation requiring examination of rough surfaces or features at a magnification range from x20 up to x20.000. The SEM enables excellent photographs of features that might be too small and rough to be detected by binocular microscope, or that would probably destroyed in the thin section preparation. The SEM's major contribution to this study is to examine the rock texture, pore space and

delicate pore fillings. Apart from the SEM studies, EDS was also be used in order to have better understanding about the chemical composition (elements investigation) of particular grains observed in the SEM.

(FE-SEM Model FEI Nova Nano SEM 230) scanning electron microscope fitted with EDS was used for this study. Samples were broken into small pieces of approximately 10 mm size in order to be easily mounted on the stubs which were placed into the vacuum chamber of the SEM. The samples were coated with gold alloy to nullify the electric charge that develops on the surface due to bombardment of electrons. The samples were finally placed in holders (platinum disc), which in turn placed in SEM chamber.

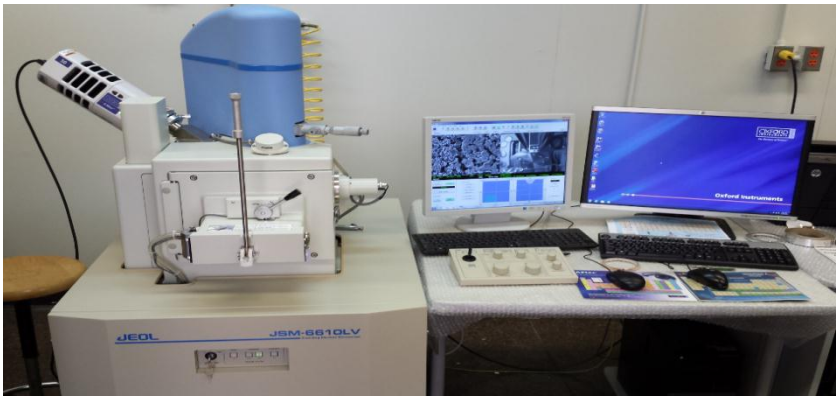

Figure 3.8 The Scanning Electron Microscopy (SEM) setup.

3.4 Core Sequestration Apparatus

A schematic diagram of experimental setup is shown in Figure 3.9. The main components of the apparatus are stainless steel core holder, syringe (ISCO) pump, pressure gauges, high temperature oven, carbon dioxide supply, and carbon dioxide accumulator. A brief description of each component is described below:

3.4.1 Core Holder

A Hassler type stainless steel core holder (aging cell) was used to perform the experiments of this work. It can accommodate about 30 cm long cores and the maximum working pressure of the core holder is 10,000 psig.

3.4.2 Syringe (ISCO) Pump

The ISCO pump was used to increase the pressure to the required pressure.

3.4.3 Pressure Gauges

Pressure gauges were used to measure the overburden pressure. The pressure gauges can measure the pressures up to 5000 psi.

3.4.4 High Temperature Oven

The core holder cells were placed in a temperature controlled oven. The oven can heat up to 150 ºC.

3.4.5 Carbon Dioxide Supply

Carbon dioxide gas cylinder (1000 psi) was used to transfer CO_2 to the accumulator.

3.4.6 Carbon Dioxide Accumulator

High pressure carbon dioxide gas accumulator (2000 psi) was used to inject CO_2 inside the cell.

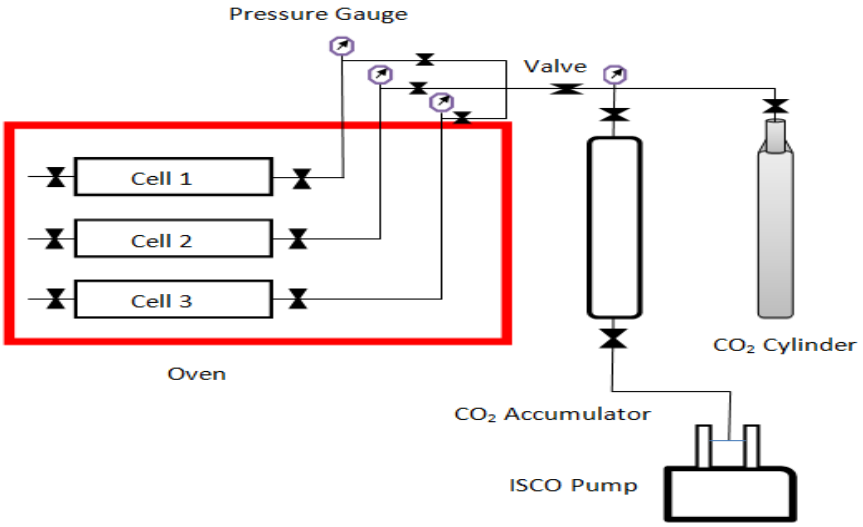

Figure 3.9 A schematic diagram of core sequestration setup.

3.5 Experimental Procedure

3.5.1 Saturation and Porosity Measurement

- After the sample is cleaned and dried, record its weight.
- Take dimensions (length and diameter) of core sample. Record at least 5 readings of length and diameter at five different locations and take the average of them.
- Place the sample in the saturation apparatus as shown in Figure 3.10 and evacuate the sample for at least three hours.
- Close the vacuum pump valve, open the liquid valve and saturate the sample with the saturating fluid (brine). Close the liquid valve and open the vacuum pump valve to evacuate again for at least half an hour to remove the dissolved air in the saturating fluid.
- Keep the sample on saturation for about 24 hours at least.
- After saturation, take the sample and remove the excess liquid from the outer surface of the sample using unbleached, unglazed paper towels and weighs it as quickly as

possible to avoid the evaporation of liquid from the sample using a balance with a resolution of at least 0.001 gram. Record this weight as saturated weight.

- Calculate the weight of the saturating liquid by subtracting the dry weight from the saturated weight of the core (Manual for PETE 204, 2012).

$$V_{bulk} = \frac{\pi * D^2 * L}{4} \tag{3.2}$$

$$PV = \frac{M_{sat.} - M_{dry}}{\rho_{brine}} \tag{3.3}$$

$$\emptyset = \frac{PV}{V_{bulk}} \tag{3.4}$$

Where:

$\emptyset$ = Porosity (%),

PV = Pore volume of the core (cc),

$M_{sat.}$ = Weight of the core saturated with brine (gm),

M_{dry}= Weight of the dry core (gm),

ρ_{brine} = Density of the brine (gm/cc),

V_{bulk}= Bulk volume of the core (cc),

D = Core diameter (cm), and

L = Core length (cm).

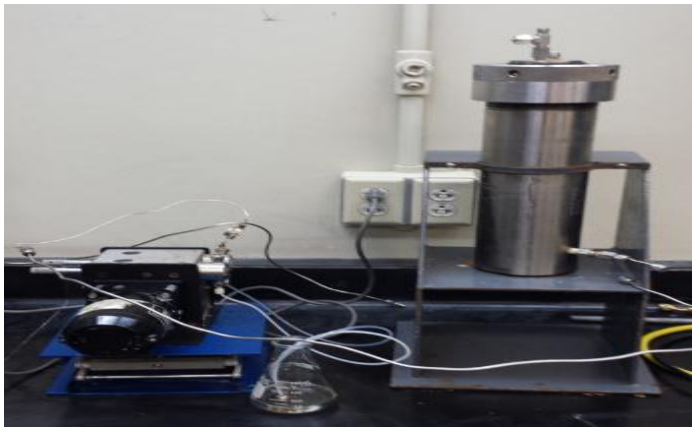

Figure 3.10 Saturation apparatus.

3.5.2 Porosity Measurement Using TPI–219 Teaching Helium Porosimeter

The basic principle behind the measurement is Boyle's law which describes the relationship between the volume of a dry ideal gas and its pressure as $P_1V_1 = P_2 V_2$. This relationship allows us to determine the volume of the grains or the volume of the void space for a rock sample using a pressure chamber. Figure 3.11 shows TPI – 219 Helium Porosimeter (Manual for PETE 204, 2012).

Figure 3.11 TPI–219 Helium Porosimeter.

3.5.3 Gas Permeability Determination Using TKA-209 Gas Permeameter

The TKA-209 (Figure 3.12) utilizes a steady-state flow technique and is operated manually. Measured pressure and flow data from the digital display meters on the front panel are used to calculate permeability after reaching a steady-state flow condition (Manual for PETE 204, 2012). The equation for standard permeability is given as:

$$K_a = \frac{2\mu_a Q_a P_a L}{A(P_1^2 - P_2^2)} * 1000 \quad (3.5)$$

Where:

K_a = Permeability to air (md),

μ_a = Air viscosity at room temperature (cP),

Q_a = Flow rate of gas calculated from meter reading at room conditions (cc/min),

P_a = Atmospheric pressure (atmospheres absolute),

P_1 = Inlet pressure (atmospheres absolute),

P_2 = Outlet pressure (atmospheres), and

L & A = Sample length (cm) and sample area (cm^2).

Figure 3.12 TKA-209 Gas Permeameter.

3.5.4 Carbon Dioxide Sequestration Procedures

A schematic diagram of experimental setup shown in Figure 3.9 was used to achieve the supercritical injection of CO_2. Carbon dioxide sequestration procedures are described below:

- The aging cells are connected by stainless steel tubing. Each cell has an inlet valve and a port connected to pressure gauges outside the oven. The outlet of each cell was permanently closed.
- Each cell was loaded with cleaned and dry core samples and the brine was poured inside the core holder around the core samples.
- After placing the dry cores in their respective cells, the vacuum was applied to the cells through the inlet valve for three hours to ensure complete removal of trapped air in the cores, in the cells, and tubings. Inlet valves were then closed before disconnecting the vacuum pump.
- The cells were placed inside the oven.
- The oven was switched on and the temperature was set to the reservoir temperature of 100 ^{o}C and left for three days.
- CO_2 gas was injected from the CO_2 accumulator into the aging cells and the pressure was increased to 2000 psi.
- The system was left for a period of time to allow CO_2 to soak into the cores.

3.6 Measurement of Mechanical Properties

The mechanical properties of the rock samples were measured on two types of samples.

- Vacuum-dried samples

- Samples that were kept under CO_2 saturation for considerable length of time (14 days, 30 days, and 90 days).

To carry out the measurement of mechanical properties, two types of tests were conducted. Each test involved different type of specimen preparation. These tests are:

- Unconfined compression test
- Indirect tensile strength test

3.6.1 Unconfined Compression Test

The uniaxial or unconfined compressive strength (UCS) test is the most common laboratory test undertaken for rock mechanics studies. The UCS test is the basic test in numerous design methods. It is carried out by using the compression machine 300 kN (Figure 3.13). Applications comprise the following: (i) estimation of the onset of compression or shear failure, (ii) estimating rock modulus for calculation of displacements and settlements, (iii) estimating the Poisson's ratio, and (iv) estimating the triaxial strength. UCS tests were conducted on the samples under dry condition.

3.6.1.1 Sample Preparation

- Take dimensions (length and diameter) of core sample. Record at least 5 readings of length and diameter at five different locations and take the average of them.
- Make sure the sample length-to-diameter ratio is between 2 to 2.5.
- Following the ASTM standards, specimens of 1.5-inch diameter and 3-inch length were prepared.
- Calculate the density of core.

3.6.1.2 Experimental Procedure

- The sample is mounted in a high pressure triaxial cell between the top and bottom steel platens. It is then fitted with two internal 0.1 inch axial linear variable differential transducers (LVDTs) and one 0.25 inch circumferential LVDT.
- The cell is connected to the displacement signal conditioning box via a cable breakout box. At this point, the LVDTs are preset within their working range with the aid of the program screen voltmeter.
- The cell is then positioned on the hydraulic frame ram piston.
- The computer program is used to run the hydraulic ram, raise the piston, and establish sample-load cell contact.
- Axial load is then applied automatically at a predetermined fixed strain rate using the system's program. Axial load, axial stress, average axial strain, and radial strain are automatically recorded and saved in a file.

Figure 3.13 Compression machine 300 kN.

3.6.1.3 Calculation

- Calculate the axial strain, ε_{axial}, for a given applied load as follows:

$$\varepsilon_{axial} = \frac{\Delta L}{L} \tag{3.6}$$

- Calculate the radial strain, ε_{radial}, for a given applied load as follows:

$$\varepsilon_{radial} = \frac{\Delta D}{D} \tag{3.7}$$

Where:

ΔL = The change in the sample length (mm),

L = The initial length of sample (mm),

ΔD = The change in the sample diameter (mm), and

D = The initial diameter of sample (mm).

- Calculate the average cross-section area, A, for the sample (mm^2).
- Calculate the axial stress, σ, for a given applied load, as follows (MPa):

$$\sigma = \frac{P}{A} \tag{3.8}$$

Where:

P = Given applied load (KN).

- Plot the graph of stress-strain data (Figure 3.14).
- Determine unconfined compressive strength (UCS) from the plot (MPa).

- Determine the Young's modulus (E) from the plot (GPa).

$$E = \frac{\Delta\sigma_{axial}}{\Delta\varepsilon_{\text{axial}}} \tag{3.9}$$

- Determine the Poisson's ratio from the plot (υ).

$$\upsilon = -\frac{\Delta\sigma_{axial}/\Delta\varepsilon_{axial}}{\Delta\sigma_{axial}/\Delta\varepsilon_{radial}} \tag{3.10}$$

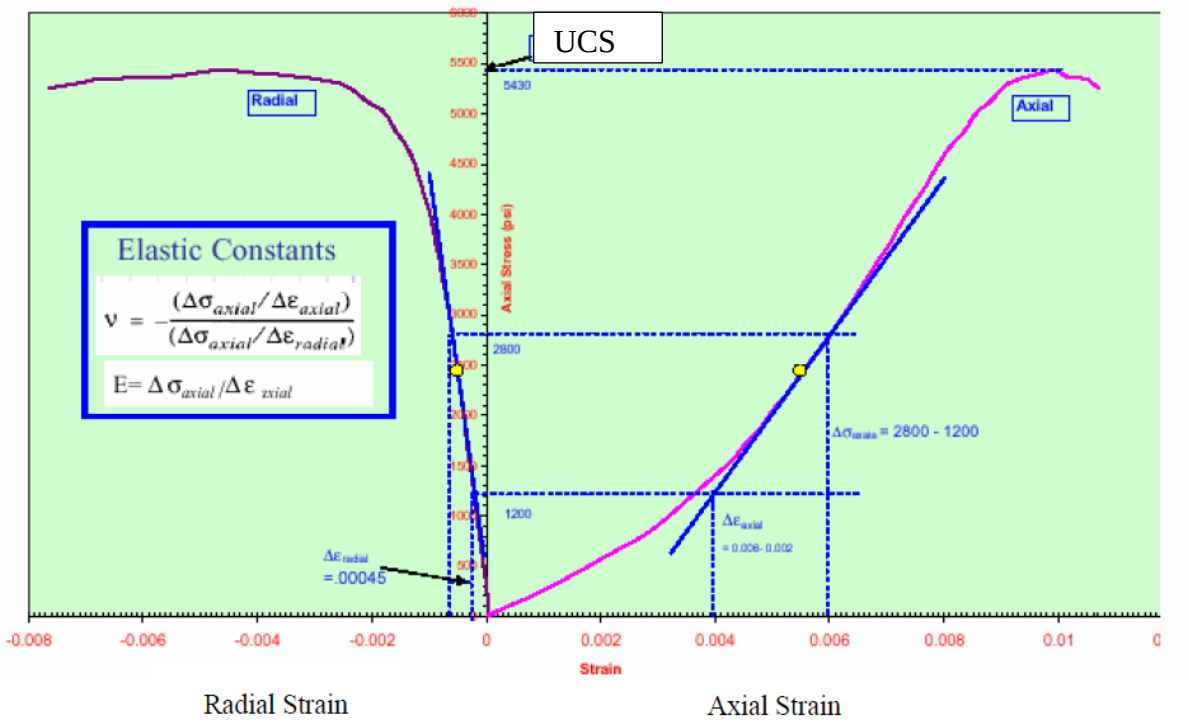

Figure 3.14 Graph of a typical stress-strain relationship.

3.6.2 Indirect Tensile Strength (ITS) Test

ITS test is a conventional and practical test used to estimate the strength of core sample. This test is conducted by Brazilian Disk as shown in Figure 3.15. Tests were conducted on dry samples under normal lab conditions.

Tensile strength of rocks plays an important role especially in the design, initiation, and propagation of fractures.

3.6.2.1 Sample Preparation

- Take dimensions (length and diameter) of core sample. Record at least 5 readings of length and diameter at five different locations and take the average of them.
- Make sure the sample length-to-diameter ratio is between 0.2 to 0.75.
- According to the ASTM standards, specimens of 1.5 inch diameter and 0.75 inch thickness were prepared from the rock cores.
- Calculate the density of core.

3.6.2.2 Experimental Procedure

- Adjust the loading press to apply a deformation rate of 2 inch per minute.
- Carefully put the sample on the lower loading strip.
- Gradually lower top loading strip to establish contact with the core.
- During the testing, ensure the two loading strips remain parallel to each other
- Apply the load to the specimen, without shock, at a controlled deformation rate of 2 inch per minute.
- Record the vertical load at failure of the specimen.

3.6.2.3 Calculation

The indirect tensile strength can be calculated as follows.

$$\mathrm{ITS} = \frac{2000 * \mathrm{P}}{3.14 * \mathrm{L} * \mathrm{d}} \tag{3.11}$$

Where:

ITS = Indirect tensile strength (MPa),

P = Maximum applied load (KN),

L = Average length of the specimen (mm), and

d = Diameter of the specimen (mm).

Figure 3.15 Indirect tensile strength machine.

3.7 Measurement of Wave Velocities

Many experiments were performed to determine the acoustic properties of the rock samples at the simulated field pressure. This task is subdivided into two major types of tests.

- Conduct velocity measurements (compressional velocity, V_p, and shear velocity, V_s) as a function of applied confining pressure on vacuum-dried samples.
- Conduct velocity measurements (compressional velocity, Vp, and shear velocity, Vs) as a function of applied confining pressure for samples after CO_2 sequestration.

The range of confining pressures in the above mentioned experiments is varied from 725 psi to 3,625 psi at suitable increments. The ultrasonic velocity measuring system was used to conduct these measurements.

3.7.1 Ultrasonic Velocity Measuring System

The ultrasonic velocity measuring system measures high quality compressional and shear wave velocities on rock cores as a function of confining pressure and pore fluid pressure. The three main elements of the system are:

- Ultrasonic transducer assembly (Figure 3.16).
- The pressure vessel and pore pressure intensifier contained in a safety enclosure (Figure 3.17).
- Data Acquisition system (Figure 3.18).

The ultrasonic transducer assembly is a matched set of transmitting and receiving transducers capable of propagating a compressional wave (P) and two polarized shear waves (S1 and S2) through a rock specimen. Samples can be tested under dry, saturated, and partially saturated conditions. The center frequency of the transducer is near 700 KHz. The transducers operate at confining pressures of up to 70 MPa. The confining pressure is developed with a hand operated hydraulic pump rated to 70 MPa. The pore pressure is generated with an intensifier rated to 70 MPa. The intensifier is controlled with a manually operated hydraulic pump.

The data acquisition system consists mainly of a microcomputer and an electronic console. The electronic console transmits and receives the compressional waves and two polarized shear waves. The wave data after necessary conversions is stored in the microcomputer.

3.7.2 Sample Preparation

- Take dimensions (length and diameter) of core sample. Record at least 5 readings of length and diameter at five different locations and take the average of them.
- Make sure the sample length is between 2 to 2.5" and the diameter is 1.5" in order to be accommodated in the sample holder.
- Apply couplant on the end faces of the sample in order to fill surface irregularities.
- Place the sample in the rubber sleeve and place it in between the two steel platens of the sample holder.
- Cut two tying wires of approximately 1.5' long. Fold each wire into two half and tighten the two ends of the sample on to the sample holder. Make sure the wires are tightened on the steel platens and not on the sample. This ensures that the confining pressure fluid doesn't enter the sample.

3.7.3 Experimental Procedure

- Remove approximately 180 ml of oil from the test chamber and fill it back into the reservoir through the funnel.
- Make sure all the valves on the front panel are off.
- Make Confining Intensifier (CI) knobs to down position and open Fill/Drain valve. Keep pumping till it gets harder (approximately for 10 mins). Immediately make CI knobs to off position and close Fill/Drain valve.
- Open Relief valve and slowly press the sample inside. Lock the sample by rotating clockwise.
- Connect the transmitter, receiver and thermocouple cables on the sample holder.
- Close Relief valve. Make CI knobs up. Open Vessel On/Off valve. Start pumping in order to reach the required confining pressure (CP). Usually the acoustic

measurements are taken starting at a CP of 5 MPa and then incremented in steps of 5 MPa till 20 MPa.

- Use the AutoLab software to record the acoustic measurements. The procedure is listed in Data Acquisition Section.
- After recording the measurements, remove the cables attached to the sample holder.
- Close the Vessel On/Off valve and open slightly the Relief and Fill/Drain valves to release the pressure. Make the two CI knobs at down position. Keep opening the Relief and Fill/Drain valves further slowly.
- Make the CI knobs to Off position. Turn the sample holder anticlockwise such that it should get relieved from the groove (Unlock).
- Close back Relief and Fill/Drain valves. Open Vessel On/Off valve. Bring CI knobs to Up position. Slightly open Fill/Drain valve.
- Keep pumping (approx. 5 min) so that a confining pressure is applied and the sample holder should come out slowly.
- After the sample holder comes out, gently pull it off and wait for about 20 mins for the oil to be dripped completely.

3.7.4 Data Acquisition

To obtain P & S-wave velocities, carry out the following steps:

- Open the AutoLab software. Click the "Start Data Acquisition" tab. This will open a new window wherein the sample information (density, length and diameter) has to be entered. Other information related to the sample such as sample name, formation name should also be entered in order to identify sample being tested. After entering

sample information click "Done". This will automatically open a window that displays the confining pressure being applied and the temperature of the cell.

- After reaching a confining pressure of 5 MPa, click "Capture" in order to transmit the acoustic waves. Then click "Accept" to record the data. Repeat this for 10, 15, and 20 MPa, respectively.
- Once readings are recorded, Click "Stop Data Acquisition" tab. Then click "Process data" tab in order to select the arrival times of P-and S-waves at different confining pressure.

Figure 3.16 Safety enclosure with pressurization system.

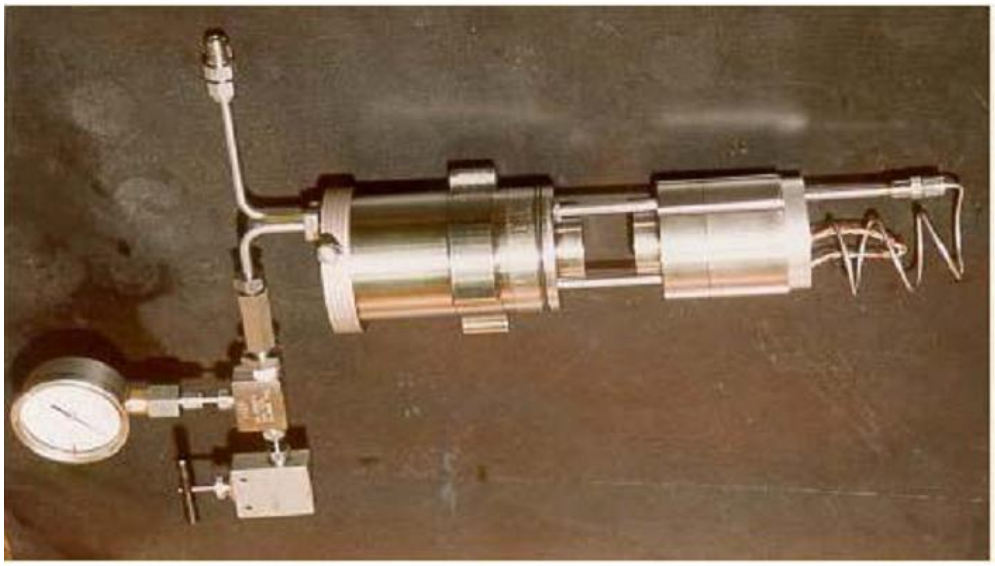

Figure 3.17 Ultrasonic transducer assembly.

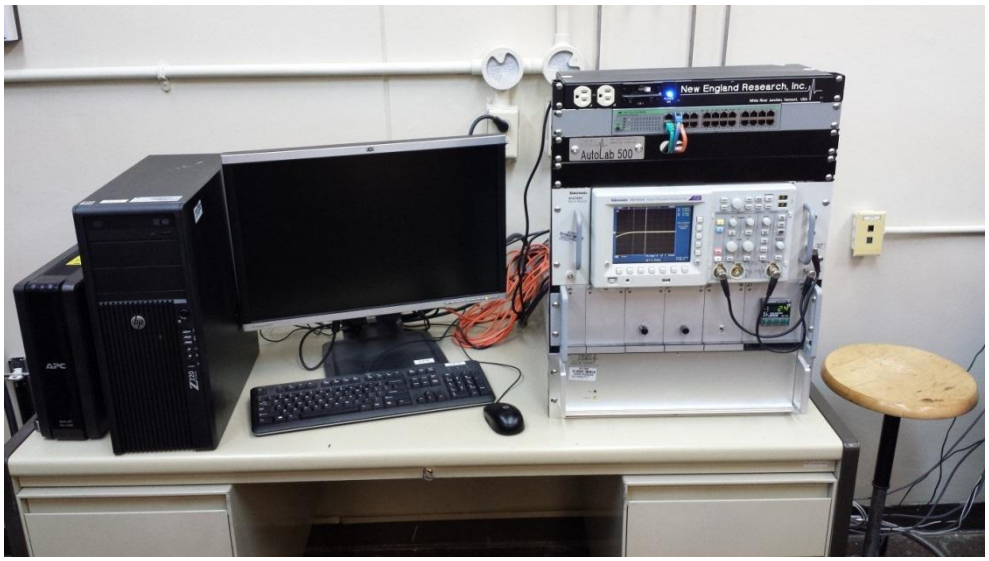

Figure 3.18 Data acquisition system.

3.7.5 Calculation

Compressional and shear wave velocities measured in this test reflect the mechanical properties, especially the Young's modulus and Poisson's ratio. These are given by:

$$E = \rho V_s^2 \frac{3V_p^2 - 4V_s^2}{V_p^2 - V_s^2} \tag{3.12}$$

$$\upsilon = \frac{V_p^2 - 2V_s^2}{2(V_p^2 - V_s^2)} \quad (3.13)$$

Where:

E= Young's modulus (GPa),

υ= Poisson's ratio,

v_p= Compressional wave velocity (m/s),

v_s = Shear wave velocity (m/s), and

ρ = Bulk density of core sample (gm/cc).

CHAPTER 4 PETROGRAPHIC AND PETROPHYSICAL ANALYSIS

4.1 Petrographic Analysis

The main objective of petrographic analysis is to determine the textural and mineralogical composition and classify the carbonate rock types. The petrographic description included thin section petrography, X-Ray Diffraction (XRD) analysis, and Scanning Electron Microscopy (SEM) analysis.

4.1.1 Thin Section Petrography

Due to the homogeneity of the Indiana limestone, Pink Deseret limestone, and Khuff limestone rock samples, three samples were prepared for thin sections, one for each.

4.1.1.1 Indiana Limestone

Peloidal echinoidal grainstone: It is a medium-to coarse-grained, moderately sorted, subrounded bioclasts (grains) including micritized peloids, echinoderms, bivalves, bryozoans, forams, gastropods, interparticle porosities with minor presence of intraparticle and moldic porosities. The pores are reduced by blocky calcite cement and calcite overgrowths. The porosity is 8% and the pore size is 50-600 microns. It is mainly composed of calcite (98%) and quartz (2%).

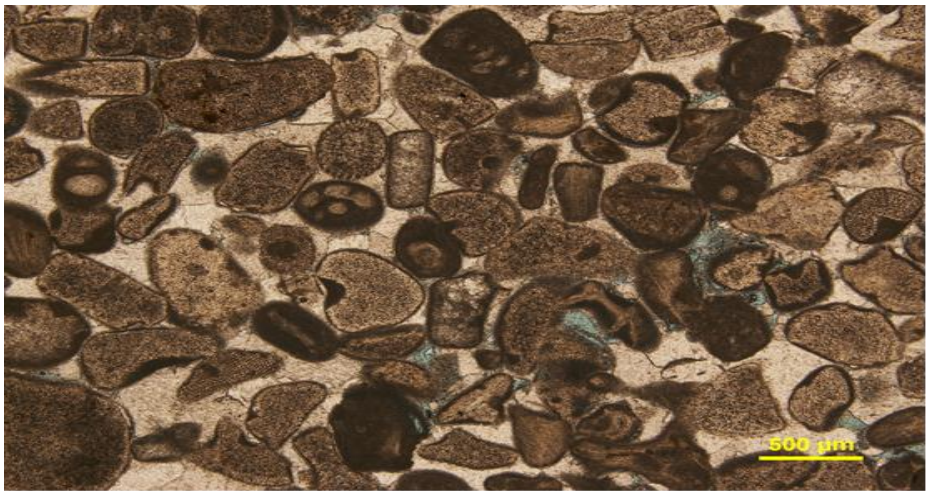

Figure 4.1 Microphotograph for thin section of Indiana limestone. The rock is peloidal echinoidal grainstone.

4.1.1.2 Pink Deseret Limestone

Peloidal echinoderm grainstone: It is a fine-grained, moderately sorted, subrounded bioclasts including micritized peloids, echinoderms, interparticle porosities with minor amounts of moldic and intraparticle porosities. The pores are reduced by syntaxial calcite overgrowths and blocky calcite cement. The porosity is 25%, and the average pore size is 50-300 microns (up to 700 micron pore). It is mainly composed of calcite (95%) and dolomite (5%).

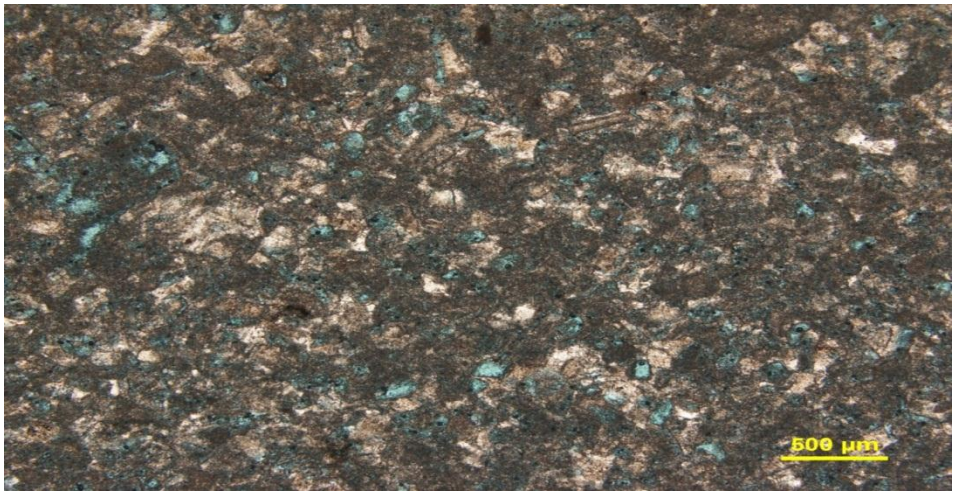

Figure 4.2 Microphotograph for thin section of Pink Deseret limestone. The rock is peloidal echinoderm grainstone.

4.1.1.3 Khuff Limestone

Oolitic grainstone: It is a medium-grained rock, very well sorted, well rounded with oolites, micritized peloids, bivalves bioclasts, Moldic porosity is dominant with blocky calcite cement. The porosity is 15% and the pore size is 50-1000 microns. It is mainly composed of calcite (95%) and dolomite (5%).

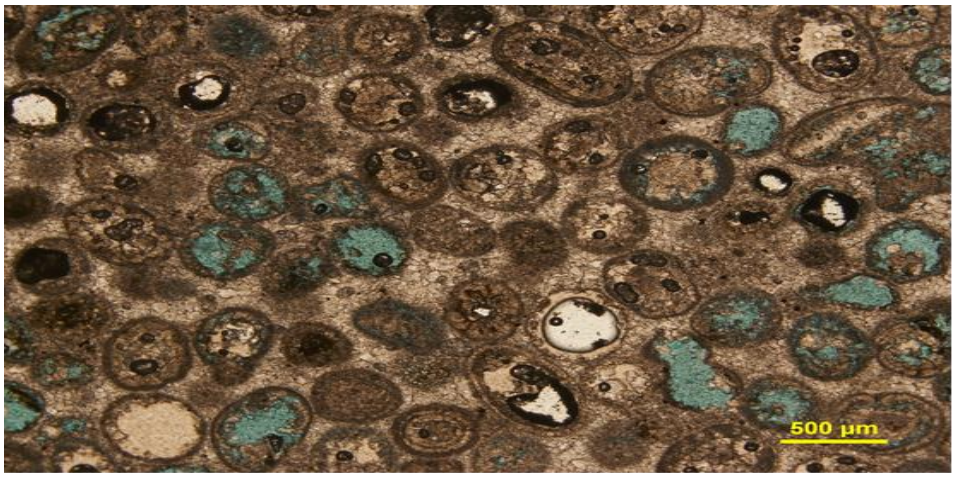

Figure 4.3 Microphotograph for thin section of Khuff limestone. The rock is oolitic grainstone.

4.1.2 X-Ray Diffraction (XRD) Analysis

In addition to thin section analysis, XRD gives the mineral composition of the core samples and determines the percentage of each mineral (quantitative analysis). Table 4.1 shows the quantitative analysis of representative core samples. It can be seen that Indiana limestone, Pink Deseret limestone, and Khuff limestone rock samples are composed of calcite except 1% quartz in Indiana limestone rock sample. These results confirm the result obtained from thin section analysis. Figures 4.4 through 4.9 show the phases for the rock samples before and after CO_2 sequestration. It can be seen from figures that the mineral composition of samples is the same before and after CO_2 storage. XRD results are presented in Appendix C.

Table 4.1 Quantitative analysis of the core samples using XRD.

Sample Name	Phase Name	Content (%)
Indiana Limestone	Calcite	99
	Quartz	1
Pink Desert Limestone	Calcite	100
	Quartz	0
Khuff Limestone	Calcite	100
	Quartz	0

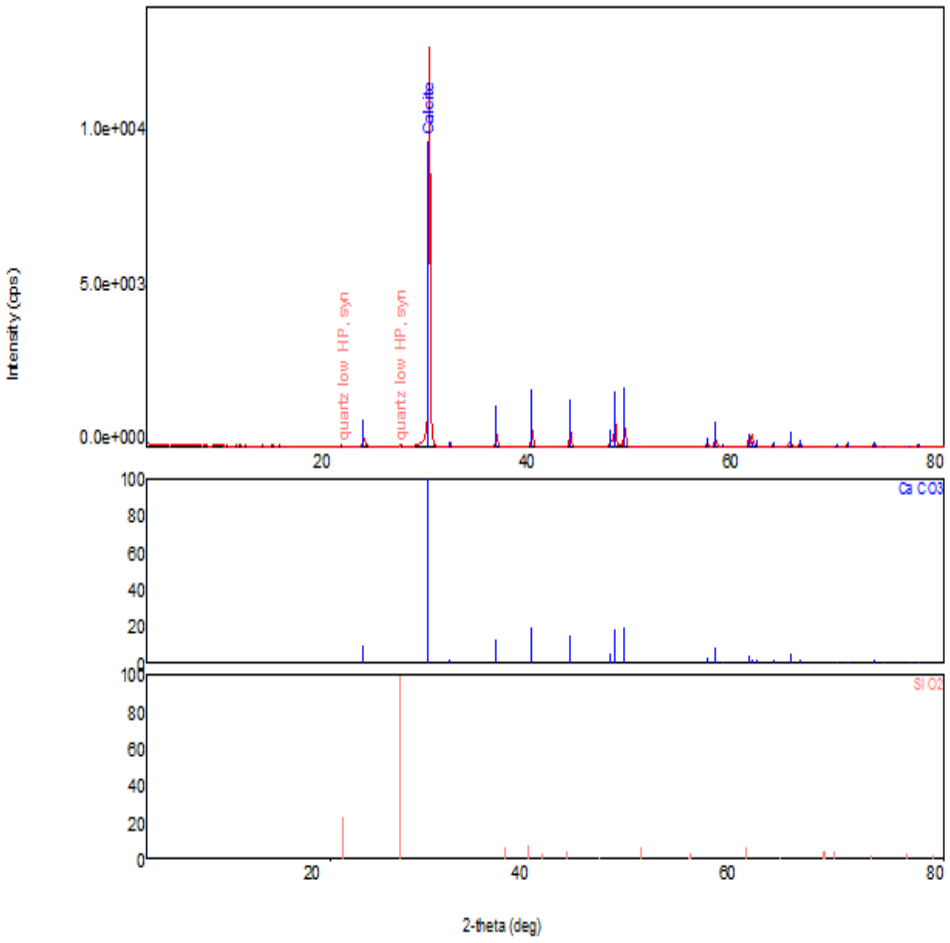

Figure 4.4 The phase identification for Indiana limestone sample before CO_2 sequestration using XRD.

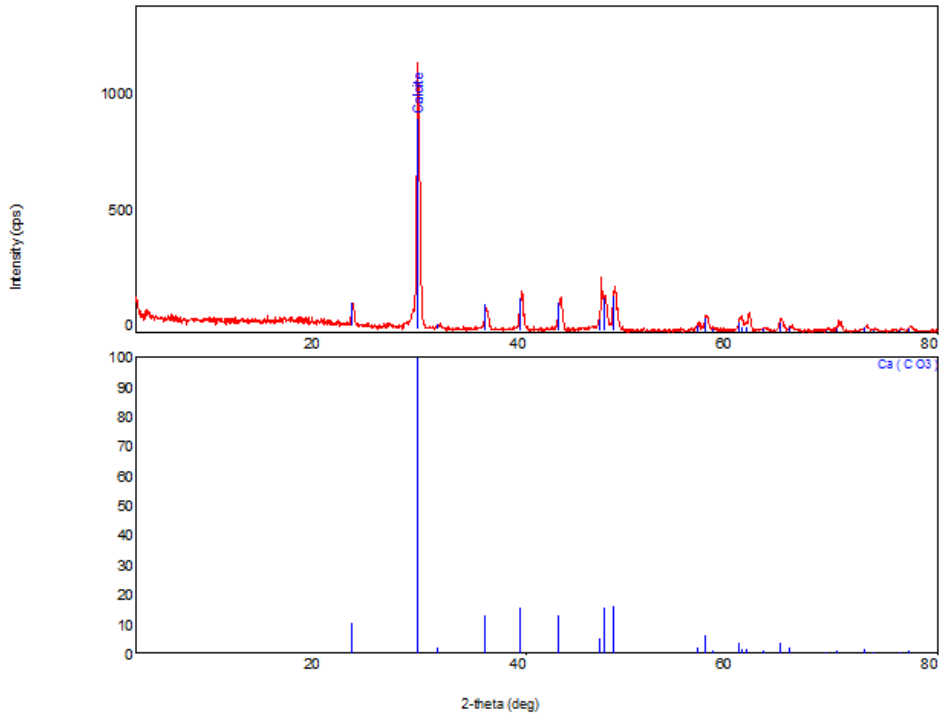

Figure 4.5 The phase identification for Indiana limestone sample after CO_2 sequestration using XRD.

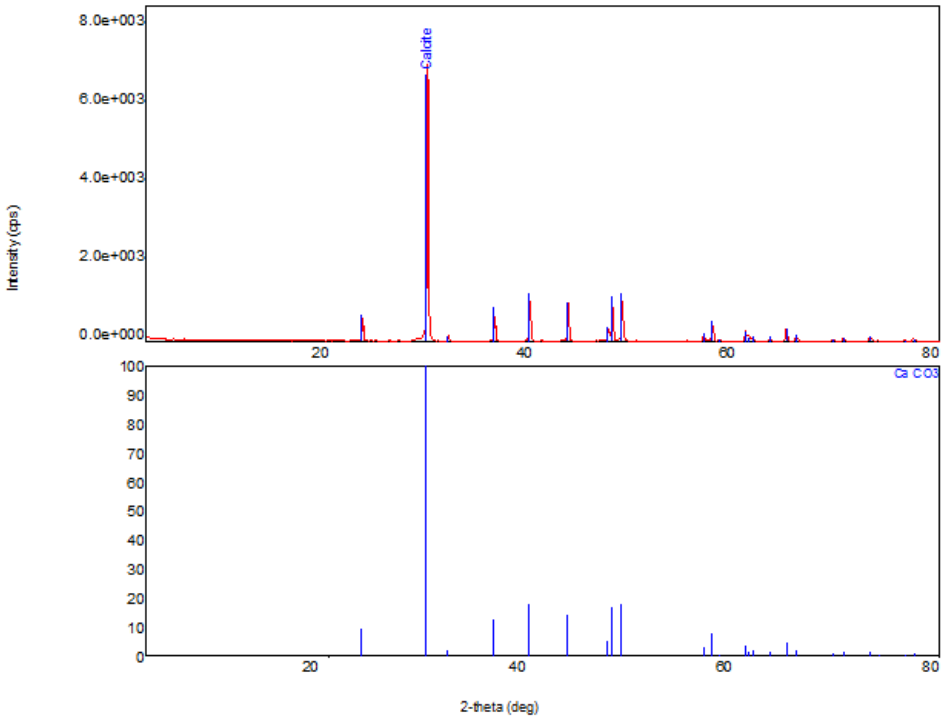

Figure 4.6 The phase identification for Pink Desert limestone sample before CO_2 sequestration using XRD.

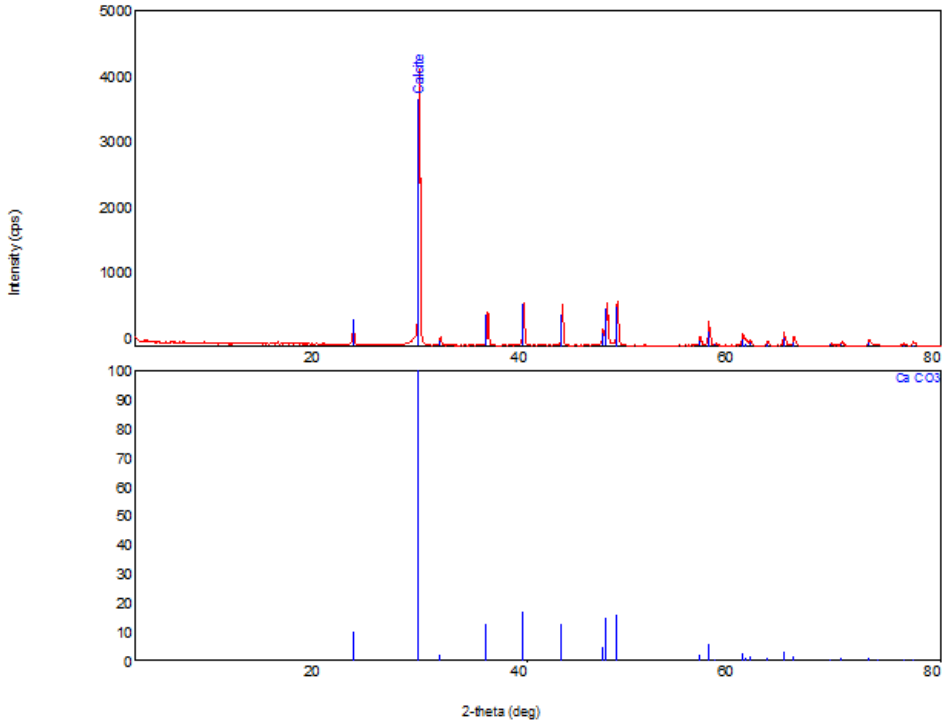

Figure 4.7 The phase identification for Pink Desert limestone sample after CO_2 sequestration using XRD.

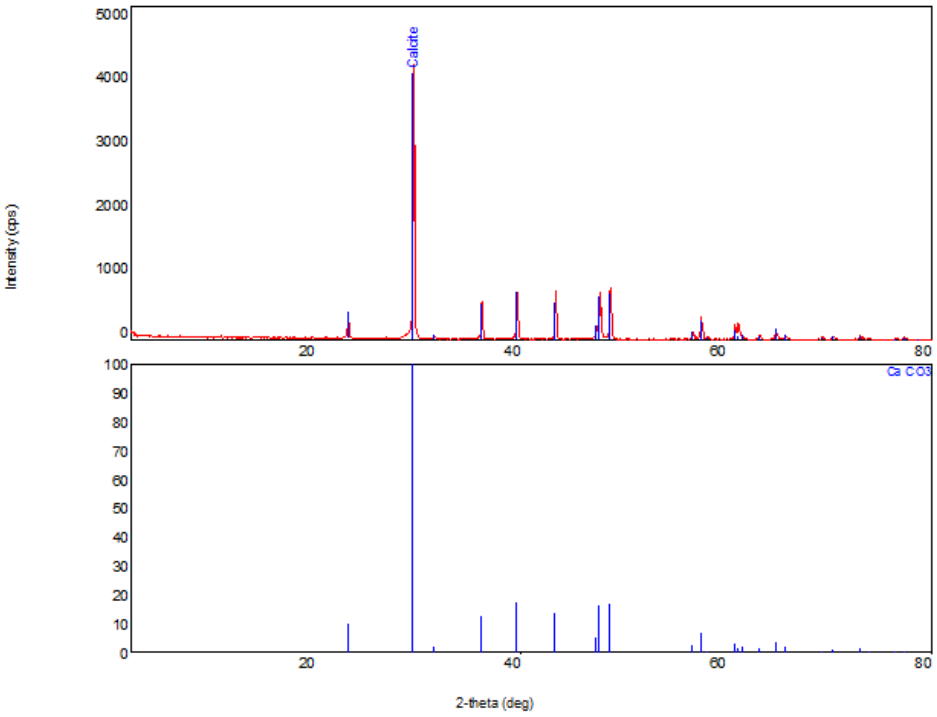

Figure 4.8 The phase identification for Khuff limestone sample before CO_2 sequestration using XRD.

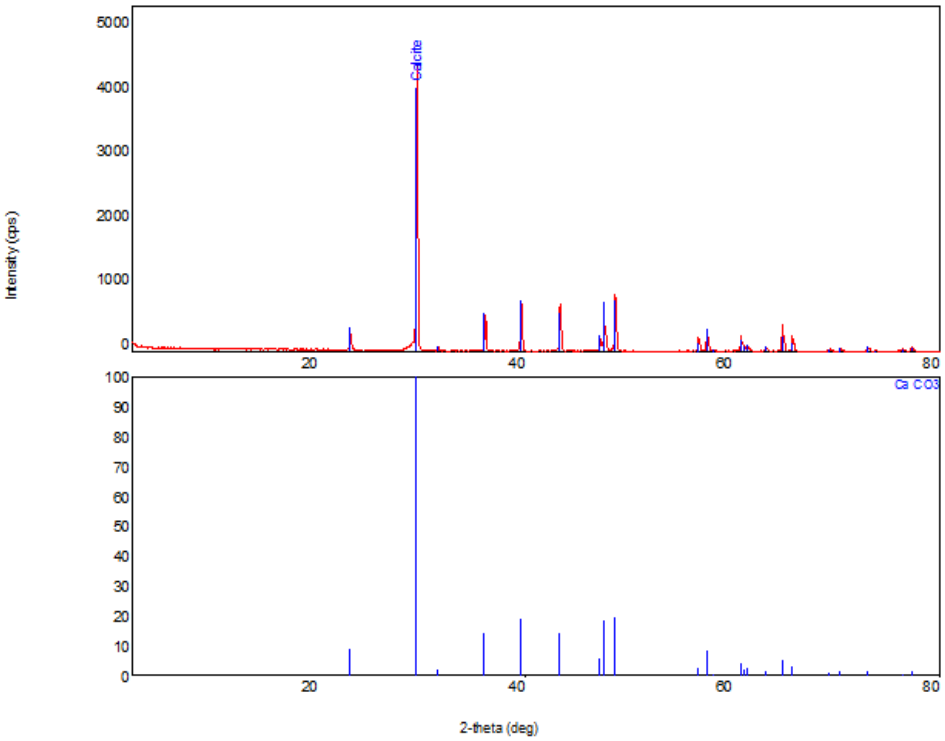

Figure 4.9 The phase identification for Khuff limestone sample after CO_2 sequestration using XRD.

4.1.3 Scanning Electron Microscopy (SEM) Analysis

The main contribution of SEM to this work is to examine the rock texture, pore space and delicate pore fillings. Apart from the SEM studies, EDS was also be used in order to have better understanding about the chemical composition of particular grains observed in the SEM. Table 4.2 shows the chemical compositions of representative core samples. It can be seen that Indiana limestone, Pink Deseret limestone, and Khuff limestone rock samples are mainly composed of three elements, oxygen (O), calcium (Ca), and carbon (C). Figures 4.10 through 4.27 show the images by using SEM for Pink Deseret limestone and Khuff limestone rock samples before and after CO_2 sequestration. Spectrums for rock samples are shown in Figures 4.28 through 4.32.

Table 4.2 Chemical compositions for different core samples using SEM.

Sample Name	Elements Weight (%)			
	O	Ca	C	Al
Indiana Limestone	31	54.6	14	0.4
Pink Deseret Limestone	21.8	64.9	13.3	
Khuff Limestone	28.4	50.5	21.1	

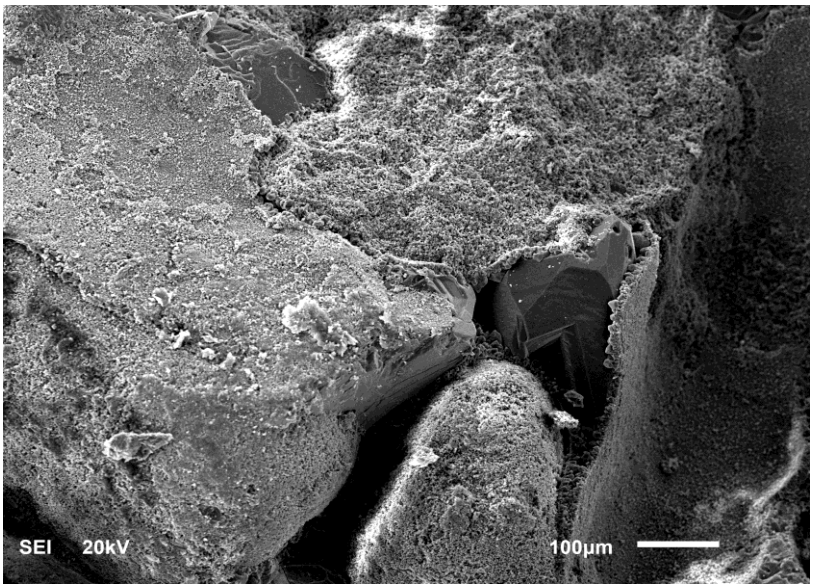

Figure 4.10 SEM microphotograph for Indiana limestone sample before CO_2 sequestration.

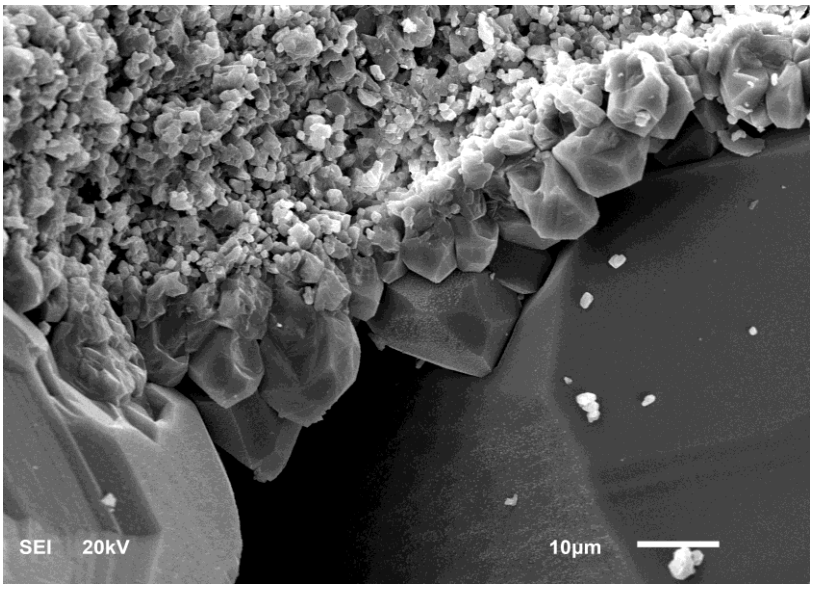

Figure 4.11 SEM microphotograph for Indiana limestone sample before CO_2 sequestration.

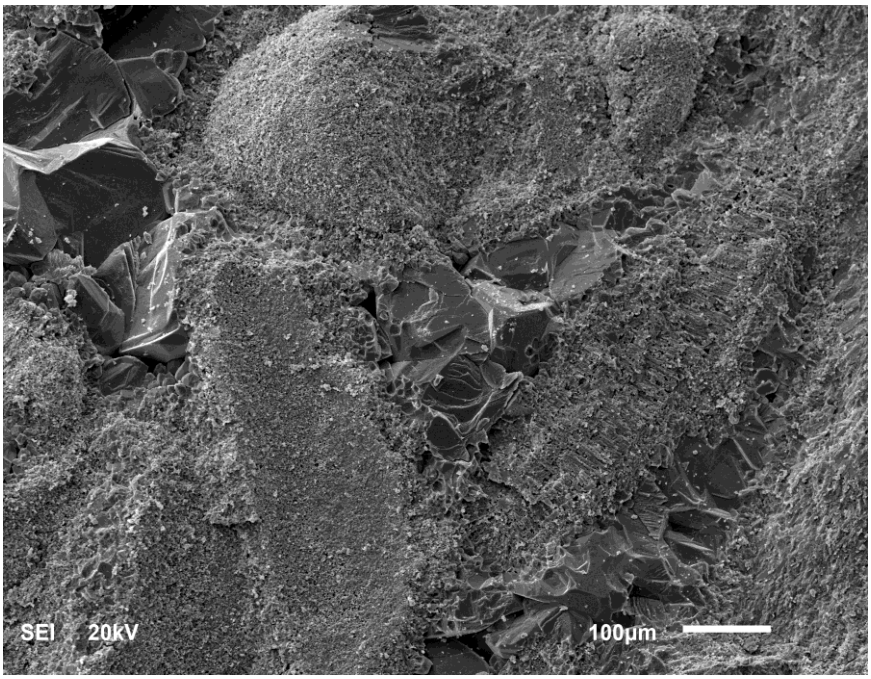

Figure 4.12 SEM microphotograph for Indiana limestone sample after CO_2 sequestration.

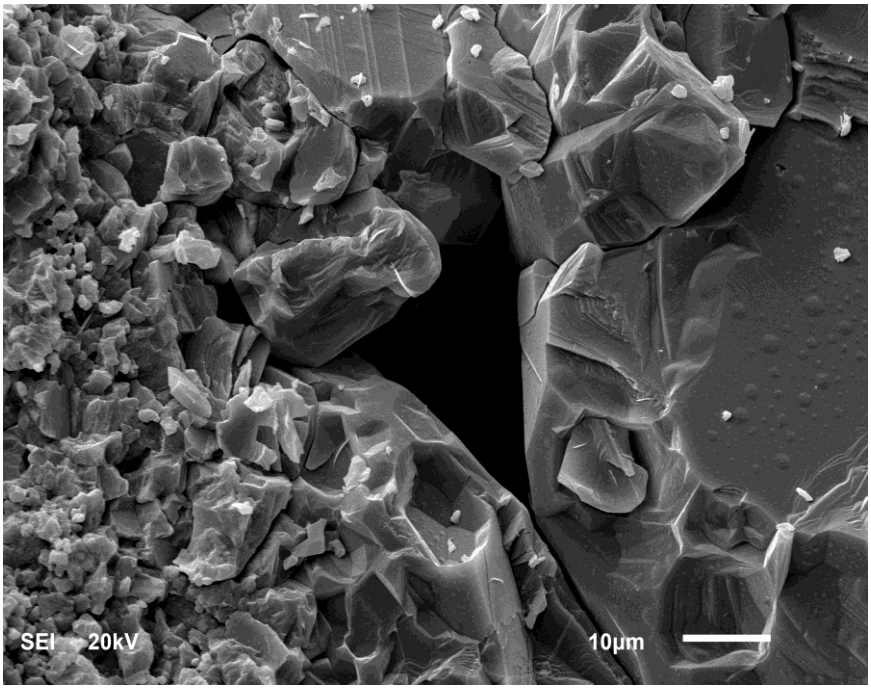

Figure 4.13 SEM microphotograph for Indiana limestone sample after CO_2 sequestration.

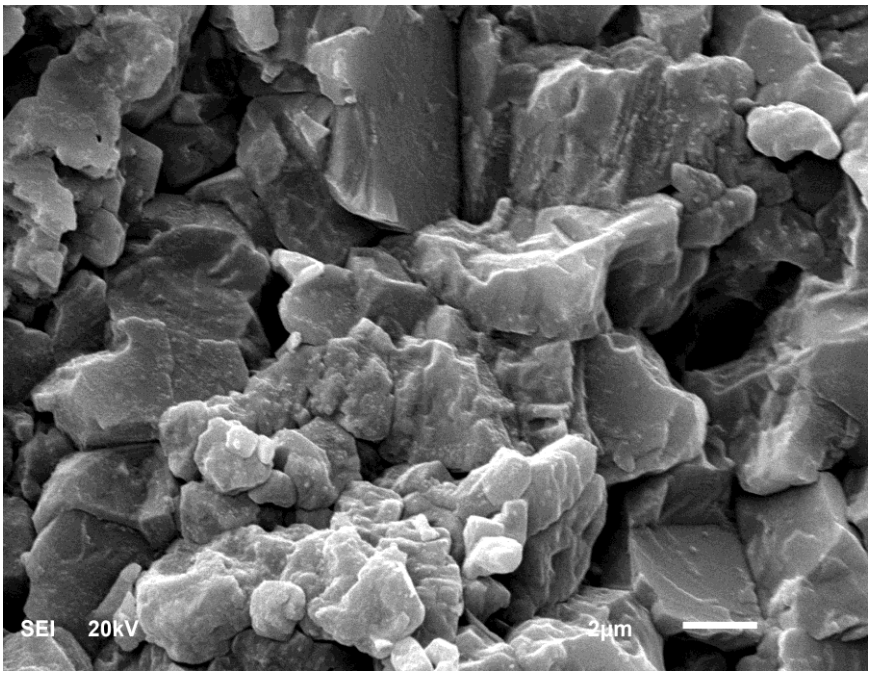

Figure 4.14 SEM microphotograph for Indiana limestone sample after CO_2 sequestration.

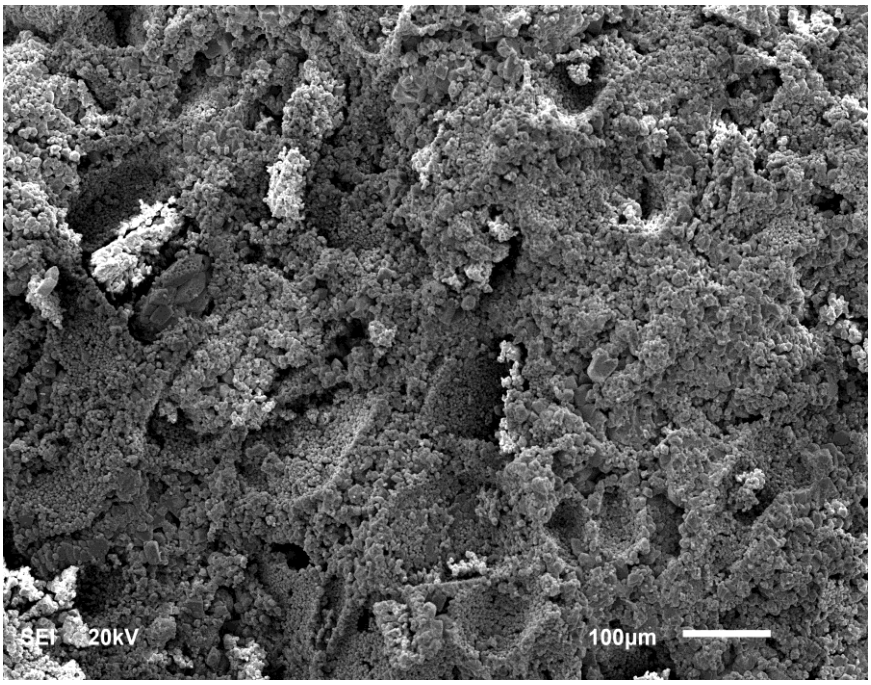

Figure 4.15 SEM microphotograph for Pink Desert limestone sample before CO_2 sequestration.

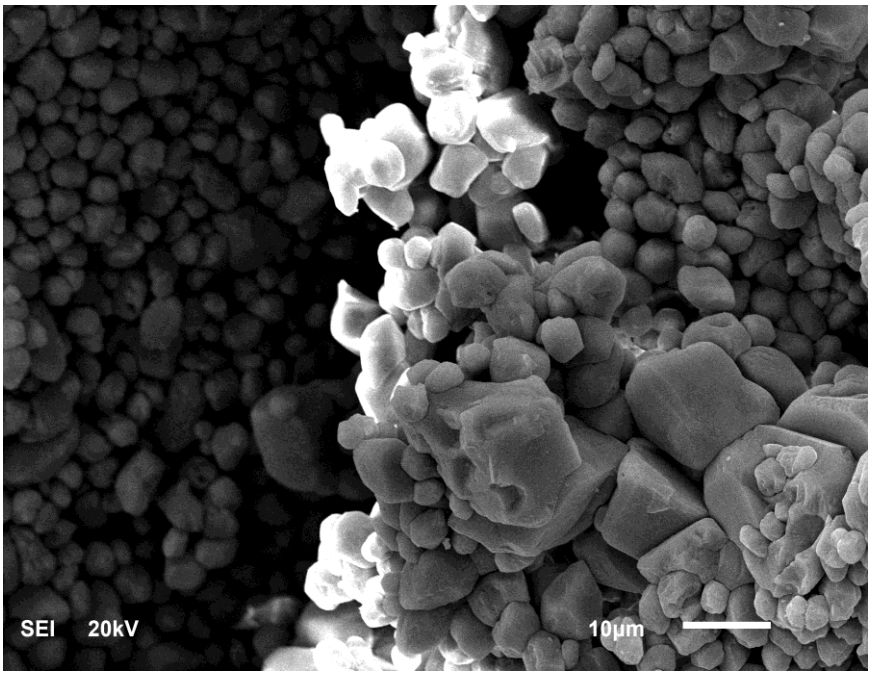

Figure 4.16 SEM microphotograph for Pink Desert limestone sample before CO_2 sequestration.

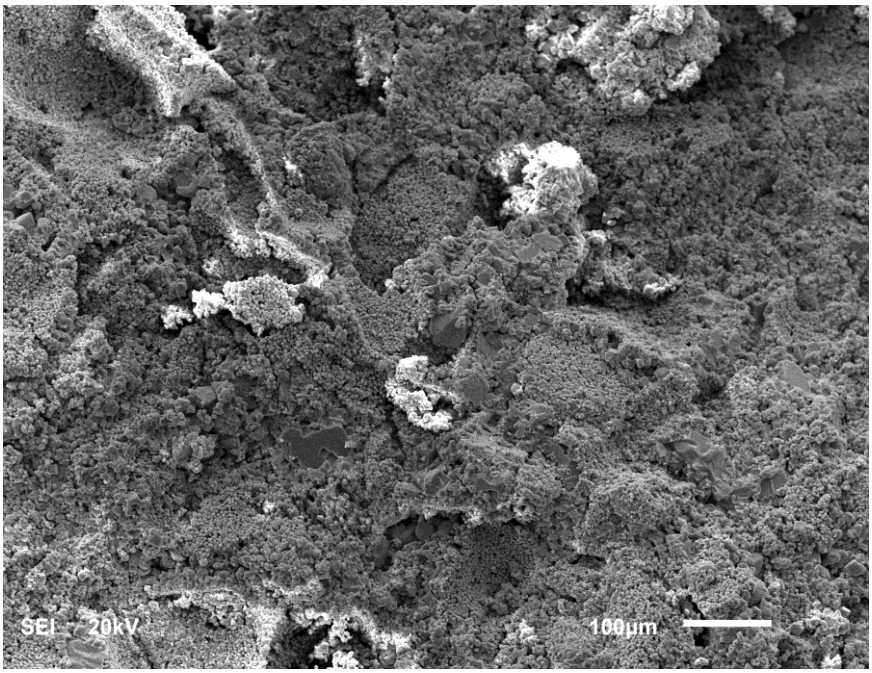

Figure 4.17 SEM microphotograph for Pink Desert limestone sample after CO_2 sequestration.

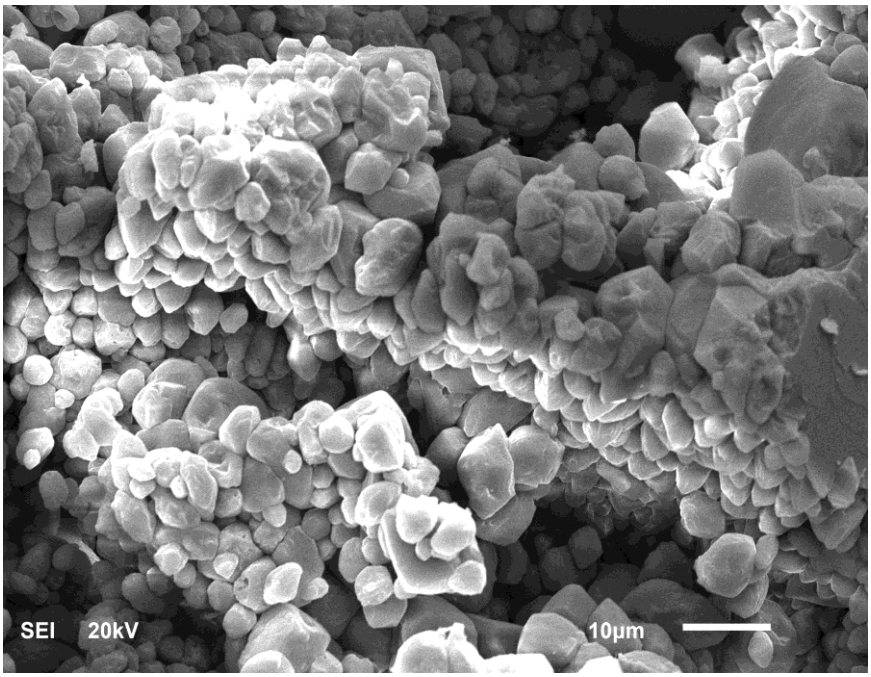

Figure 4.18 SEM microphotograph for Pink Desert limestone sample after CO_2 sequestration.

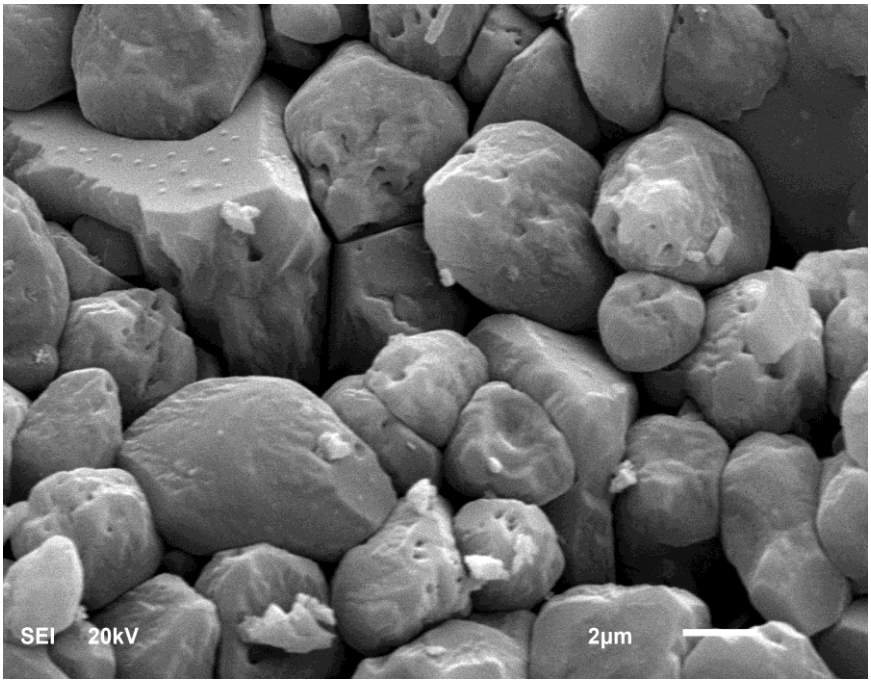

Figure 4.19 SEM microphotograph for Pink Desert limestone sample after CO_2 sequestration.

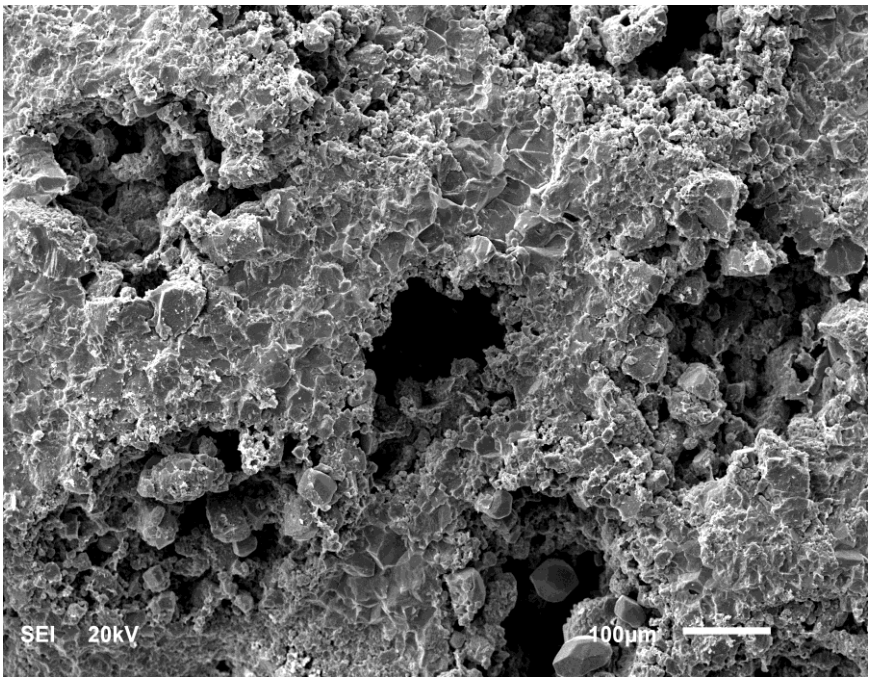

Figure 4.20 SEM microphotograph for Khuff limestone sample before CO_2 sequestration.

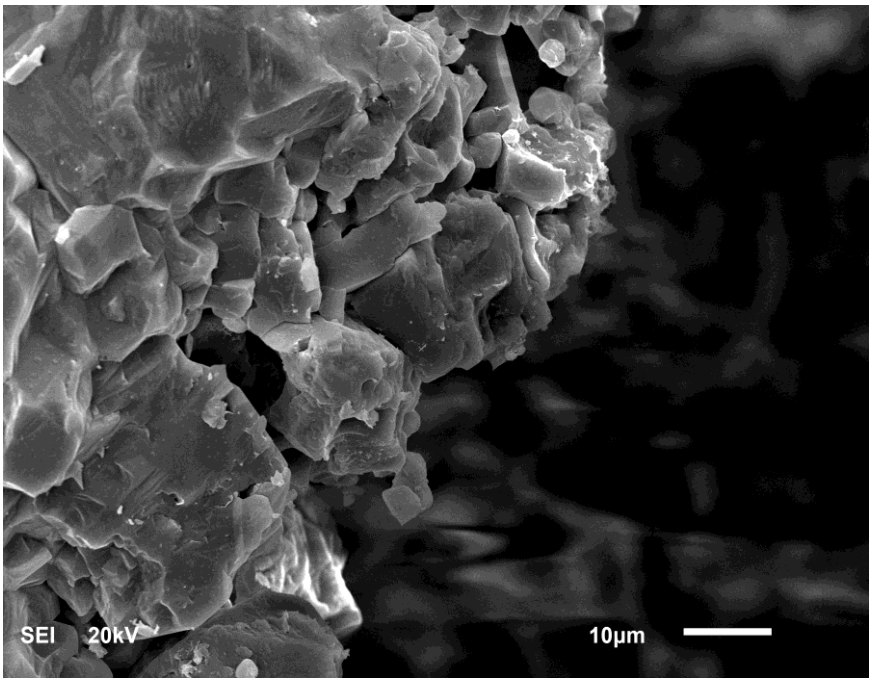

Figure 4.21 SEM microphotograph for Khuff limestone sample before CO_2 sequestration.

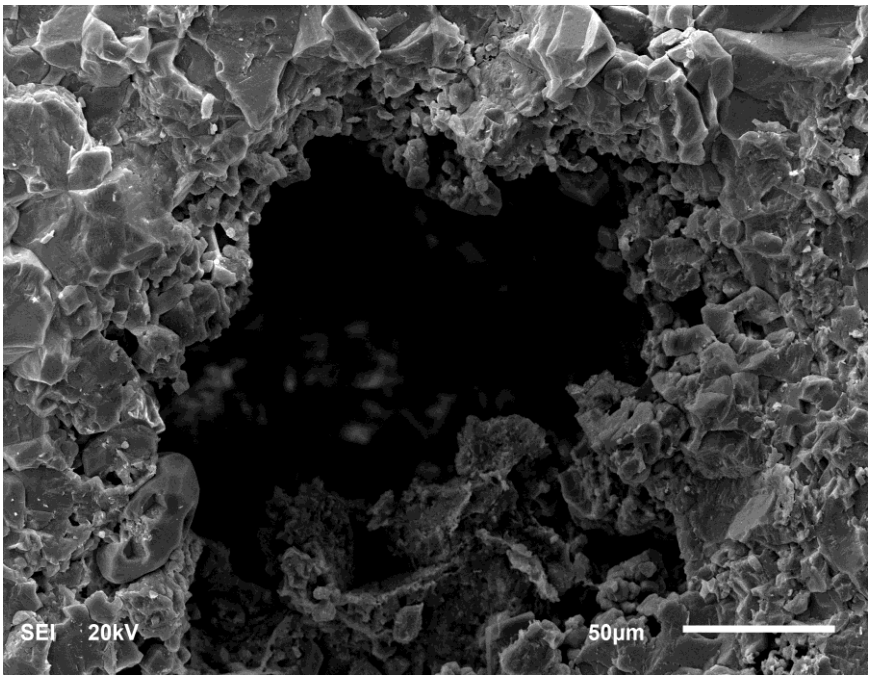

Figure 4.22 SEM microphotograph for Khuff limestone sample before CO_2 sequestration.

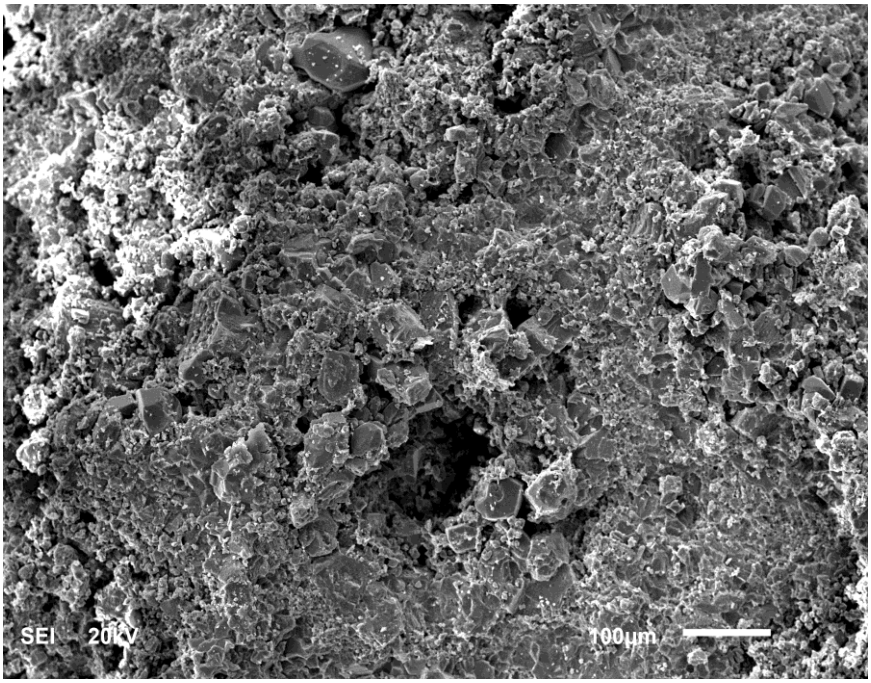

Figure 4.23 SEM microphotograph for Khuff limestone sample after CO_2 sequestration.

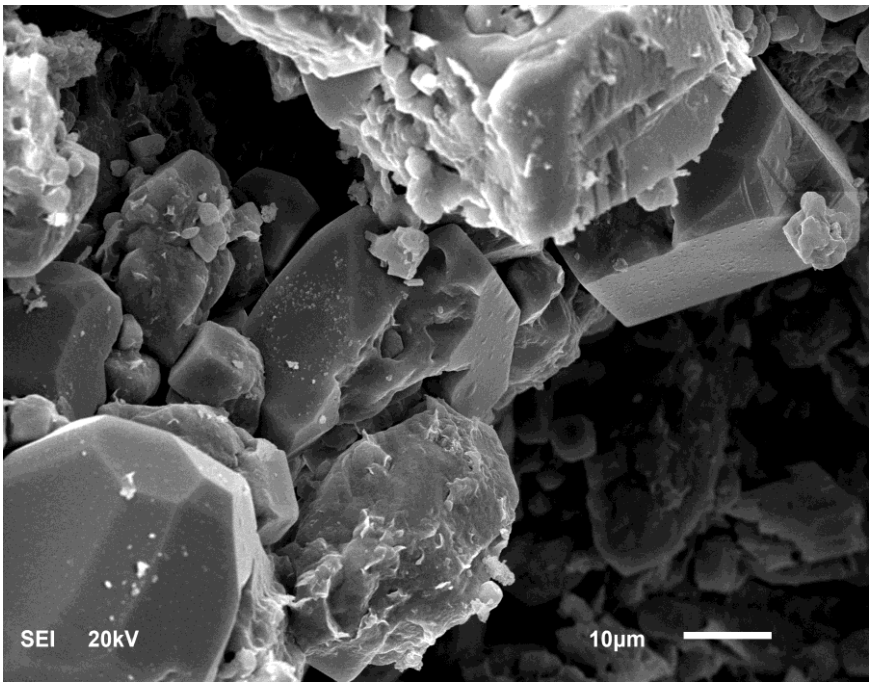

Figure 4.24 SEM microphotograph for Khuff limestone sample after CO_2 sequestration.

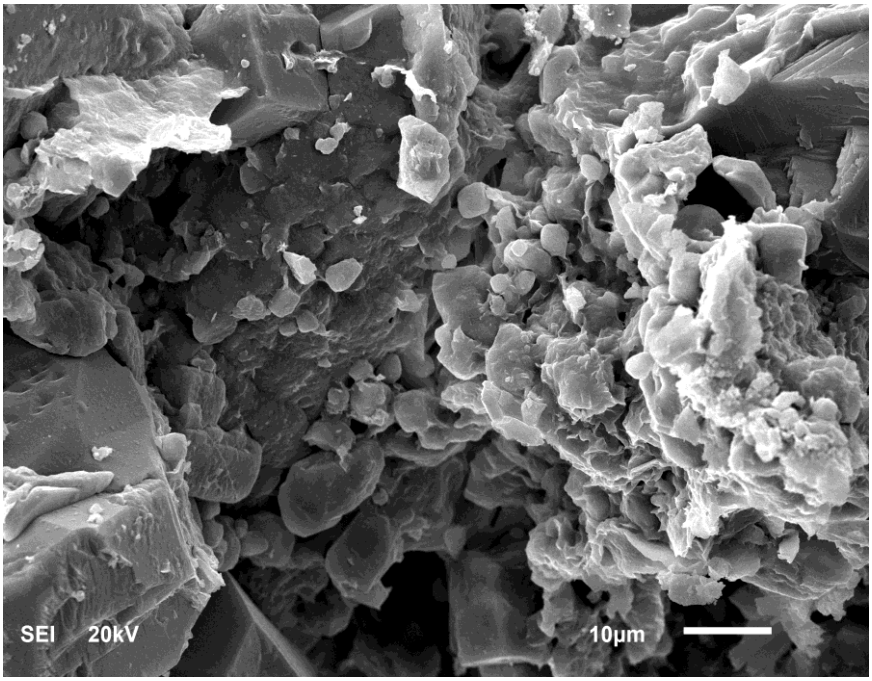

Figure 4.25 SEM microphotograph for Khuff limestone sample after CO_2 sequestration.

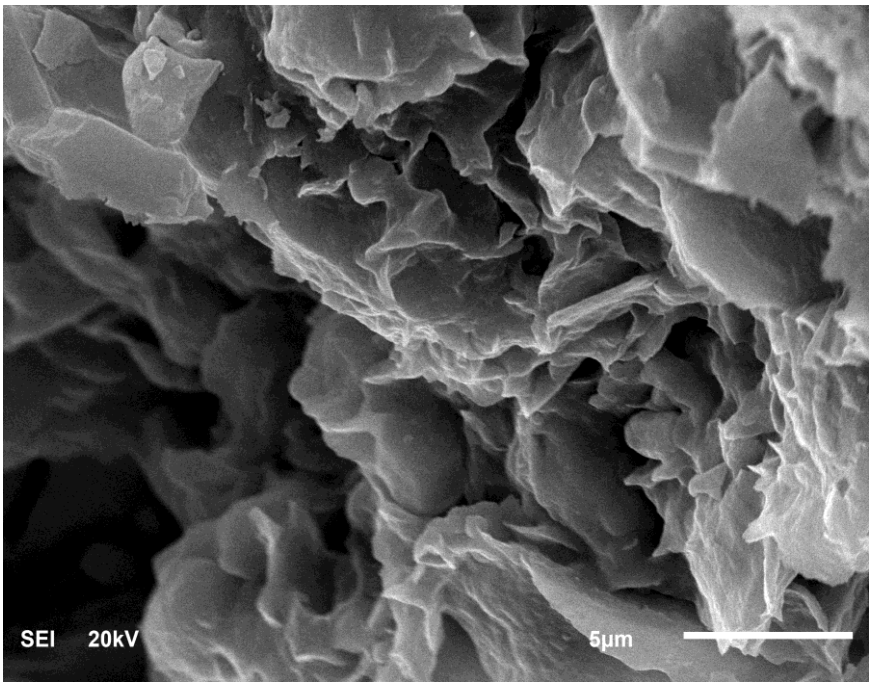

Figure 4.26 SEM microphotograph for Khuff limestone sample after CO_2 sequestration.

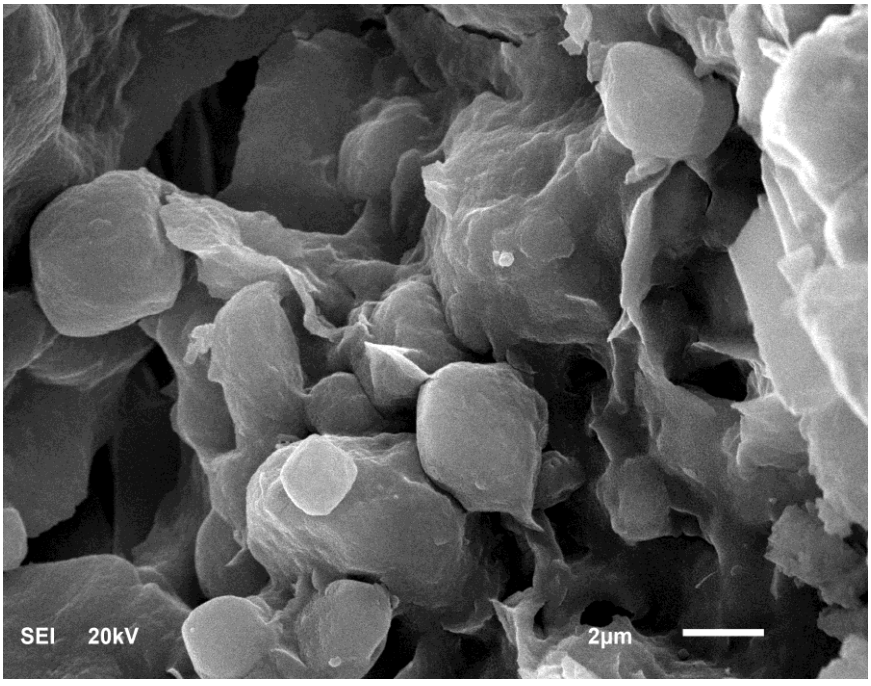

Figure 4.27 SEM microphotograph for Khuff limestone sample after CO_2 sequestration.

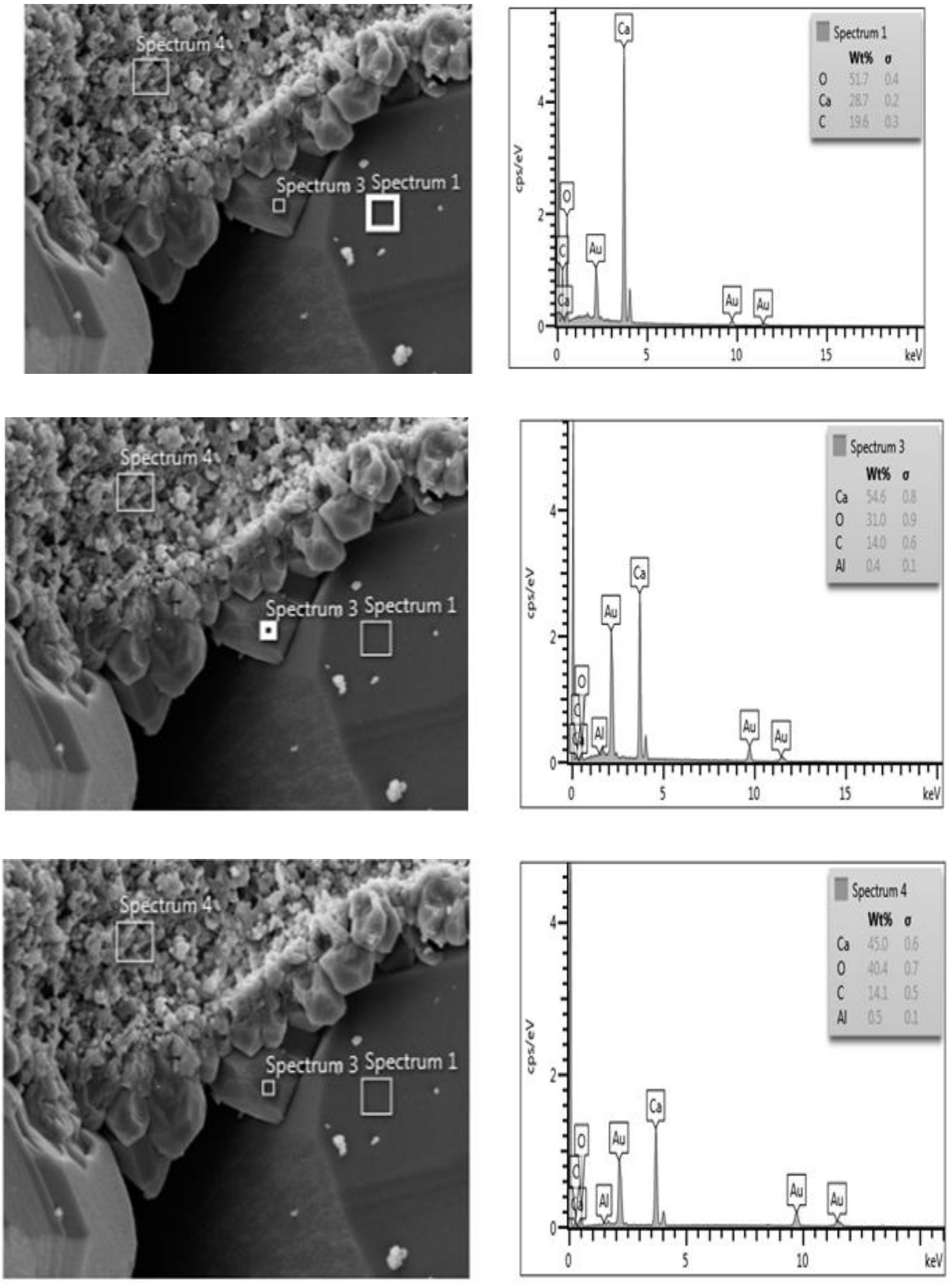

Figure 4.28 Three different locations (spectrums 1, 3, and 4) for Indiana limestone sample before CO_2 sequestration.

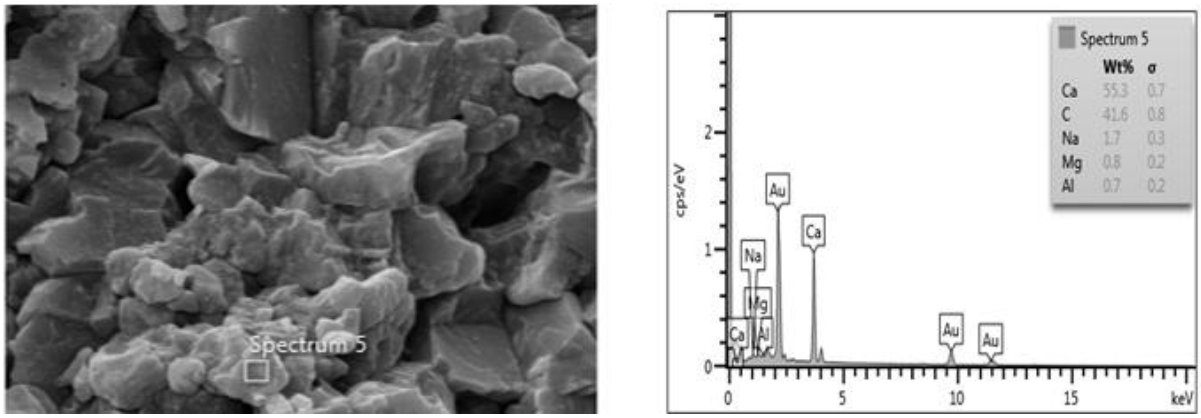

Figure 4.29 One location (spectrum 5) for Indiana limestone sample after CO_2 sequestration.

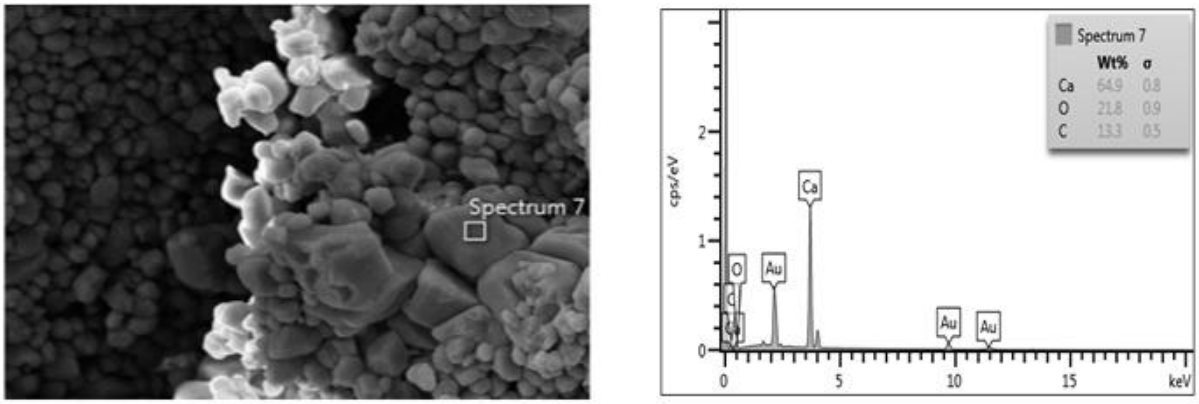

Figure 4.30 One location (spectrum 7) for Pink Desert limestone sample before CO_2 sequestration.

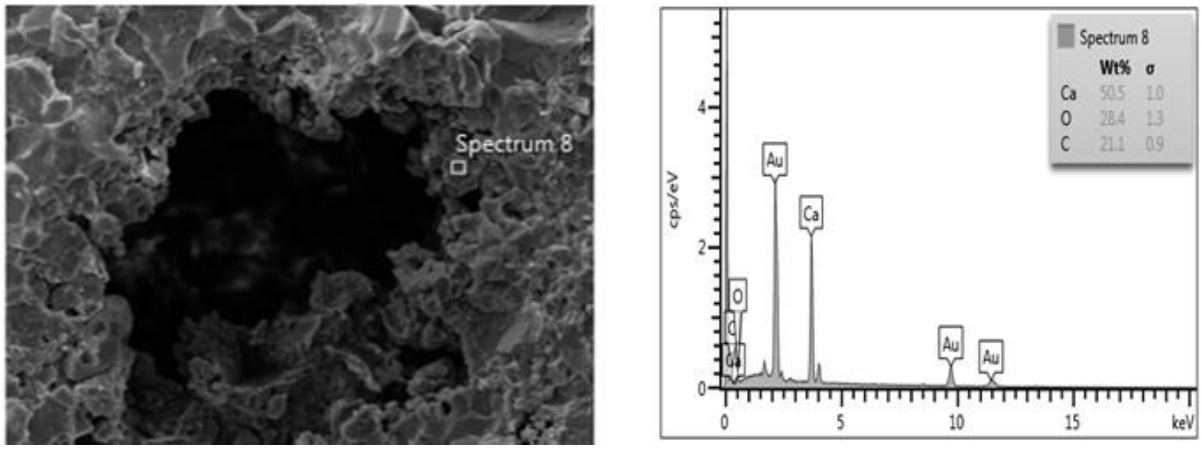

Figure 4.31 One location (spectrum 8) for Khuff limestone sample before CO_2 sequestration.

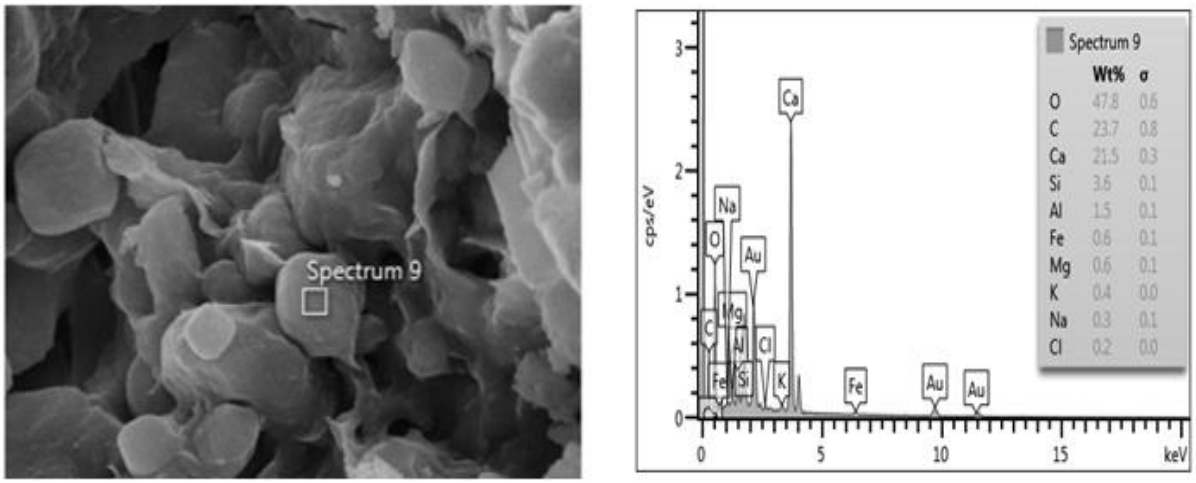

Figure 4.32 One location (spectrum 9) for Khuff limestone sample after CO_2 sequestration.

4.2 Petrophysical Analysis

The main objective of the petrophysical analysis is to determine the porosity and permeability of the core samples before soaking with CO_2 to confirm the homogeneity of the samples.

4.2.1 Porosity and Permeability Measurements

Brine porosity was determined for Indiana limestone (IL), Pink Deseret limestone (PL), and Khuff limestone (KL), and cap rock shale (SH) samples. Basic properties of these samples are given in Table 4.3. Moreover, porosity by using helium gas-expansion and liquid permeability from gas permeability and verification of Klinkenberg effect by using TKA-209 Permeameter was measured for six samples from Pink Deseret limestone rocks to address the impact of CO_2 sequestration on petrophysical properties as shown in Table 4.4.

Table 4.3 Basic core properties.

Sample ID	Length (cm)	Dia (cm)	Bulk Vol. (cc)	Brine Porosity (%)
IL-10-2	5.115	3.748	56.429	6.721
PL-S-1-A	5.274	3.795	59.639	26.067
PL-S-1-B	5.167	3.795	58.433	26.842
PL-S-2-A	5.152	3.790	58.127	27.792
PL-S-3-A	5.139	3.788	57.912	26.127
PL-S-3-B	5.173	3.788	58.251	28.745
KL-S-1-A	5.148	3.799	58.346	15
SH-4-81	5.226	3.735	57.266	0.83
SH-4-95	5.343	3.728	58.336	1.11
IL-15-2	7.691	3.742	84.569	7.324
IL-15-3	7.653	3.748	84.437	7.194
PL-U-1-A	7.768	3.793	87.797	26.022
PL-U-2-A	7.665	3.793	86.605	25.68
PL-U-3-B	7.8	3.793	88.156	26.652
PL-T-1-A	2.058	3.786	23.712	26.740
PL-T-1-B	2.057	3.788	23.179	26.332
PL-T-2-A	2.096	3.788	23.626	26.634
PL-T-3-C	1.927	3.79	22	26.005

Table 4.4 Liquid permeability and gas porosity of specimens.

Sample ID	L (cm)	D (cm)	Bulk Vol. (cc)	Gas Porosity (%)	Liquid Permeability(md)
PL-K-1	2.605	3.786	29.327	29.326	19.1168
PL-K-2	2.631	3.79	29.69	29.682	15.144
PL-K-3	2.585	3.785	29.082	29.086	20.4233
PL-K-4	2.602	3.786	29.29	29.293	17.9973
PL-K-5	2.564	3.788	29.896	28.895	18.0569
PL-K-6	2.57	3.786	29.934	28.932	16.2066

4.2.2 Nuclear Magnetic Resonance (NMR)

Three experiments were conducted to measure the porosity of Pink Desert limestone samples by using NMR before CO_2 storage as presented in Table 4.5.

Table 4.5 Porosity values by using NMR.

Sample No	Porosity Before Sequestration (%)
DL-S-1-A	23.85
DL-S-2-B	24.25
DL-S-3-B	26.08

CHAPTER 5 RESULTS AND DISCUSSION

5.1 Introduction

Experimental work was carried out to investigate the impact of CO_2 sequestration on the petrophysical and mechanical properties of formation rocks exposed to long time periods of CO_2 sequestration. Petrophysical and mechanical measurements were taken on Indiana limestone, Pink Desert limestone, Khuff limestone, and cap rock shale samples.

5.2 Effect of CO_2 Sequestration on Petrophysical Properties

Gas porosity and liquid permeability were measured for six samples from the selected Pink Desert limestone (PL) block to study the effect of CO_2 sequestration on petrophysical properties. From the measurements, it is found that the grain density ranges from 2.81 to 2.82 g/cm^3 indicating the same mineralogy for the same block. The samples are PL-K-1, PL-K-2, PL-K-3, PL-K-4, PL-K-5, and PL-K-6 , and they were soaked with CO_2 for 7 days, 14 days, 30 days, 60 days, 90 days, and 120 days, respectively. Table 5.1 shows the gas porosity and liquid permeability before and after CO_2 sequestration. The results showed that after CO_2 exposure for 7 days, there is a slight increase in the porosity value from 30.623 to 30.957%. On the other hand, there is a medium increase in the permeability value from 19.116 to 23.575 md. The change in the porosity and permeability results from the two interdependent and competing processes: the calcite dissolution (Equation 5.3) and the resulting mechanical compaction due to pressure.

However, after the soaking with CO_2 from 14 days to 90 days, the porosity and permeability diminished. This was due to the precipitation of interaction products, mostly calcium carbonate (Equation 5.4). After120 days, the porosity increased from 30.215 to 30.913%,

and the permeability increased from 18.057 to 25.378 md. These results explain the difficulty of understanding the processes of dissolution and precipitation.

$$CO_2 + H_2O \leftrightarrow H_2CO_3 \quad (5.1)$$

$$H_2CO_{3\,(aq)} \leftrightarrow H^+_{(aq)} + HCO^-_{3\,(aq)} \quad (5.2)$$

$$CaCO_3 + H^+ \leftrightarrow Ca^{2}_{(aq)} + CO^-_{2\,(aq)} + H_2O \quad (5.3)$$

$$Ca^{2}_{(aq)} + HCO^-_{3\,(aq)} \leftrightarrow H^+_{(aq)} + CaCO_{3\,(s)} \quad (5.4)$$

Table 5.1 Gas porosity and liquid permeability before and after CO_2 sequestration for different time periods.

Sample ID	Time (days)	Gas Porosity Before Sequestration (%)	Gas Porosity After Sequestration (%)	Liquid Permeability Before Sequestration (md)	Liquid Permeability After Sequestration (md)
PL-K-1	7	30.623	30.957	19.1168	23.5754
PL-K-2	14	28.329	27.816	15.144	13.9685
PL-K-3	30	31.644	31.239	20.4233	19.2837
PL-K-4	60	31.024	29.592	20.0378	18.5838
PL-K-5	90	29.096	28.079	16.2066	15.0127
PL-K-6	120	30.215	30.913	18.0569	25.3782

Also, porosity was measured for three Pink Desert limestone samples by using NMR as shown in Table 5.2. The samples are PL-S-1-A, PL-S-2-B, and PL-S-3-B, and they were subjected to CO_2 for different time periods, namely, 14 days, 30 days, and 90 days, respectively. The results showed that the values of porosity decreased slightly after CO_2 sequestration due to the precipitation of calcite.

Table 5.2 Porosity by using NMR before and after CO_2 sequestration.

Sample No	Porosity Before Sequestration (%)	Porosity After Sequestration (%)
PL-S-1-A	23.85	23.4
PL-S-2-B	24.25	23.9
PL-S-3-B	26.08	25.8

5.3 Effect of CO_2 Sequestration on the Acoustic Properties

Ultrasonic velocity measurements were taken on one Indiana limestone (IL) sample, six Pink Desert limestone (PL) samples, two Khuff limestone (KL) samples, and two cap rock shale (SH) samples. Sample IL was used to measure acoustic properties before and after sequestration for 90 days. The six PL samples were tested for three sequestration periods of 14, 30, and 90 days for two samples each. The two KL samples were tested for 90 days. Also, two SH samples were tested for 30 days.

Figure 5.1 shows the comparison of compressional and shear wave velocities for sample IL-10-2 before and after CO_2 sequestration for 90 days. It can be seen from the figure that P-wave velocities range between 4774-5222 m/s for dried sample while P-wave velocities for post-CO_2 treated (90 days) sample decreased to 4447-4978 m/s, a 5.7% decrease. Also, the pre-injection S-wave velocities range between 2596-2791.5 m/s, while the post-injection velocities range between 2577-2800 m/s, a decrease in 0.2%.

In order to quantify the effect of CO_2 sequestration on the mechanical properties of the rock samples, the dynamic Young's modulus and Poisson's ratio were calculated using the compressional and shear wave velocities data as the input values in equations 2.4 and 2.5. The test results showed that after CO_2 sequestration for 90 days, the Young's modulus and Poisson's ratio values for sample IL-10-2 decreased when compared with these values for the same sample which was not subjected to CO_2 sequestration as shown in Figures 5.2 and 5.3, respectively.

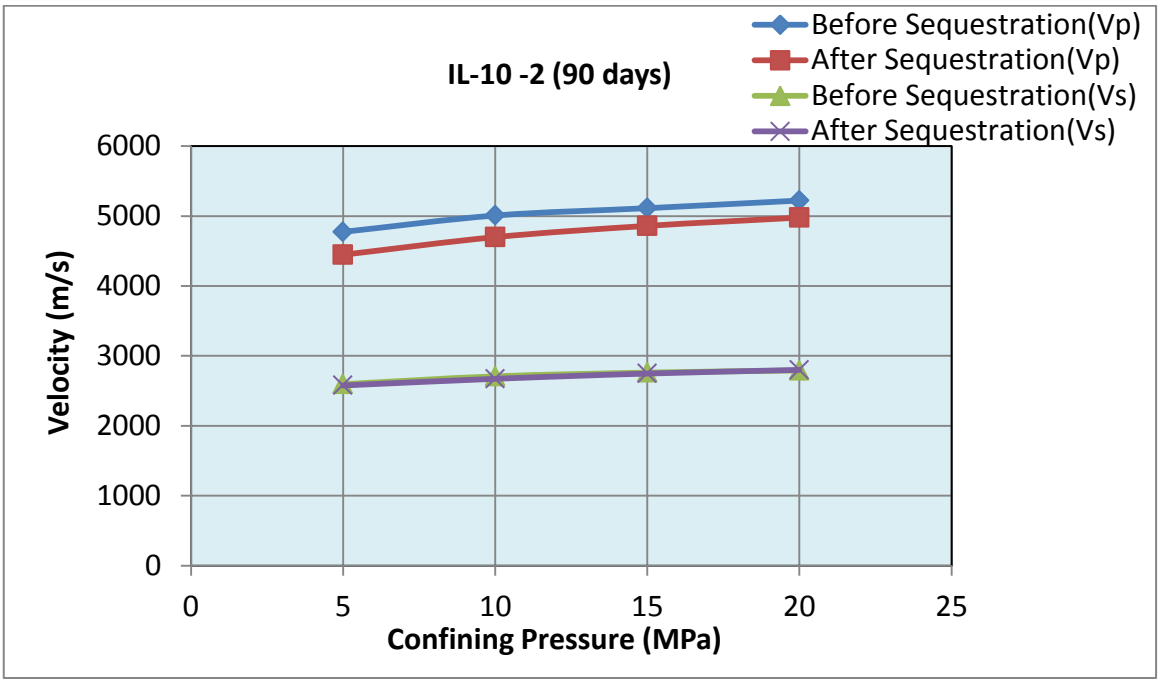

Figure 5.1 Comparison of compressional and shear wave velocities of Indiana limestone sample (IL-10-2) before and after CO_2 sequestration for 90 days.

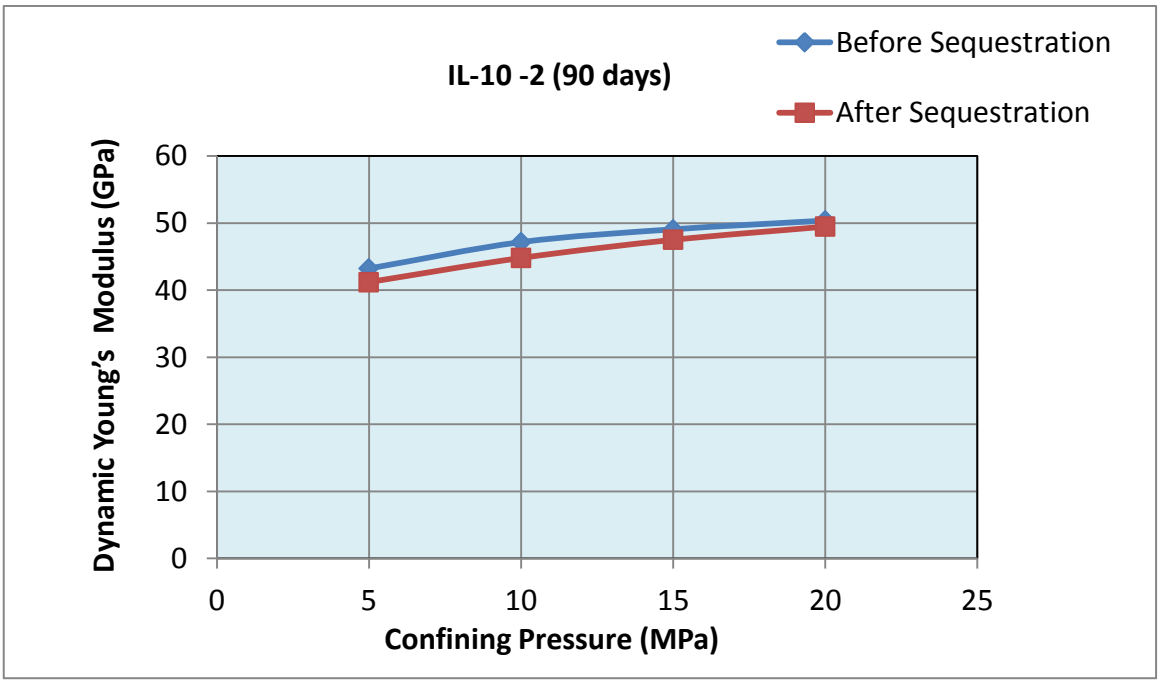

Figure 5.2 Comparison of Young's modulus of Indiana limestone sample (IL-10-2) before and after CO_2 sequestration for 90 days.

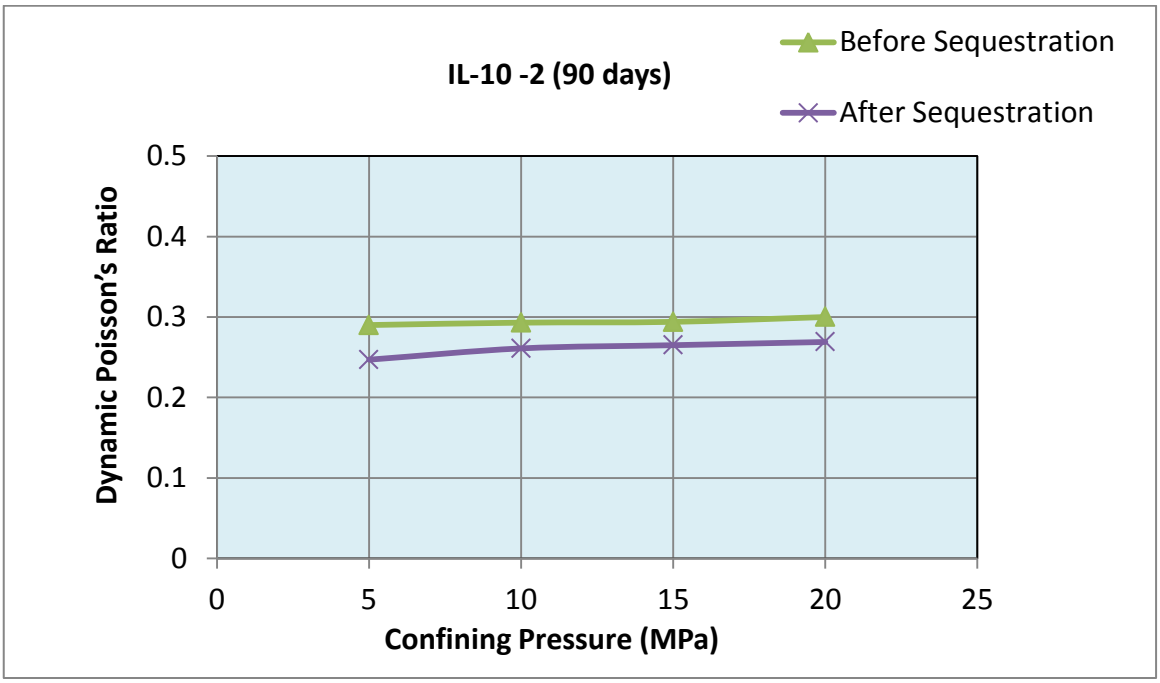

Figure 5.3 Comparison of Poisson's ratio of Indiana limestone sample (IL-10-2) before and after CO_2 sequestration for 90 days.

For PL samples, the acoustic measurements were performed on the samples before and after soaking with CO_2 for different time periods, viz., 14 days, 30 days, and 90 days, to investigate the effect of CO_2 sequestration on the mechanical properties and the effect of time periods. Figure 5.4 shows that for sample PL-S-1-A, the P-wave and S-wave velocities exhibited values between 3870-3935 m/s and 2179-2221 m/s, respectively, which decreased to 3628-3863 m/s (-4%) and 2069-2187 m/s (-3.3%), respectively, after soaking with CO_2 for 14 days. Also, a reduction in Poisson's ratio and Young's modulus was noted after CO_2 sequestration for 14 days as presented in Figures 5.5 and 5.6, respectively.

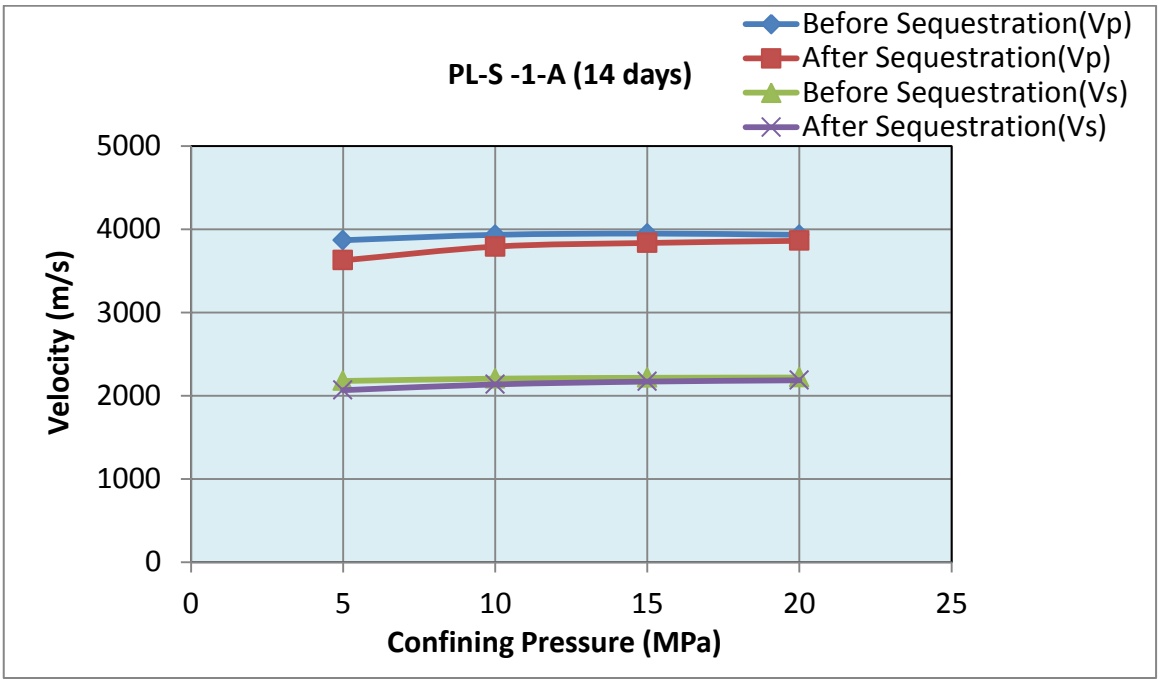

Figure 5.4 Comparison of compressional and shear wave velocities of Pink Desert limestone sample (PL-S-1-A) before and after CO_2 sequestration for 14 days.

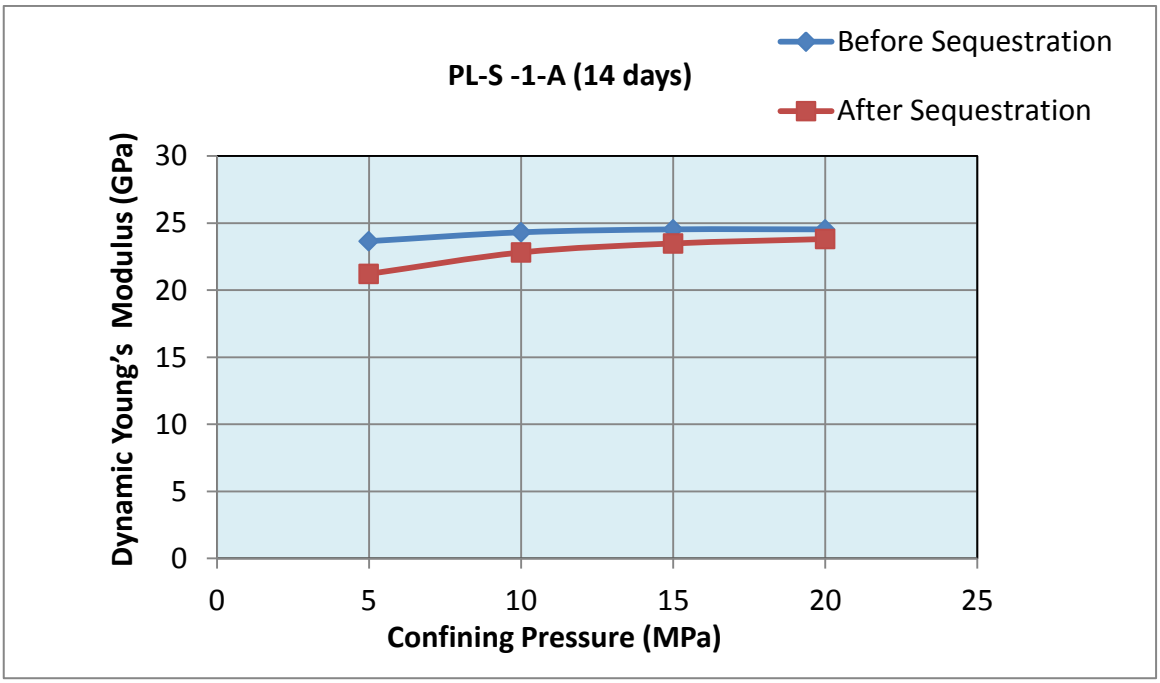

Figure 5.5 Comparison of Young's modulus of Pink Desert limestone sample (PL-S-1-A) before and after CO_2 sequestration for 14 days.

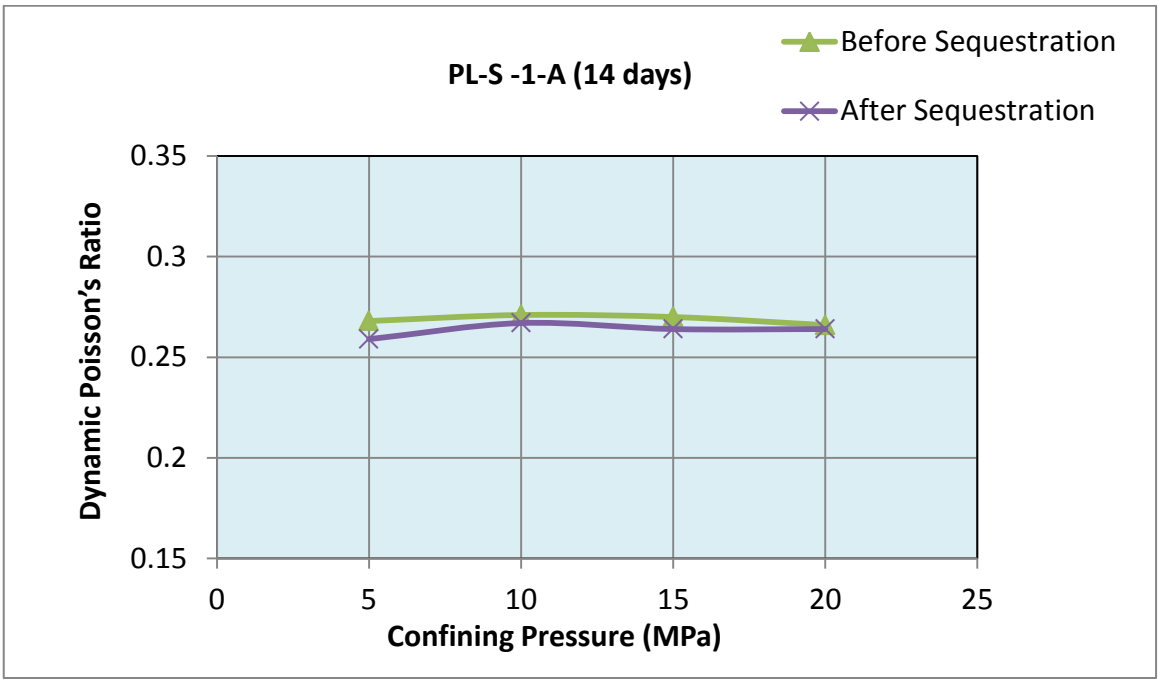

Figure 5.6 Comparison of Poisson's ratio of Pink Desert limestone sample (PL-S-1-A) before and after CO_2 sequestration for 14 days.

Figure 5.7 shows that for Khuff limestone sample KL-S-1-A, the P-wave and S-wave velocities exhibited values between 4687-4834 m/s and 2584-2640 m/s, respectively, which decreased significantly to 3462-4227 m/s (-19.24%) and 1820-2307 m/s (-21%), respectively, after soaking with CO_2 for 90 days. Also, a considerable reduction in the stiffness of the sample was noted after CO_2 sequestration for 90 days, where Young's modulus decreased sharply after the sequestration as presented in Figure 5.8. For example, the percentage of reduction in Young's modulus reached 23.7 % at 25 MPa confining pressure. Also, for sample KL-S-1-B, the P-wave, and S-wave velocities, and Young's modulus reduced drastically after CO_2 sequestration as presented in Figures 5.9 and 5.10, respectively. Since the stiffness is directly related to velocities, the observed behavior matches with the equations 2.4 and 2.5 that relate these measurements.

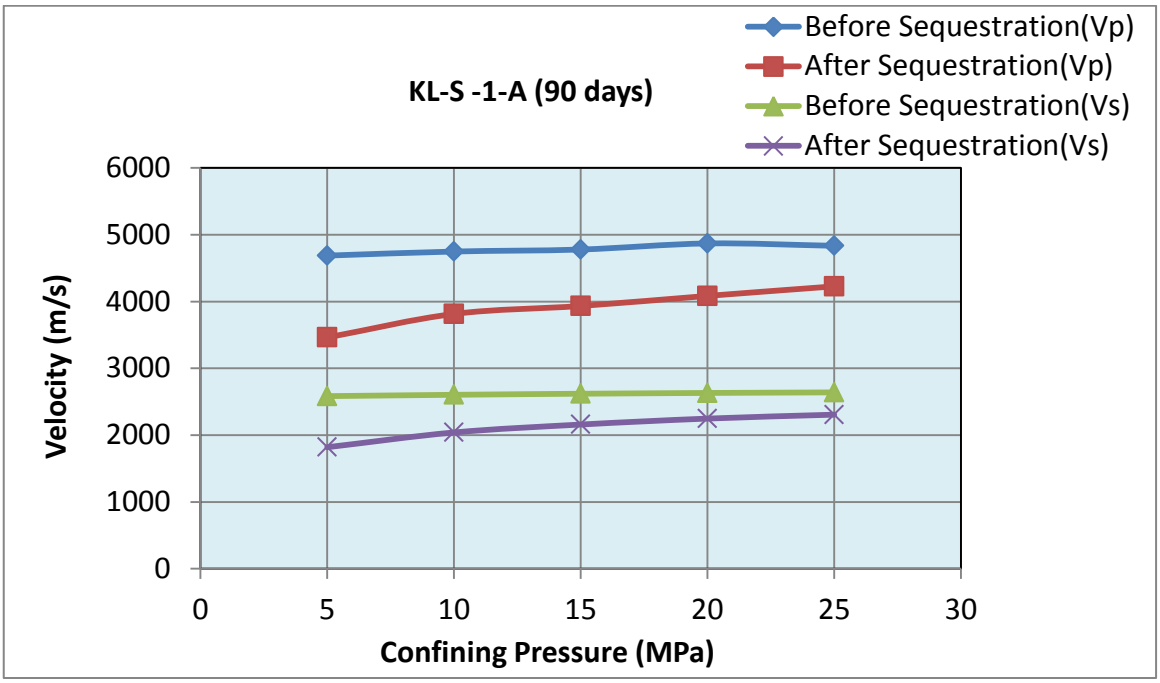

Figure 5.7 Comparison of compressional and shear wave velocities of Khuff limestone sample (KL-S-1-A) before and after CO_2 sequestration for 90 days.

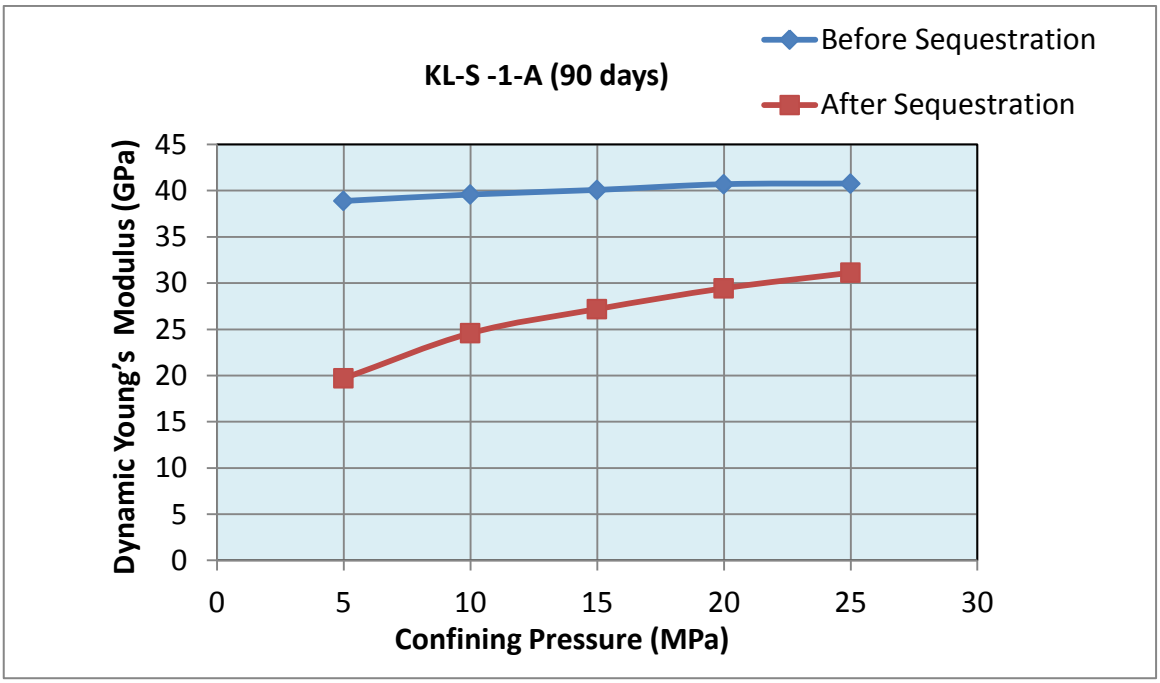

Figure 5.8 Comparison of Young's modulus of Khuff limestone sample (KL-S-1-A) before and after CO_2 sequestration for 90 days.

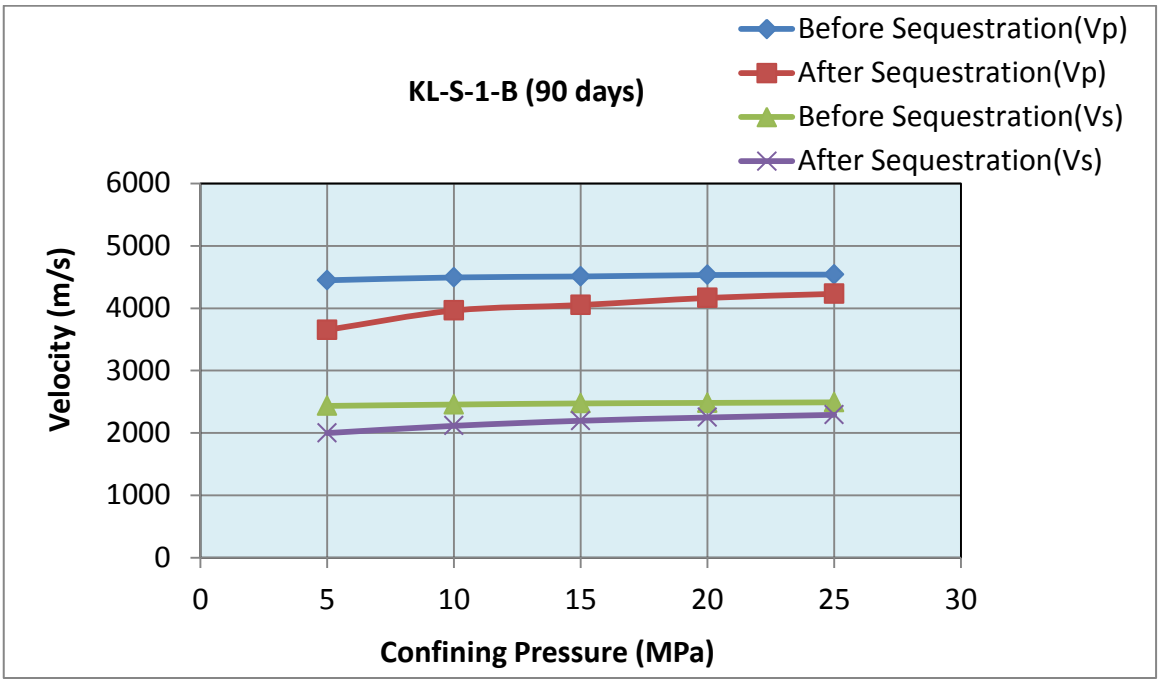

Figure 5.9 Comparison of compressional and shear wave velocities of Khuff limestone sample (KL-S-1-B) before and after CO_2 sequestration for 90 days.

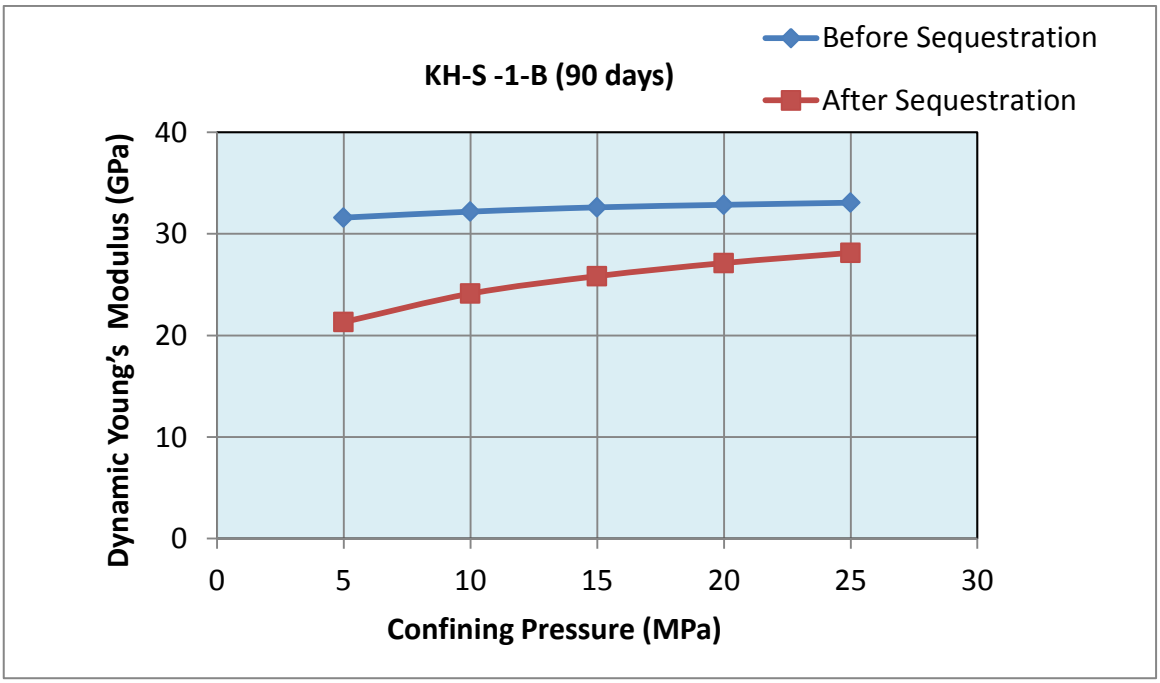

Figure 5.10 Comparison of Young's modulus of Khuff limestone sample (KL-S-1-B) before and after CO_2 sequestration for 90 days.

In addition to carbonate rocks, two cap rock shale (SH) samples were subjected to CO_2 for 30 days to study the impact of geological sequestration of CO_2 on the mechanical properties of cap rocks. Figure 5.11 shows the dynamic Young's modulus for samples SH-C-81, and SH-C-95 before and after CO_2 sequestration. The results indicated that the dynamic Young's modulus of two samples decreased. It means that cap-rock sealing and integrity were affected by sequestration CO_2.

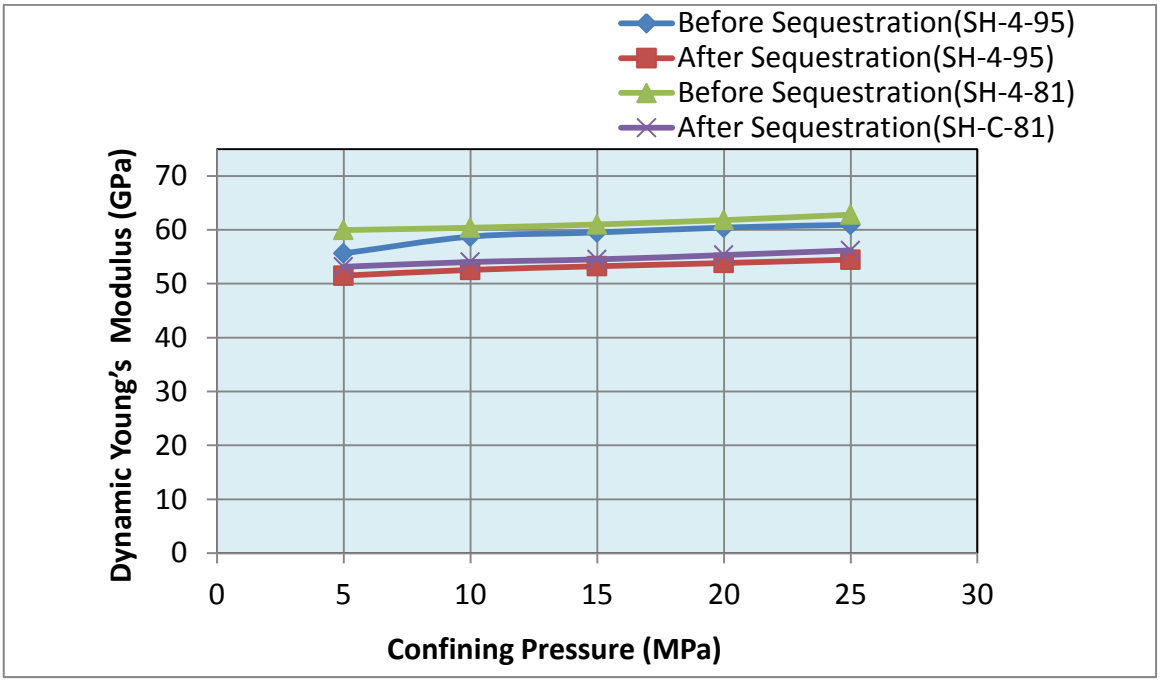

Figure 5.11 Comparison of Young's modulus for two cap rock shale (SH) samples (SH-4-95, and SH-4-81) before and after CO_2 sequestration for 30 days.

In general, the results showed a decrease in elastic properties of rocks after sequestration of supercritical CO_2 as confirmed by the reduction in P-and S-wave velocities. The observed change is derived from the solubility of the injected CO_2 in the water of the pores and around them resulting in low pH solution. The low pH solution leads the chemical dissolution of calcite which softens grain contacts, collapses the rock frame, and alters pore space geometry and thus changes the mechanical properties of the rocks. Before CO_2 sequestration, the

crystals of Indiana limestone had sharp edges. After CO_2 sequestration was conducted, these edges were transformed to smooth ones as shown in Figure 5.12.

Figure 5.13 shows that the pores of Pink Desert limestone were cleaned after CO_2 storage due to the dissolution of cement between them. For Khuff limestone, some micro pores were created after soaking with CO_2 compared to the case before soaking with CO_2 due to the dissolution of calcite as shown in Figure 5.14. The dissolution was confirmed by the micro CT scan images as shown in Figures 5.15 through 5.17. In addition, presence of calcite minerals in brine samples and the moderately large wormholes confirmed the dissolution of calcite as shown in Figures 5.18 and 5.19, respectively. Since Khuff samples showed significant decrease in the mechanical properties, it shows that each individual rock has to be studied for its response to of CO_2 sequestration in order to accurately determine its changes.

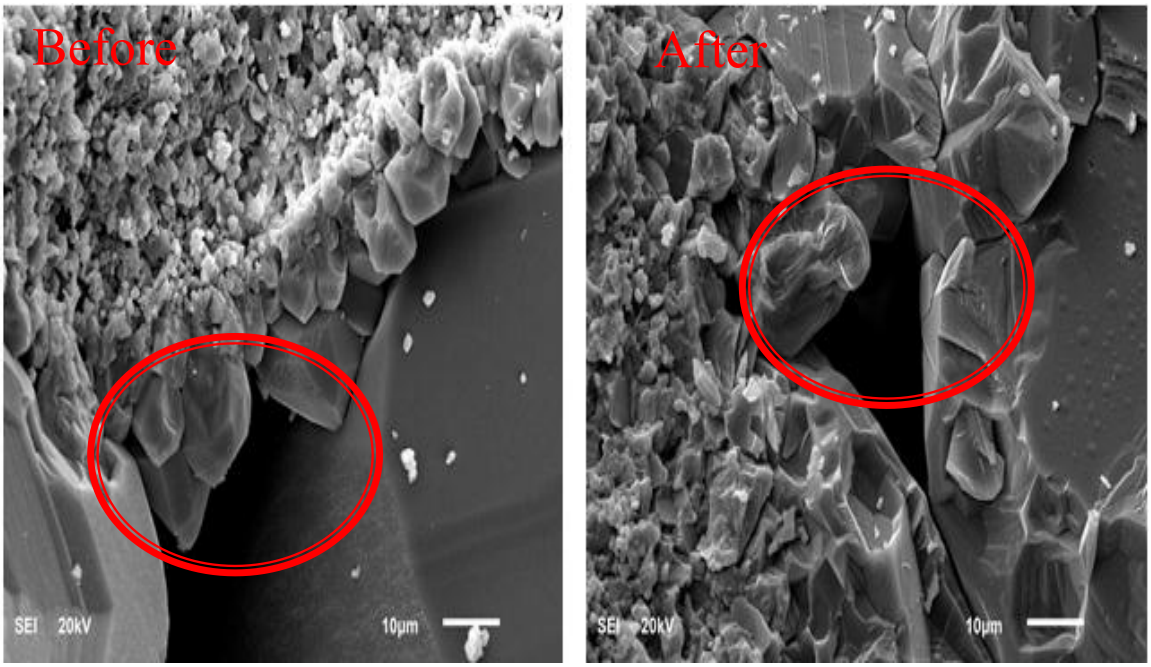

Figure 5.12 SEM microphotograph for Indiana limestone sample before and after CO_2 sequestration.

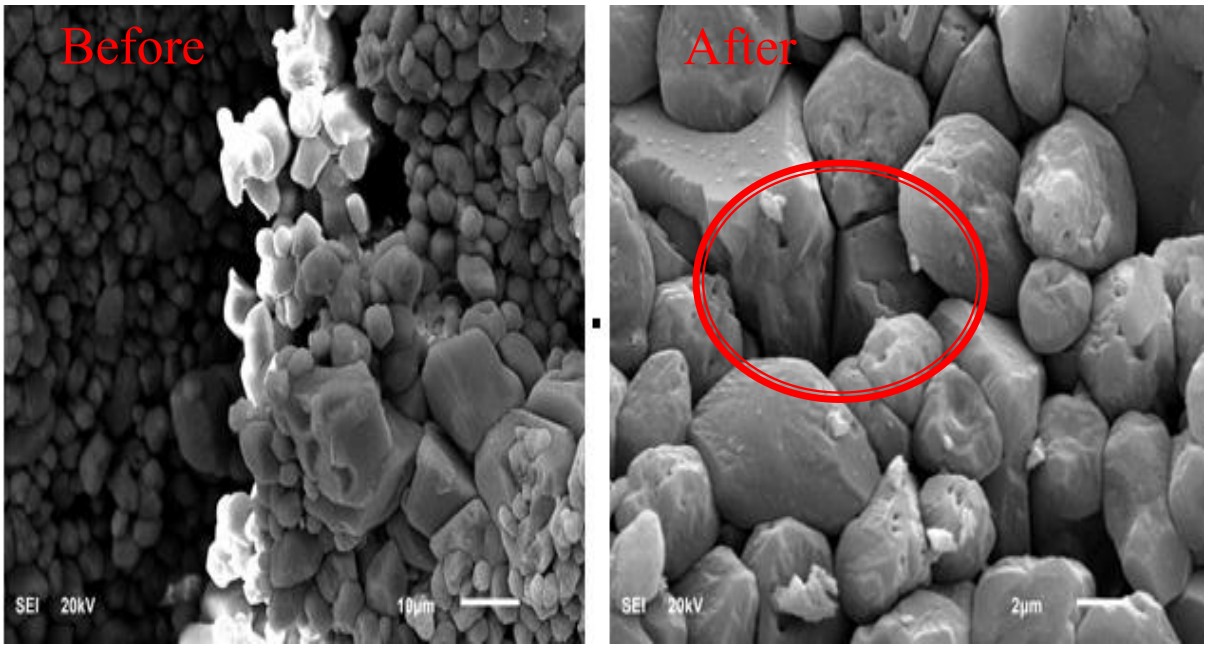

Figure 5.13 SEM microphotograph for Pink Desert limestone sample before and after CO_2 sequestration.

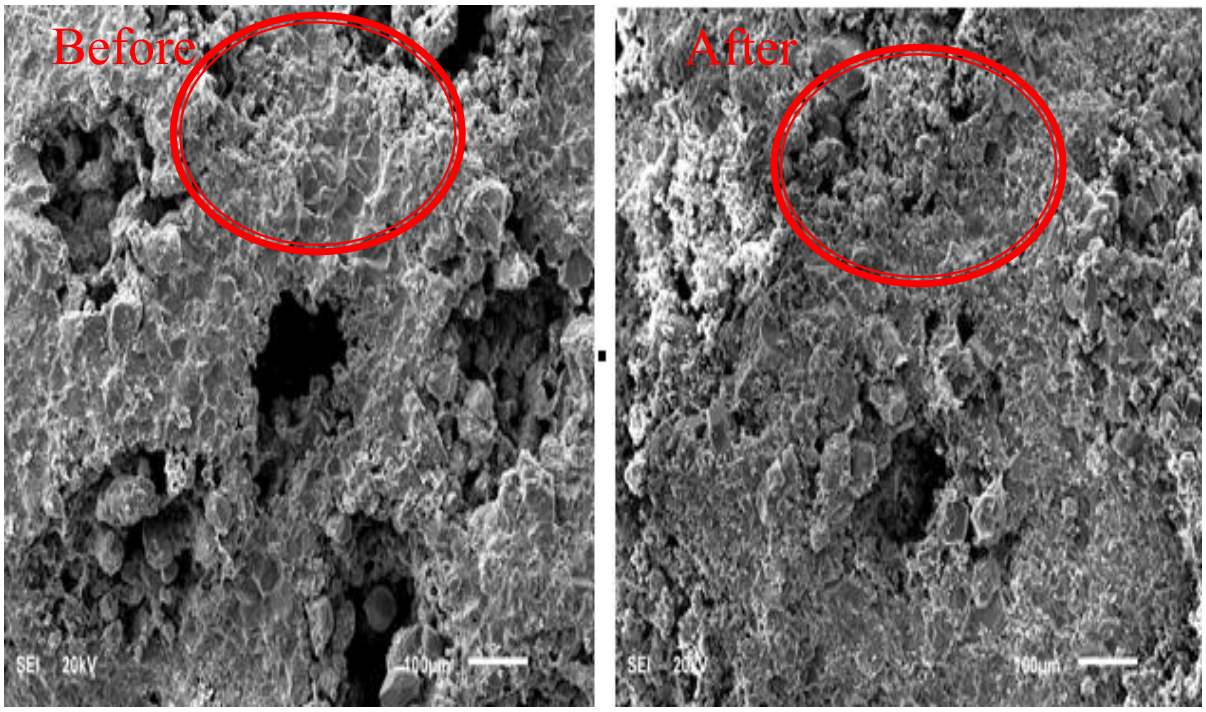

Figure 5.14 SEM microphotograph for Khuff limestone sample before and after CO_2 sequestration.

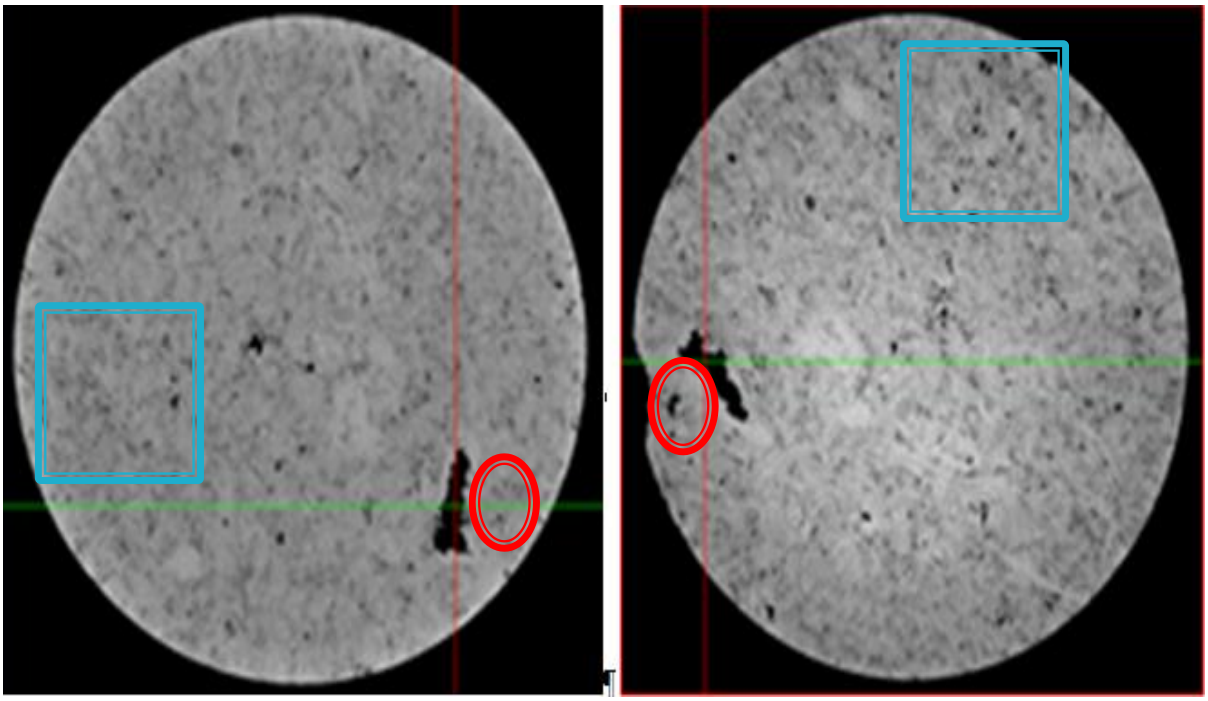

Figure 5.15 Micro CT scan image for Indiana limestone sample before and after CO_2 sequestration.

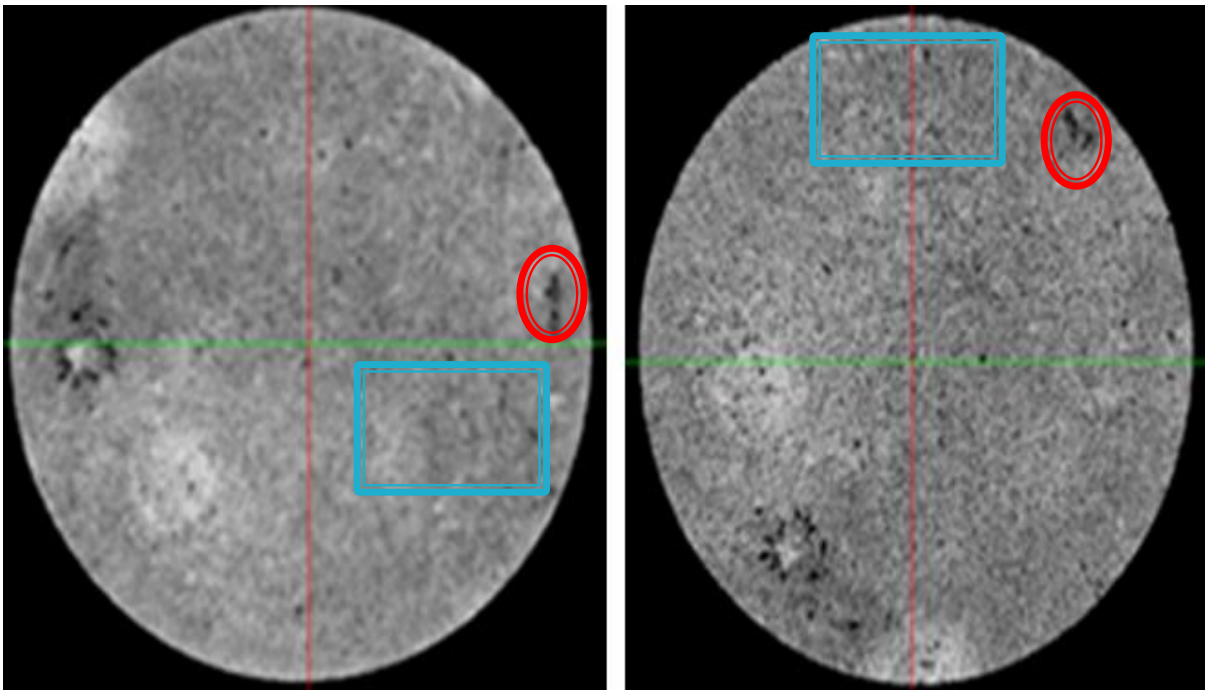

Figure 5.16 Micro CT scan image for Pink Desert limestone sample before and after CO_2 sequestration.

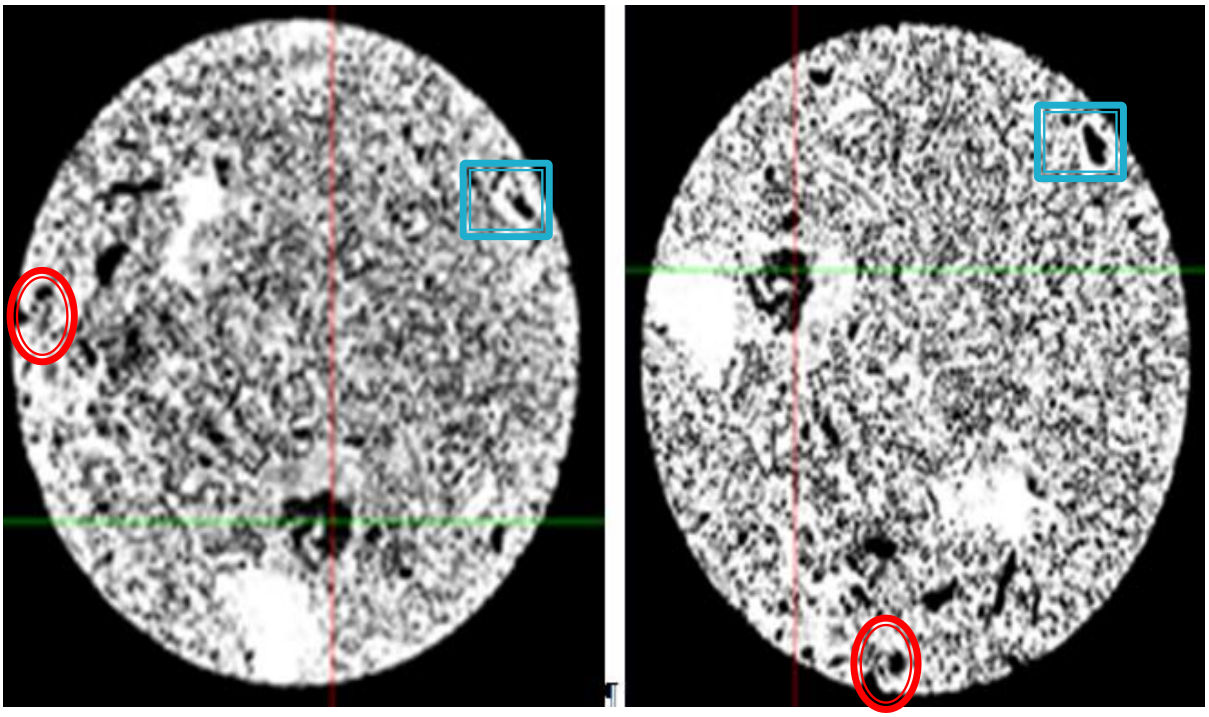

Figure 5.17 Micro CT scan image for Khuff limestone sample before and after CO_2 sequestration.

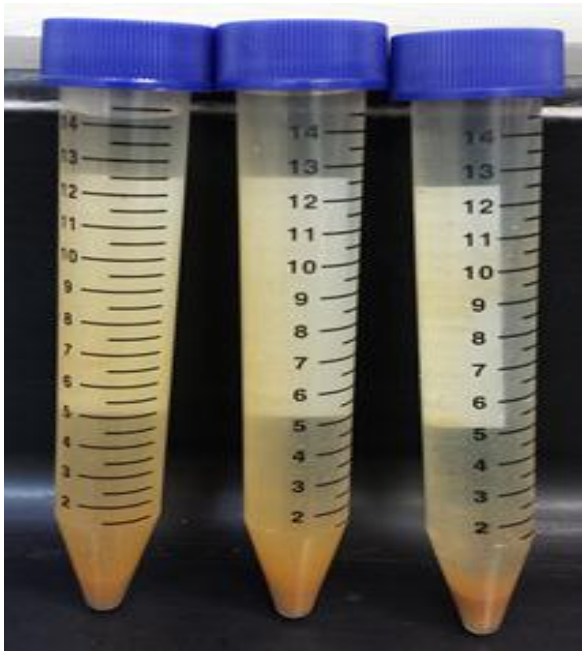

Figure 5.18 The presence of calcite minerals in brine samples.

Figure 5.19 Pink Desert limestone samples before and after CO_2 sequestration.

To compare the effect of duration of CO_2-brine contact time (solubility time) on these properties, three homogenous samples PL-S-1-A, PL-S-2-A and PL-S-3-B were subjected to supercritical injection of CO_2 under a pressure of 2000 psi for 14 days, 30 days, and 90 days, respectively. Figure 5.20 shows that at 15 MPa, the percentage of reduction in Young's modulus which represents the stiffness of rock increased with increase in the time period of CO_2 sequestration. For sample PL-S-1-A which soaked with CO_2 for short period (14 days), the percentage of reduction was 4.28% and increased to 5.32% for sample PL-S-2-A which subjected to CO_2 for 30 days. Also, this percentage reached 6.02 % when CO_2 stored for longer time (90 days) as happened in sample PL-S-3-B. However, there is no clear trend for Poisson's ratio.

One can see that CO_2 storage changed the formation fluid to become more reactive to the rock. In other words, the geochemical interaction between CO_2, brine, and rock is time dependent making changes in rock mechanical properties also time dependent. Samples in which CO_2 was stored for longer times exhibited greater change in mechanical properties compared to those in which CO_2 was stored for shorter time.

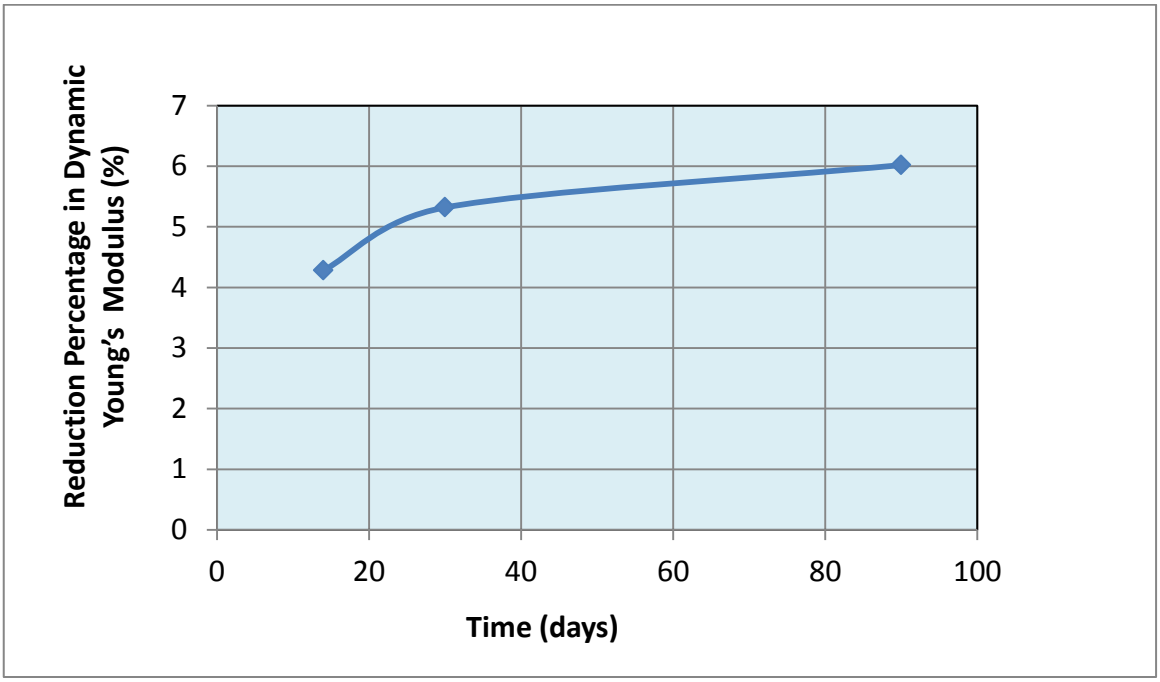

Figure 5.20 Effect of sequestration time periods on Young's modulus of Pink Desert Limestone samples (PL-S-1-A, PL-S-2-A, and PL-S-3-B) at 15 MPa.

Also, to address the effect of sequestration of CO_2 on rocks with different mechanical properties, each sample from Indiana limestone, Pink Desert limestone, and Khuff limestone were soaked with CO_2 for 90 days. Figure 5.21 shows the percentage of reduction in Young's modulus after CO_2 sequestration for the different rocks types. It can be seen from the table that a significant reduction in Young's modulus was in Khuff limestone despite its higher initial stiffness compared to Pink Desert limestone. The lowest effect of CO_2 sequestration observed in Indiana limestone. The significant reduction in mechanical properties of Khuff limestone after CO_2 sequestration is most probably due to the porosity type which is moldic. Also, the pore size of Khuff limestone is the biggest compared to other rocks which increased the contact area with CO_2.

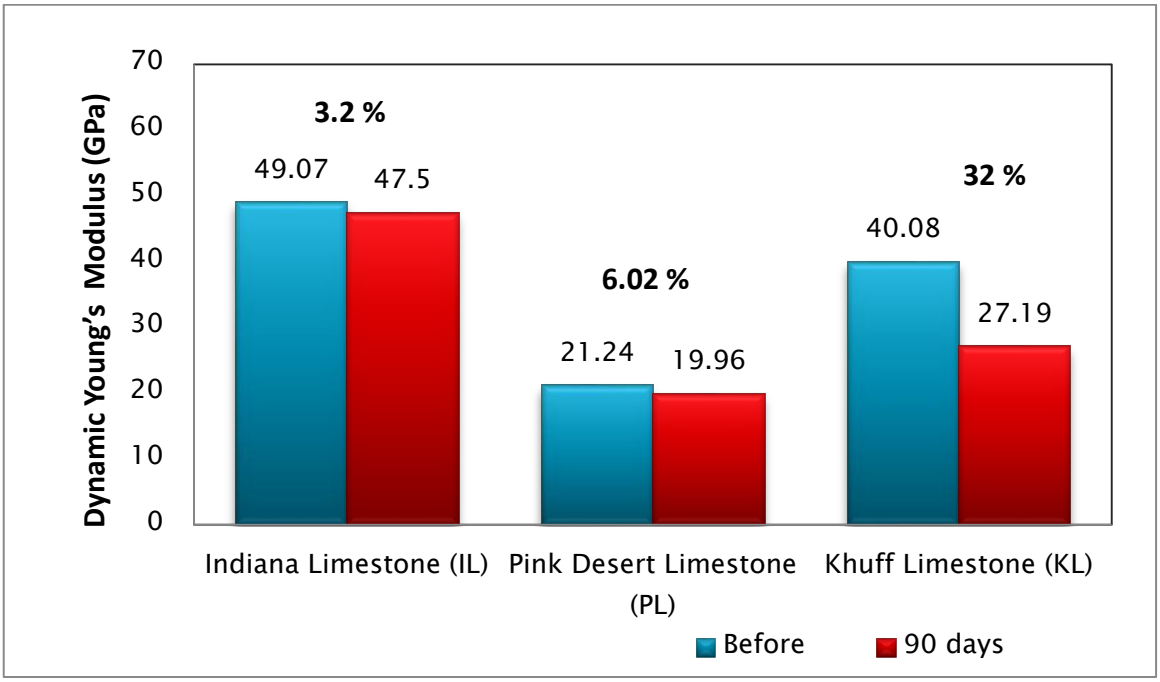

Figure 5.21 Reduction percentage in Young's modulus for different rock types subjected to CO_2 sequestration for 90 days.

5.4 Effect of CO_2 Sequestration on Static Elastic Moduli and Unconfined Compressive Strength

A summary of the UCS test results for IL samples is provided in Table 5.3. Typical stress-strain curves for IL and PL samples are presented in Appendix B. The data shows that the supercritical sequestration of CO_2 for long time period caused noticeable changes both in unconfined compressive strength and elastic properties. Sample IL-15-2 was tested before subjecting to CO_2 sequestration while an identical sister sample IL-15-3 was tested after having undergone CO_2 sequestration for long period of time (90 days). It was noted that there is a reduction in the static values for Poison's ratio (υ) and Young's modulus (E) for the post-CO_2 treated, where υ decreased from 0.316 to 0.296 and (E) dropped from 23.436 GPa to 16.282 GPa. Also, unconfined compressive strength decreased from 36 MPa to 33 MPa.

For Pink Desert limestone samples, the measurements were conducted on four homogenous samples. Sample PL-U-2 was tested before soaking with CO_2. Samples PL-U-1-A, PL-U-2-A, and PL-U-3-B were tested after CO_2 sequestration for different time periods, viz., 14 days, 30 days, and 90 days, respectively. Figures 5.22 through 5.24 show that after CO_2 sequestration, the mechanical properties of rocks including static values for Poison's ratio (υ) and Young's modulus (E), and unconfined compressive strength decreased. Moreover, Figures 5.22 through 5.24 show the effects of CO_2 storage time on elastic properties and strength for PL samples. Overall, we can see from these figures that the percentage of reduction in elastic properties and strength increased with time. It means that, the rock became less stiff after increasing the duration of CO_2-brine contact time (solubility time). An exception was for sample PL-U-3-B, where a slight increase in Young's modulus was observed after 90 days compered to sample PL-U-2-A which was soaked with CO_2 for 30 days. This may be due to the difference in the constituents of sister sample.

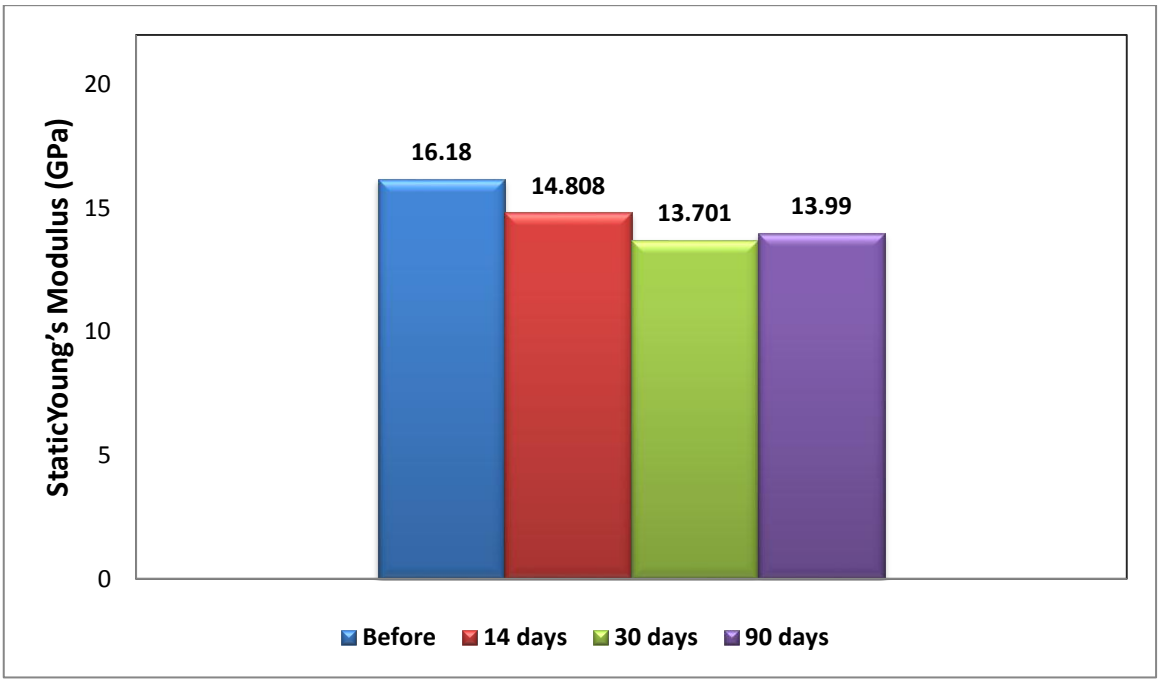

Figure 5.22 Effect of sequestration time periods on Young's modulus of Pink Desert limestone samples (PL-U-2, PL-U-1-A, PL-U-2-A, and PL-U-3-B).

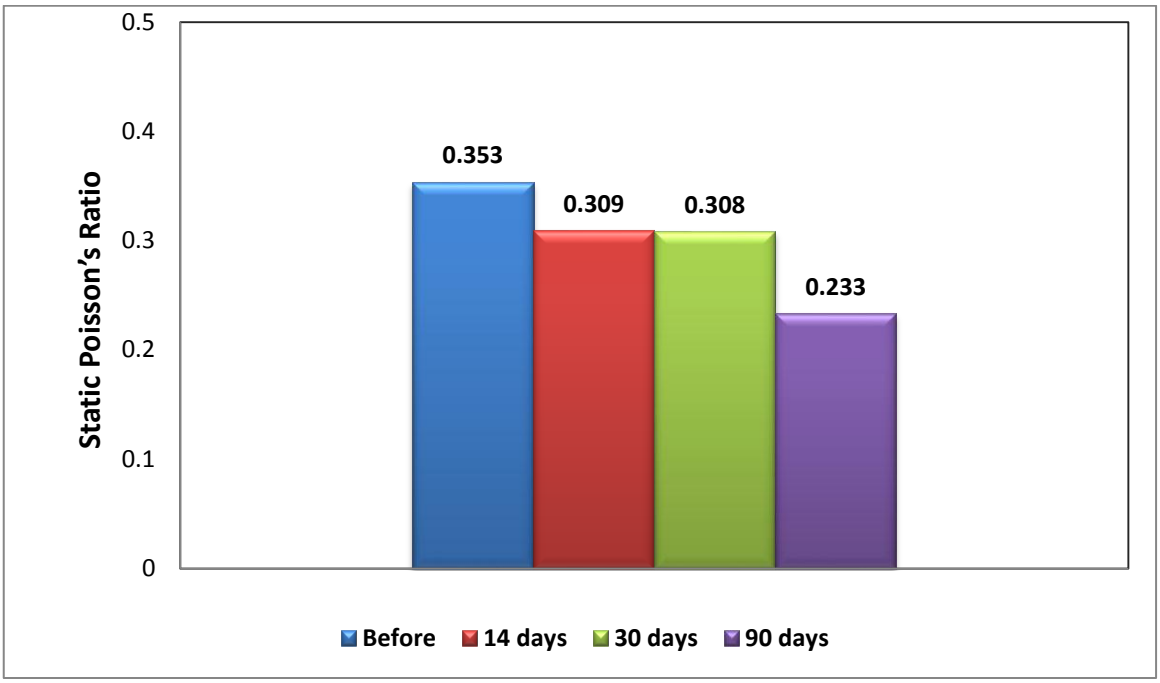

Figure 5.23 Effect of sequestration time periods on Poison's ratio of Pink Desert limestone samples (PL-U-2, PL-U-1-A, PL-U-2-A, and PL-U-3-B).

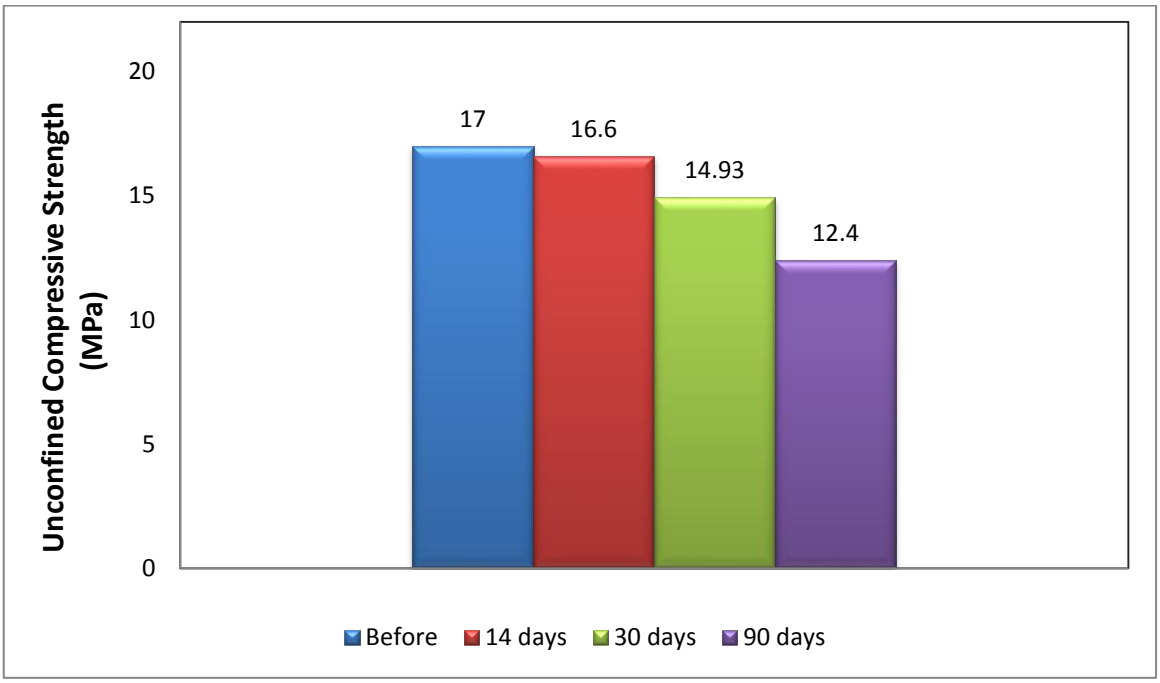

Figure 5.24 Effect of sequestration time periods on unconfined compressive strength of Pink Desert limestone samples (PL-U-2, PL-U-1-A, PL-U-2-A, and PL-U-3-B).

Table 5.3 Static values of Young's modulus and Poison's ratio and unconfined compressive strength values of Indiana limestone samples.

Property	Indiana Limestone		
Sample No	IL-15-2	IL-15-3	
Test Condition	Before CO_2 Sequestration	After CO_2 Sequestration (90days)	Reduction Percentage
UCS(MPa)	36	33	8.33
E (GPa)	23.436	16.282	30
υ	0.316	0.296	6.33

To investigate the impact of the disposal of CO_2 into deep saline aquifer rocks with different mechanical properties by using unconfined compression test, six samples from Indiana limestone, Pink Desert limestone, and Khuff limestone core samples were tested one before and one after CO_2 sequestration (90 days). Figure 5.25 shows that the percentage of reduction in the strength of Indiana limestone sample is 8.33% which increased to 27% in Pink Desert limestone sample. Also, this percentage increased to 30% in Khuff limestone sample. Generally, the results obtained from unconfined compression tests are in conformity with the results obtained from ultrasonic velocity measurements.

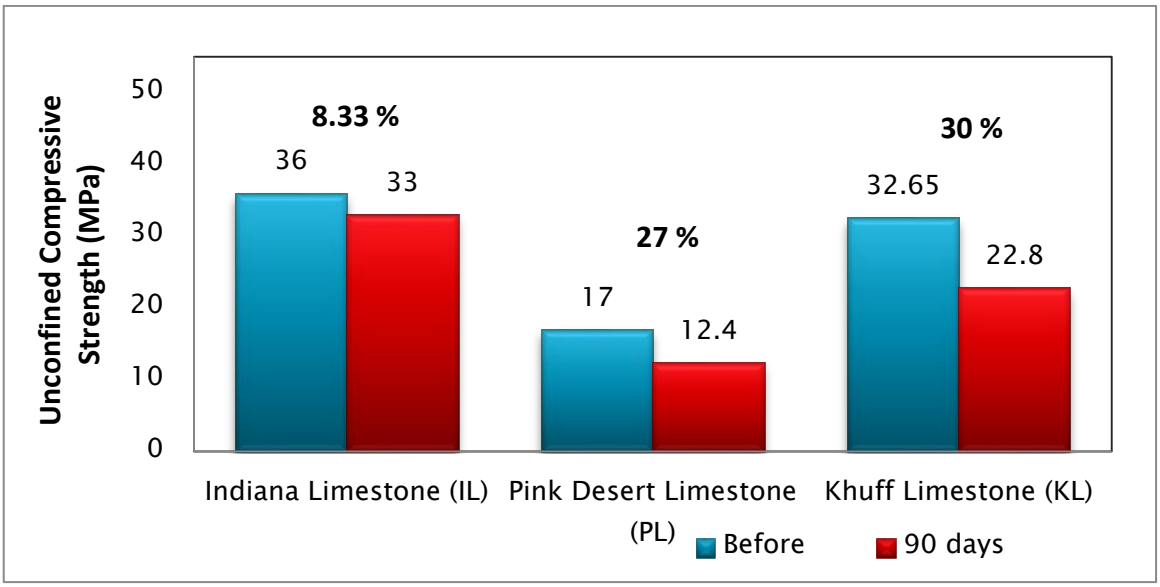

Figure 5.25 Reduction percentage in unconfined compressive strength for different rock types subjected to CO_2 sequestration for 90 days.

5.5 Effect of CO_2 Sequestration on Indirect Tensile Strength

In addition to the previous tests, indirect tensile strength test was conducted to study the effect of supercritical CO_2 sequestration and the effect of duration of CO_2-brine contact time (solubility time) on the indirect tensile strength of Pink Desert limestone, and Khuff limestone core samples.

Figure 5.26 and Table 5.4 show the indirect tensile strength values for Pink Desert limestone samples obtained from the tests. For sample PL-T-1-B which was soaked with CO_2 for a short time period (14 days), a slight decrease in indirect tensile strength from 199.137 to 199.128 psi was observed when compared to the indirect tensile strength of dried sister sample PL-T-1-A. On the other hand, for sample PL-T-2-A which was tested after having undergone CO_2 sequestration for a medium period of time (30 days), the indirect tensile strength reduced from 199.137 to 158 psi (-20.65%) in comparison with the untreated sample DL-T-1-A. Also, when sample PL-T-3-C was subjected to CO_2 for 90 days, reduction in indirect tensile strength was further reduced to 28.3%.

Table 5.5 shows that for sample KL-T-1-B which was soaked with CO_2 for longer time period (90 days), a significant decrease in tensile strength from 278 to 165 psi was observed when compared to the tensile strength of dried sister sample KL-T-1-D. When comparing the percentage reduction in indirect tensile strength (Figure 5.27), it is clear that the effect of CO_2 storage (90 days) on Khuff limestone rocks is very high, where the percentage reduction reached 34.3%. However, this value reached 28.3% in Pink Desert limestone rocks.

We can see from the results that the percentage of reduction in tensile strength increased with increasing the time period of CO_2 sequestration and the effect on Khuff limestone was very

significant. We expect more effect on the strength of rocks after storage for longer time periods.

Table 5.4 Indirect tensile strength values of Pink Desert limestone samples.

Property	Pink Desert Limestone			
Sample No	PL-T-1-A	PL-T-1-B	PL-T-2-A	PL-T-3-C
Test Condition	Before CO_2 Sequestration	After CO_2 Sequestration (14days)	After CO_2 Sequestration (30days)	After CO_2 Sequestration (90days)
Indirect Tensile Strength (psi)	199.137	199.128	158	142.8

Table 5.5 Indirect tensile strength values of Khuff limestone samples.

Property	Khuff Limestone	
Sample No	KL-T-1-B	KL-T-3-D
Test Condition	Before CO_2 Sequestration	After CO_2 Sequestration (90days)
Indirect Tensile Strength (psi)	278	165

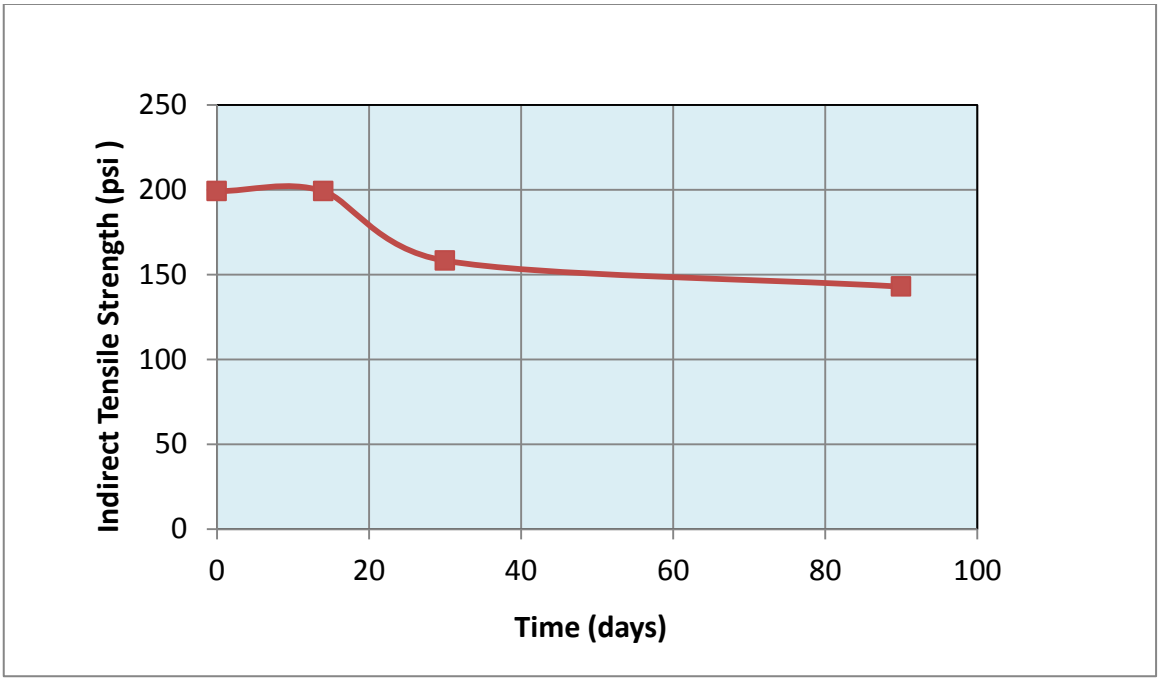

Figure 5.26 Indirect tensile strength (ITS) of Pink Desert limestone samples (PL-T-1-A, PL-T-1-B, PL-T-2-A, and PL-T-3-C) at different time periods.

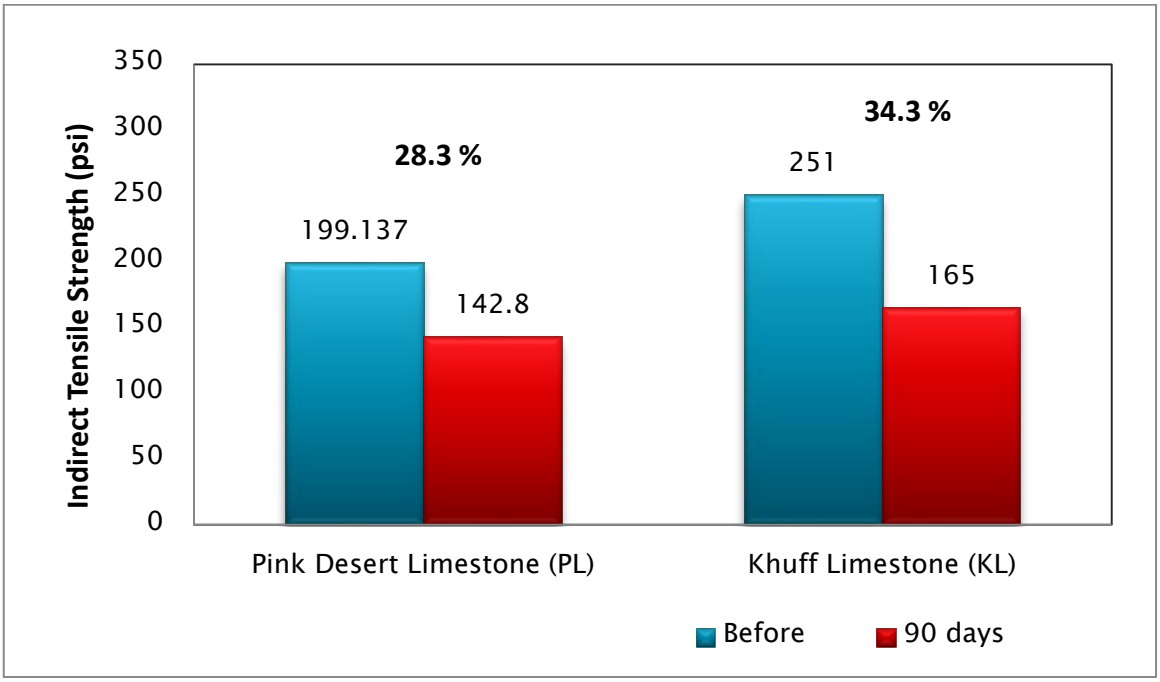

Figure 5.27 Reduction percentage in indirect tensile strength for different rock types subjected to CO_2 sequestration for 90 days.

5.6 Concluding Remarks

Overall, we can see from the ultrasonic velocity, static elastic moduli, unconfined compressive strength, and indirect tensile strength measurements which were done before and after CO_2 sequestration for different carbonate aquifer rocks that CO_2 sequestration has a significant effect on the mechanical parameters. The reason for this phenomenon is the dissolution of CO_2 in formation brine forming carbonic acid which dissolves some soluble carbonate grains and thereby softens grain contacts, collapses the rock frame, and alters rock pore structure. In addition, the impact of CO_2 storage depends on the time for the reaction between CO_2, brine, and rock. Longer exposure leads to greater changes in the properties. Moreover, the significant impact of CO_2 storage was noted on Khuff limestone when compared with Indiana limestone and Pink Desert limestone. Among the rocks that are

studied in this program, the good candidate carbonate rock for geologic sequestration of CO_2 is Indiana limestone rocks.

CHAPTER 6 IMPACT OF CO_2 SEQUESTRATION ON ENGINEERING OPERATIONS

The effect of CO_2 sequestration on the rock mechanical properties is a key parameter to be studied that will help in assessing the deep saline aquifer performance in the process of geological sequestration to get safe and effective long-term storage. As we have seen from this study, mechanical properties of the carbonate rock aquifers were affected by CO_2 sequestration. In this part, Impact of CO_2 sequestration on engineering operations is discussed in brief.

The results obtained from this study showed that the supercritical sequestration of CO_2 for long time period caused noticeable changes both in unconfined compressive strength (UCS) and elastic properties of carbonate rocks. For instance, Khuff limestone sample was tested before subjecting to CO_2 sequestration while an identical sister sample was tested after having undergone CO_2 sequestration for long period of time (90 days). It was observed that there is a reduction in unconfined compressive strength for the post-CO_2 treated sample, where UCS decreased from 32.65 MPa to 22.8 MPa. To clarify the change in the strength on failure of rocks, Mohr circle was plotted from unconfined compression test results as shown in Figure 6.1. Since UCS test doesn't give angle of internal friction, a value of 20° is assumed in this case and a failure envelope was plotted. Even if the angle of internal friction remains the same after CO_2 sequestration, as assumed here and shown in the figure, there is a significant fall of failure envelope towards the weaker side.

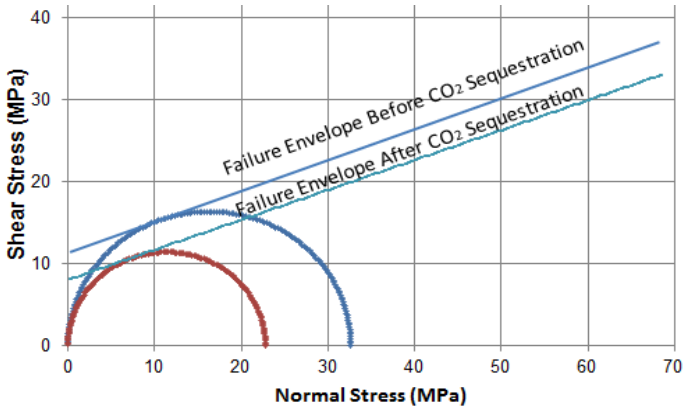

Figure 6.1 Mohr circles and failure envelopes for Khuff limestone samples before and after CO_2 sequestration.

6.1 Borehole Instability

A case of borehole instability is presented here as one of the most important petroleum engineering operations. Let us take a vertical borehole with the following assumptions:

Depth = 7000 ft

Radius of wellbore = 12 in

Wellbore pressure = 3000 psi

Vertical stress (σ_v) = 7000 psi

Max. Horizontal stress (σ_H) = 5635 psi

Min. horizontal stress (σ_h) = 4000 psi

In such a case, the stresses around the wellbore wall at a point (Figure 6.2) are given as:

Vertical stress (σ_v) = 7000 psi (48.275 MPa)

Radial stress (σ_r) = P_w = 3000 psi (20.69 MPa)

Circumferential stress (σ_θ) = 3 σ_H – σ_h – P_w = 3*5635 – 4000 – 3000 = 9905 psi (68.31 MPa) (in the direction of σ_H, i.e., at points A and B).

Circumferential stress (σ_θ) = 3 σ_h – σ_H – P_w = 3*4000 – 5635 –3000 = 3365 psi (23.2 MPa) (in the direction of σ_h , i.e., at points C and D).

It can be seen from the results that the worst case stress scenario is at points A and B as shown in Figure 6.2. Therefore in such a case, if the stress in an aquifer is close to failure envelope (Figure 6.3), then after sequestration, there is a strong possibility that the existing wellbores or new wellbore will become unstable.

If P_w = 11600 psi, then

Circumferential stress (σ_θ) = 3 σ_H – σ_h – P_w = 3*5200 – 4000 – 11600 = 0 psi

In such a case, if tensile strength is decreased like what happened in this study, there will be fracture in the formation after CO_2 sequestration compared to the case before sequestration as shown in Figures 6.2 and 6.4, again to borehole instability. Alternatively if fracturing is to be carried out in this formation, the materials property values corresponding to these after CO_2 sequestration have to be used.

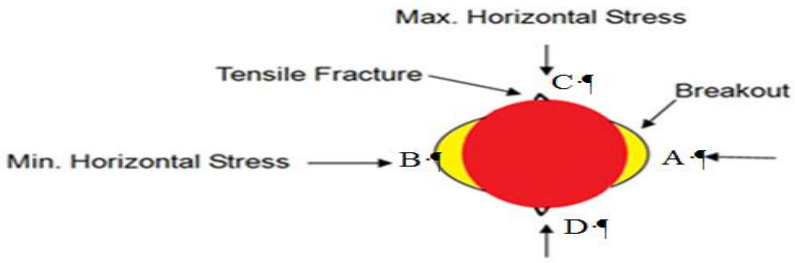

Figure 6.2 Stresses around a vertical borehole.

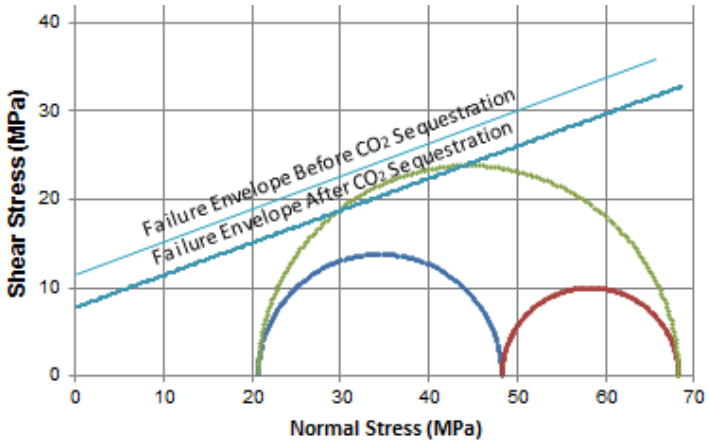

Figure 6.3 Mohr circles for stresses around the wellbore wall and failure envelopes for Khuff limestone samples before and after CO_2 sequestration.

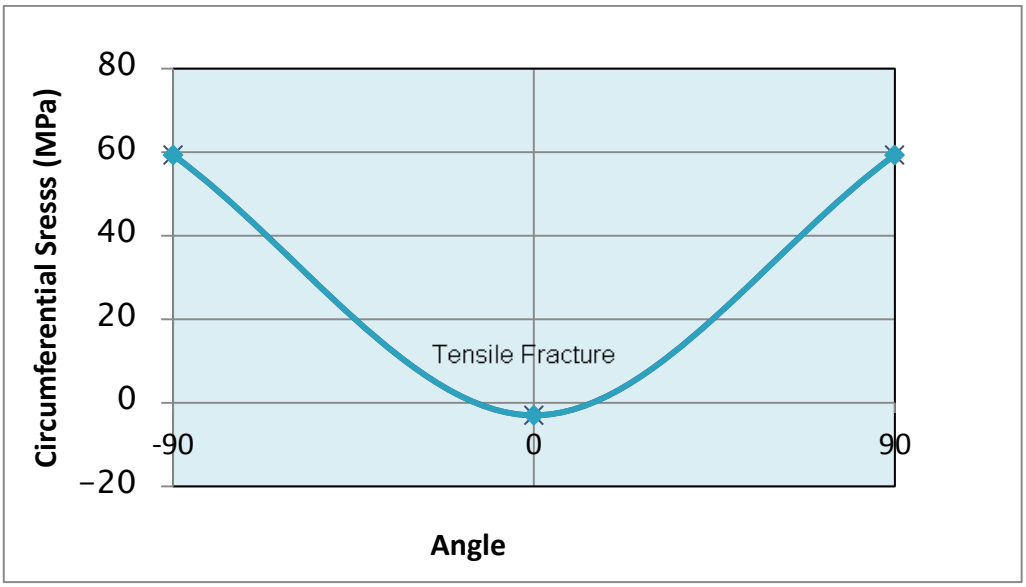

Figure 6.4 Tensile fracture after CO_2 sequestration.

6.2 Aquifer Compaction

On the basis of the results obtained from the unconfined compression test results before and after CO_2 sequestration, it was shown that the static Young's modulus (E) for the samples subjecting to CO_2 sequestration was decreased compared to the values for samples which were not having undergone CO_2 sequestration. Figure 6.5 shows the stress-strain curve for

two samples from Pink Desert limestone rocks before and after CO_2 sequestration. The results indicated that after soaking with CO_2 for one month, the static value of Young's modulus (E) decreased from 16.18 to 13.701 GPa. To explain the compaction resulting from the reduction in Young's modulus, 14 MPa axial stress was chosen. It can be seen from the figure that there is extra strain (ε) after CO_2 sequestration.

If we assume Poison's ratio (υ) = 0 or close to zero, we can then calculate axial strain:

The extra strain = $\Delta\varepsilon = 0.00114$

Extra compaction in the aquifer (let us take the thickness of 500 ft) = 0.00114*500 = 0.57 ft.

This compaction may cause a number of problems to casing. Additionally, this may lead to change in the permeability of the aquifer.

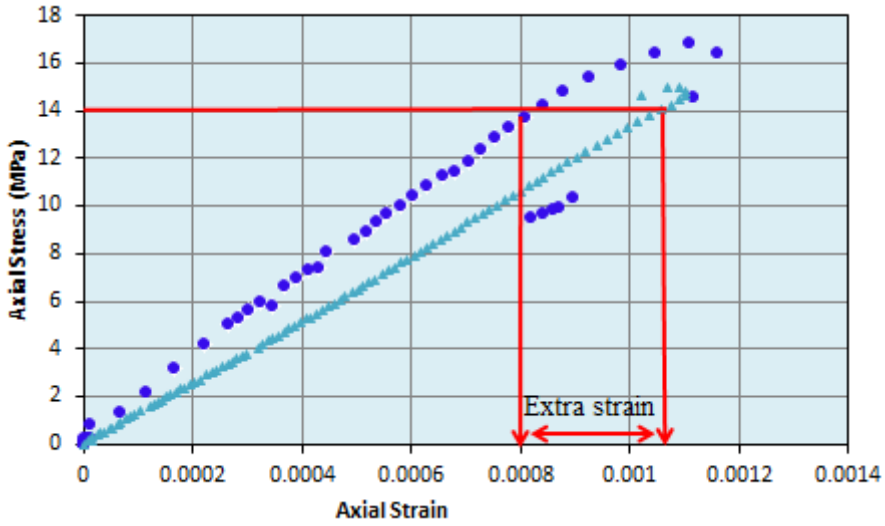

Figure 6.5 Stress-strain curve for Pink Desert limestone samples before and after CO_2 sequestration.

CHAPTER 7 CONCLUSION AND RECOMMENDATIONS

7.1 Conclusions

Carbonate and cap rocks were tested to investigate the effect of CO_2 sequestration on the mechanical properties of these rocks at supercritical conditions (2000 psi and 100 ºC) for varying time periods. Based on the results obtained, the following conclusions can be drawn:

1. CO_2 sequestration affected the mechanical properties of the carbonate rocks investigated in this work, viz., Indiana limestone, Pink Desert limestone, and Khuff limestone as well as cap rocks.
2. The observed effect is derived from the solubility of the injected CO_2 in the water of the pores and around them resulting in low pH solution which leads the chemical dissolution of calcite. This process softens the grain contacts, collapses the rock frame, and alters pore space geometry and thus changes the mechanical properties of the rocks.
3. The duration of CO_2-brine contact time has an effect on the mechanical properties of the rock samples. The effect on Pink Desert limestone which was subjected to CO_2 for longer period of time (90 days) was found to be more than the effect on the same limestone treated with CO_2 for a shorter period (30 days). Samples treated for the shortest time period (14 days) were found to exhibit the least change in the mechanical properties. Hence, it is expected that the effect on the mechanical properties of rocks increases with storage time.
4. The reason for the effect of time is that the solubility of CO_2 increases with time making the formation fluid to become more reactive to the rock. In other words, the

geochemical interaction between CO_2, brine, and rock is time dependent making changes in rock mechanical properties also time dependent.

5. The significant impact of CO_2 storage was noted on Khuff limestone when compared with Indiana limestone and Pink Desert limestone despite its higher initial stiffness compared to Pink Desert limestone.
6. The significant reduction in the mechanical properties of Khuff limestone after CO_2 sequestration is most probably due to the porosity type which is moldic. Also, the pore size of Khuff limestone is the biggest compared to other rocks which increased the contact area with CO_2.
7. The good candidate carbonate rock for geologic sequestration of CO_2 is Indiana limestone because the relative effect on this rock was minimum compared to other carbonate rocks.

7.2 Recommendations

In this study, we would suggest the following future works:

1. Conduct tests for longer storage time.
2. Tests on other carbonate aquifer and reservoir rocks (Arab and Khuff formations) in Saudi Arabia to evaluate their stability for CO_2 sequestration.
3. Evaluate the effect of CO_2 sequestration on the mechanical properties of seal rocks like anhydrite or tight-carbonate mudstone from Saudi Arabia.
4. Study the effect of CO_2 sequestration on heterogeneous carbonate rocks.
5. Use SEM and micro CT scan for more details about the effect of CO_2 sequestration on grain contacts, pore space geometry and rock frame, etc.

REFERENCES

[1] Abdulraheem, A., Ahmed, M., Vantala, A., and, Parvez, T. 2009. Prediction of Rock Mechanical Parameters for Hydrocarbon Reservoirs Using Different Artificial Intelligence Techniques. Paper SPE 126094 presented at the 2009 SPE Saudi Arabia Section Technical Symposium and Exhibition held in Al Khobar, Saudi Arabia, 09–11 May.

[2] Alam, M., Hjuler, M., Christensen, H., and Fabricius, I. 2011. Impact of Supercritical CO_2 Injection on Petrophysical and Rock Mechanics Properties of Chalk: An Experimental Study on Chalk from South Arne Field, North Sea. Paper SPE 147056 presented at the SPE Annual Technical Conference and Exhibition held in Denver, Colorado, USA, 30 October–2 November.

[3] Alam, M., and Fabricius, I. 2012. Influence of effective stress coefficient on mechanical failure of chalk. Paper ARMA 12-286 presented at the 46th US Rock Mechanics / Geomechanics Symposium held in Chicago, IL, USA, 24-27 June.

[4] Alam, M., Hjuler, M., Christensen, H., and Fabricius, I. 2012. Change of Static and Dynamic Elastic Properties due to CO_2 Injection in North Sea Chalk. Paper D047 presented at 74th EAGE Conference & Exhibition incorporating SPE EUROPEC 2012 Copenhagen, Denmark, 4-7 June.

[5] Bachu, S. 2000. Sequestration of CO_2 in geological media: criteria and approach for site selection in response to climate change. Energy Conversion & Management, 41: 953-970.

[6] Bachu, S. 2003. Screening and ranking of sedimentary basins for sequestration of CO_2 in geological media in response to climate change, Environmental Geology, 44(3), 277-289.

[7] Bahara, M., and Liu, K. 2008. Measurement of the Diffusion Coefficient of CO_2 in Formation Water under Reservoir Conditions: Implications for CO_2 Storage. Paper SPE 116513 presented at the SPE Asia Pacific Oil & Gas Conference and Exhibition in Perth, Australia, 20-22 October.

[8] Bruant, R., Guswa, A., Celia, M., and Peters, C. 2002. Safe Storage of CO_2 in Deep Saline Aquifers. Environmental Science & Technology, Volume 36, Issue 11, p. 240-245.

[9] DOE (U. S. Department of Energy). 1999. Carbon Sequestration Research and Development, U. S. DOE/SC/FE-1, Washington, D. C., available at www. ornl. gov/carbon_sequestration.

[10] Egermann, P., Bazin, B., and Vizika, O. 2005. An Experimental Investigation of Reaction-Transport Phenomena during CO_2 Injection. Paper SPE 93674 presented at the 14th SPE Middle East Oil & Gas Show and Conference held in Bahrain International Exhibition Centre, Bahrain, 12–15 March.

[11] Firoozabadi, A., and and Cheng, P. 2010. Prospects for Subsurface CO_2 Sequestration. Journal Vol. 56, No. 6.

[12] Fjaer, E., Holt, R., Horsrud, P., Raaen, A., and Risnes, R. 2008. Petroleum related rock mechanics. 2nd Edition. ISBN: 978-0-444-50260-5.

[13] Gale, J. 2004. Geological storage of CO_2: What do we know, where are the gaps and what more needs to be done?. Energy, 29(9-10), 1329-1338.

[14] Gharbia, O., Bijeljica, B., Boekb, E., and Blunta, M. 2013. Changes in Pore Structure and Connectivity Induced by CO_2 Injection in Carbonates: a Combined Pore-Scale Approach. Energy Procedia 00 (2013) 000–000.

[15] Gledhill, D., and Morse, J. 2004. Dissolution kinetics of calcite in NaCl–$CaCl_2$–$MgCl_2$ brines at 25 °C and 1 bar pCO_2. Aquatic Geochemistry 10 (1–2) (2004), pp. 171–190.

[16] Goldberg, D., Takahashi, T., and Slagle, A. 2008. Carbon dioxide sequestration in deep-sea basalt. Proceedings of the National Academy of Sciences, 105(29), 9920-9925.

[17] Gomez, J. 2006. Geomechanical Performance Assessment of CO_2 – EOR Geological Storage Projects. Calgary University, Alberta. PhD Thesis.

[18] Grigg, R., and Svec, R. 2006. CO_2 Transport Mechanisms in CO2/Brine Coreflooding. Paper SPE 103228 presented at the SPE Annual Technical Conference and Exhibition held In San Antonio, Texas, 24-27 September.

[19] Grigg, R., and Svec, R. 2003. Co-Injected CO_2-Brine Interactions with Indiana Limestone. Paper SCA 2003-19 presented at the International Symposium of the Society of Core Analysts held in Pau, France, 21-24 September.

[20] Grigg, R., and Svec, R. 2008. Injectivity Changes and CO_2 Retention for EOR and Sequestration Projects. Paper SPE 110760 presented at the SPE/DOE Improved Oil Recovery Symposium held in Tulsa, Oklahoma, 19-23 April.

[21] Gritto, R., Daley, T., and Myer, L. 2003. Joint cross-well and single-well seismic studies of CO_2 injection in an oil reservoir. Geophysical Prospecting, 2004, 52, 323–339.

[22] Gunter, W., Wiwchar, B., and Perkins, E. 1997. Aquifer disposal of CO_2 rich greenhouse gases: extension of the time scale of experiment for CO_2 sequestration reactions by geochemical modelling. Mineralogy and Petrology, 59: 121-140.

[23] Gupta, A. 2010. Capacity and Constraints for Carbon Dioxide Sequestration in Aquifers and Depleted Oil/Gas Reservoirs in Carbonate Environment. Paper SPE 135595 presented at the SPE International Conference on CO_2 Capture, Storage, and Utilization held in New Orleans, Louisiana, USA, 10–12 November.

[24] Harris, J., Langan, R, Fasnacht, T., Melton, D., Smith, B. Sinton, J., and Tan, H. 1996. Experimental verification of seismic monitoring of CO_2 injection in carbonate reservoirs. Seismic Lithology 6: McElroy Reservoir Characterization Project. SL 6. 1.

[25] Holloway, S. 1997. Safety of the underground disposal of carbon dioxide. Energy Conversion & Management, 38: S241-S245.

[26] Herzog, H. 2001. What future for Carbon capture and sequestration?. Environmental Science & Technology, 7: 148-153.

[27] Izgec, O., Demiral, B., Bertin, H., and Akin, S. 2005. Experimental and Numerical Investigation of Carbon Sequestration in Saline Aquifers. Paper SPE 94697 presented at SPE/EPA/DOE Exploration and Production Environmental Conference held in Galveston, Texas, 7-9 March.

[28] Izgec, O., Demiral, B., Bertin, H., and Akin, S. 2005. CO_2 Injection in Carbonates. Paper SPE 93773 presented at the SPE Western Regional Meeting held in Irvine, CA, 30 March-1 April.

[29] Izgec, O., Demiral, B., Bertin, H., and Akin, S. 2006. Experimental and Numerical Modeling of Direct Injection of CO_2 into Carbonate. Paper SPE 100809 presented at

the SPE Annual Technical Conference and Exhibition held in San Antonio, Texas, 24-27 September.

[30] Jaeger, U. 2005. Social Conditions of Technological Change The Case of Carbon Capture and Storage. University of Potsdam, German. MS thesis.

[31] Kim J., Xue, Z., and Toshifumi, M. 2010. Experimental Study on CO_2 Monitoring and Saturation with Combined P-wave Velocity and Resistivity. Paper SPE 130284 presented at the CPS/SPE International Oil & Gas Conference and Exhibition in China held in Beijing, China, 8–10 June.

[32] Le Gallo, Y., Coullens, P., and Manai, T. 2002. CO_2 Sequestration in Depleted oil and Gas Reservoirs. Paper SPE 74104 presented at the SPE International Conference on Health, Safety and Environment in Oil and Gas Exploration and Production, Kuala Lumpur, Malaysia, 20- 22 March.

[33] Liteanu, E. 2009. Response of carbonate rocks and wellbore cement to supercritical CO_2 injection and long-term storage. Utrecht University, Netherlands. ISBN/EAN: 978-90-5744-171-4. PhD Thesis.

[34] Masoudi, R., Abd Jalil, M., Press, D., Lee, K., Tan, C., and Anis, L., Schlumberger; Darman, N., and Othman, M. 2013. An Integrated Reservoir Simulation-Geomechanical Study on Feasibility of CO_2 Storage in M4 Carbonate Reservoir, Malaysia. Paper IPTC 15029 presented at the International Petroleum Technology Conference held in Bangkok, Thailand, 7–9 February.

[35] Mohamed, I., He, J., Mahmoud, M., and Nasr-El-Din, H. 2010. Effects of Pressure, CO_2 Volume, and the CO_2 to Water Volumetric Ratio on Permeability Change during CO_2 Sequestration. Paper SPE 136394 presented at the Abu Dhabi International Petroleum Exhibition & Conference held in Abu Dhabi, UAE, 1–4 November.

[36] Mohamed, I., He, J., and Nasr-El-Din, H. 2011. Permeability Change during CO_2 injection in Carbonate Rock: A Coreflood Study. Paper SPE 140943 presented at the SPE Production and Operations Symposium held in Oklahoma City, Oklahoma, USA, 27–29 March.

[37] Mohamed, I., He, J., and Nasr-El-Din, H. 2012. Carbon Dioxide Sequestration in Dolomite Rock. Paper IPTC 14924 presented at the International Petroleum Technology Conference held in Bangkok, Thailand, 7–9 February.

[38] Mohamed, I., He, J., and Nasr-El-Din, H. 2013. Effect of Brine Composition on CO_2/Limestone Rock Interactions during CO_2 Sequestration. Journal of Petroleum Science Research (JPSR) Volume 2 Issue 1.

[39] Mohapatra, A., Rai, C., SPE, Sondergeld, C., and Richards, T. 2012. Laboratory Study of Velocity Variations during CO_2 Flooding in Tuscaloosa Sandstone. Paper SPE 159515 presented at the SPE Annual Technical Conference and Exhibition held in San Antonio, Texas, USA, 8-10 October.

[40] Myer, L. 2001. Laboratory Measurement of Geophysical Properties for Monitoring of CO_2 Sequestration. (LRMyer@lbl. gov; 510/486-6456).

[41] National Energy and Technology Laboratory, NETL. 2009. Carbon Sequestration Storage Web Page, www. netl. doe. gov/technologies/carbon_seq/core_rd/storage. html.

[42] Nguyen, D. 2003. Carbon Dioxide Geological Sequestration: Technical and Economic Review. Paper SPE 81199 presented at the SPE/EPA/DOE Exploration and Production Environmental Conference, San Antonio, Texas, USA, 10-12 March.

[43] Nur, A., Vanorio, T., and Diaz, E. 2011. Effects of Carbon Dioxide Injection in Reactive Carbonates: Computational Rock Physics Basis for Time-Lapse Monitoring. Paper SPE-SAS-1186 presented at the 2011 SPE Saudi Arabia Section Technical Symposium and Exhibition held in Al Khobar, Saudi Arabia, 15–18 May.

[44] Petroleum Department. "Manual for PETE 204". Lab handbook. King Fahd University Of Petroleum & Minerals. Saudi Arabia. 2012. Print.

[45] Riano, V. 2012. Thermo-Hydro-Mechanical Impacts of Carbon Dioxide (CO_2) Injection in Deep Saline Aquifers. Technical University of Catalonia (UPC-BarcelonaTech), Spain. PhD Thesis.

[46] Rosenbauer, R., Koksalan, T., and Palandri, J. 2005. Experimental investigation of CO_2–brine–rock interactions at elevated temperature and pressure: Implications for CO_2 sequestration in deep-saline aquifers. Fuel Processing Technology 86 (2005) 1581– 1597.

[47] Vanorio, T., Nur, A., and Diaz, E. 2011. The Rock Physicochemical Basis for Time-Lapse Seismic Reservoir Monitoring of CO_2 Injection. Paper SPE 149031 presented at the SPE/DGS Saudi Arabia Section Technical Symposium and Exhibition held in Al-Khobar, Saudi Arabia, 15–18 May.

[48] Vialle S., and Vanorio, T. 2010. Laboratory measurements of elastic properties of carbonate rocks during injection of reactive CO_2-saturated water. Geophysical Research Letters, Vol. 38, L01302, doi: 10.1029/2010GL045606, 2011.

[49] Wang, Z., and Nur, A. 1989. Effect of CO_2 flooding on wave velocities in rocks and hydrocarbons. Soc. Petr. Eng. Res. Eng., Vol. 3, pp. 429-439.

[50] Wang, Z, Cates, M., and Langa, T. 1996. Seismic monitoring of CO_2 flooding in a carbonate reservoir: rock physics study. Chevron Petroleum Technology Company S L 6 . 5.

[51] Xuejun, Z., Zhengwen, Z., Hong, L., and, Alyssa, B. 2009. Laboratory Testing on Geomechanical Properties of Carbonate Rocks for CO_2 Sequestration. Paper ARMA 09-011 presented at Asheville 2009, the 43rd US Rock Mechanics Symposium and 4th U. S. -Canada Rock Mechanics Symposium, held in Asheville, NC June 28th – July 1.

[52] Zeng, Z., Jakupi, A., Bigelow, T., Grigg, R., Kringstad, J., Belobraydic, M., and Zhou, X. 2009. Laboratory Observation of CO_2 Phase Transition Induced Seismic Velocity Change. Paper ARMA 08-329 presented at San Francisco 2008, the 42nd US Rock Mechanics Symposium and 2nd U. S. -Canada Rock Mechanics Symposium, held in San Francisco, June 29- July 2.

APPENDIX-A (NMR RESULTS)

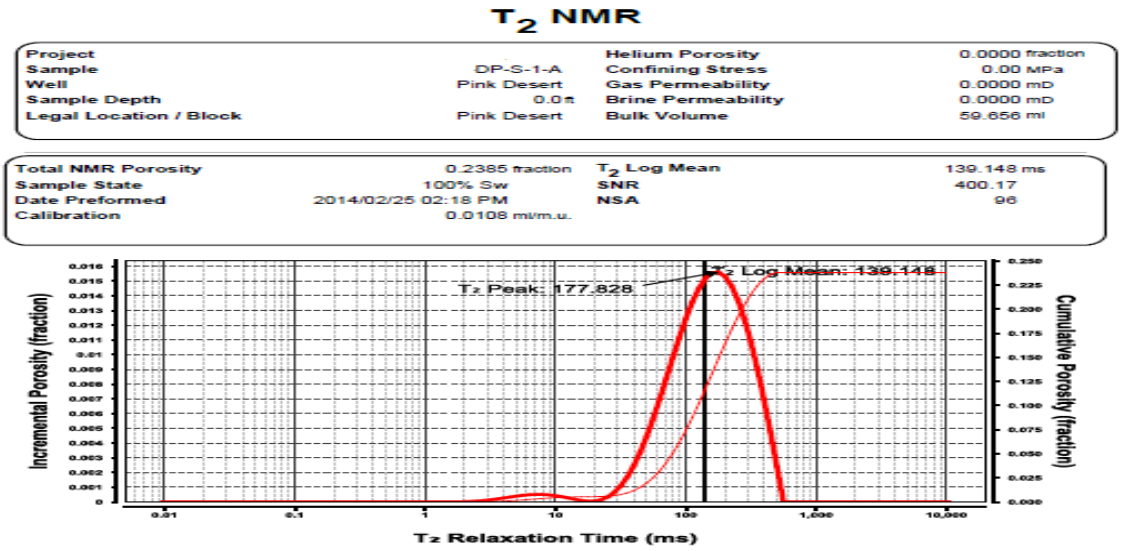

Figure A.1 Relaxation time vs. cumulative porosity for sample (PD-S-1-A) before CO_2 sequestration.

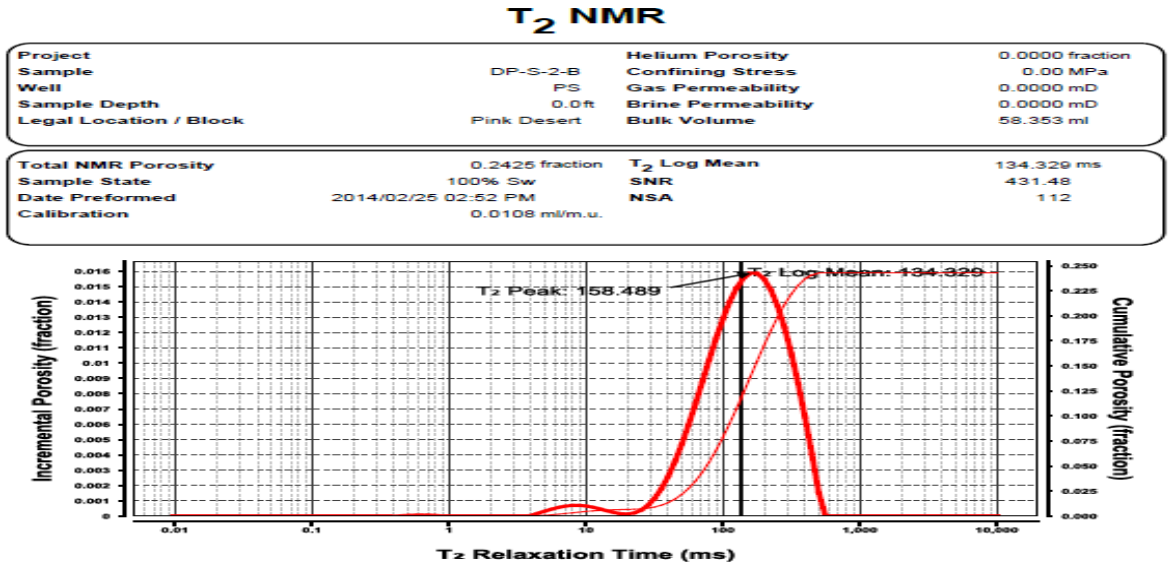

Figure A.2 Relaxation time vs. cumulative porosity for sample (PD-S-2-B) before CO_2 sequestration.

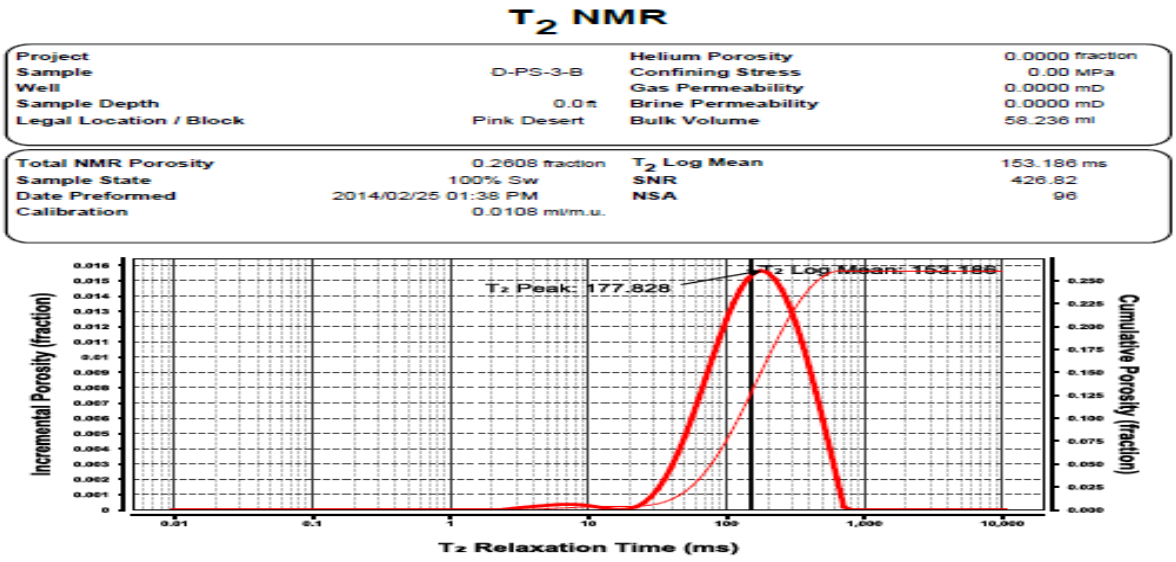

Figure A.3 Relaxation time vs. cumulative porosity for sample (PD-S-3-B) before CO_2 sequestration.

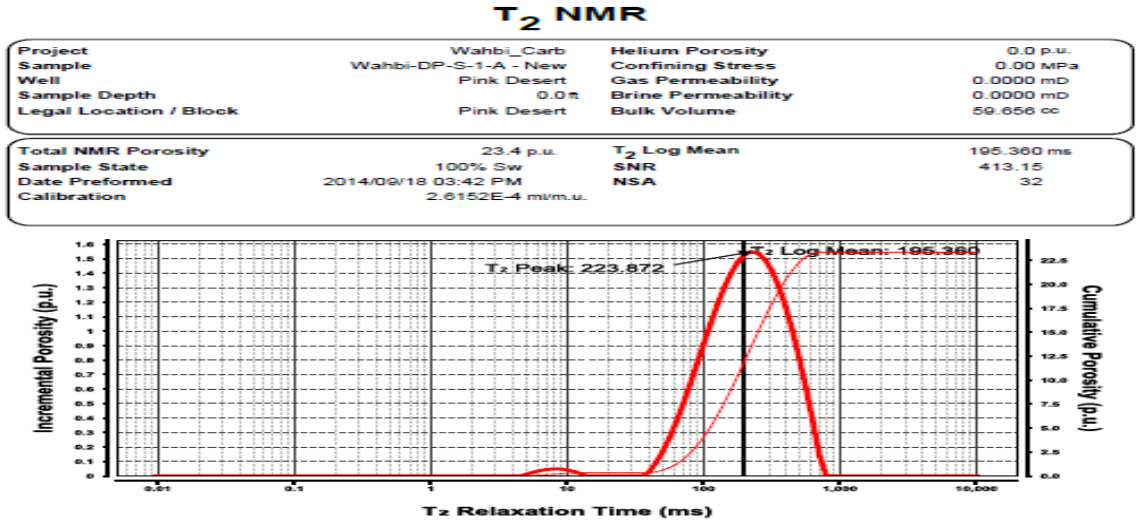

Figure A.4 Relaxation time vs. cumulative porosity for sample (PD-S-1-A) after CO_2 sequestration (14 days).

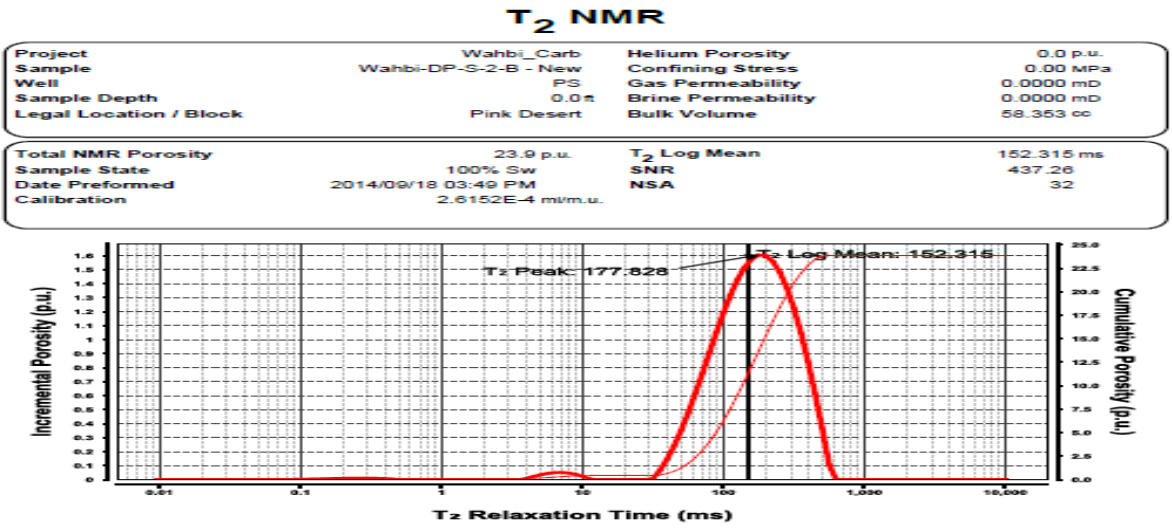

Figure A.5 Relaxation time vs. cumulative porosity for sample (PD-S-2-B) after CO_2 sequestration (30 days).

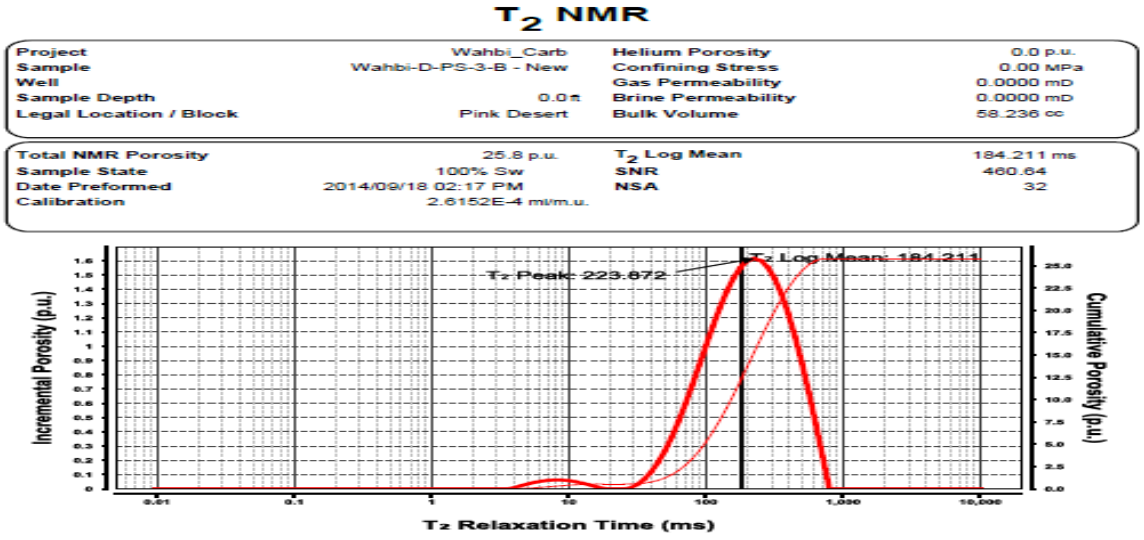

Figure A.6 Relaxation time vs. cumulative porosity for sample (PD-S-3-B) after CO_2 sequestration (90 days).

APPENDIX-B (UNCONFINED COMPRESSION TEST RESULTS)

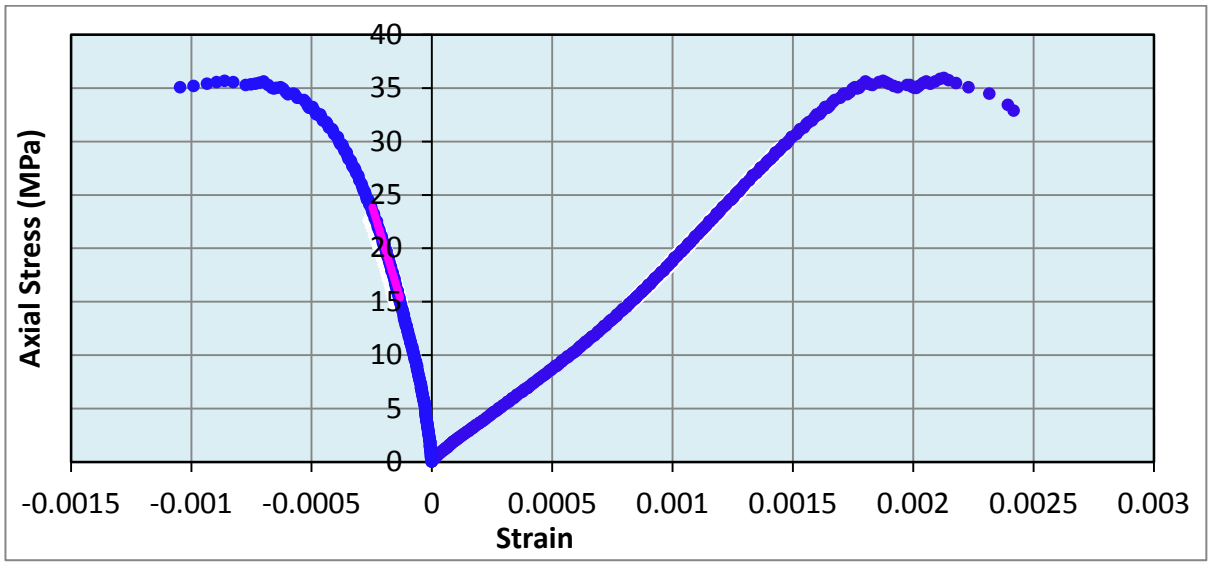

Figure B.1 Stress-strain curve for Indiana limestone sample (IL-15-2) before CO_2 sequestration.

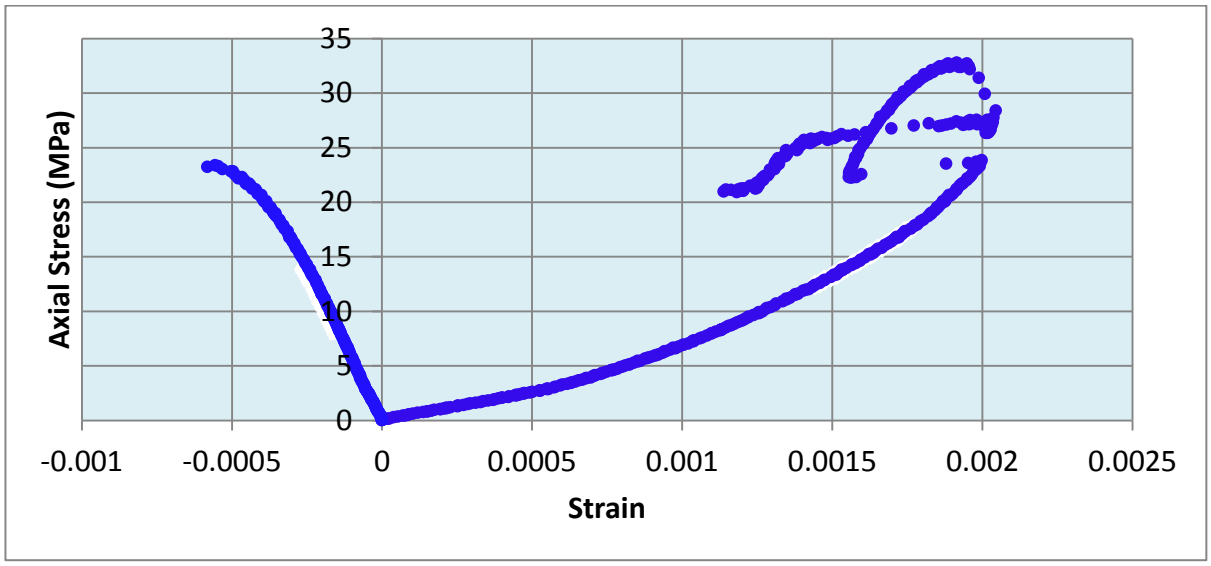

Figure B.2 Stress-strain curve for Indiana limestone sample (IL-15-3) after CO_2 sequestration (90 days).

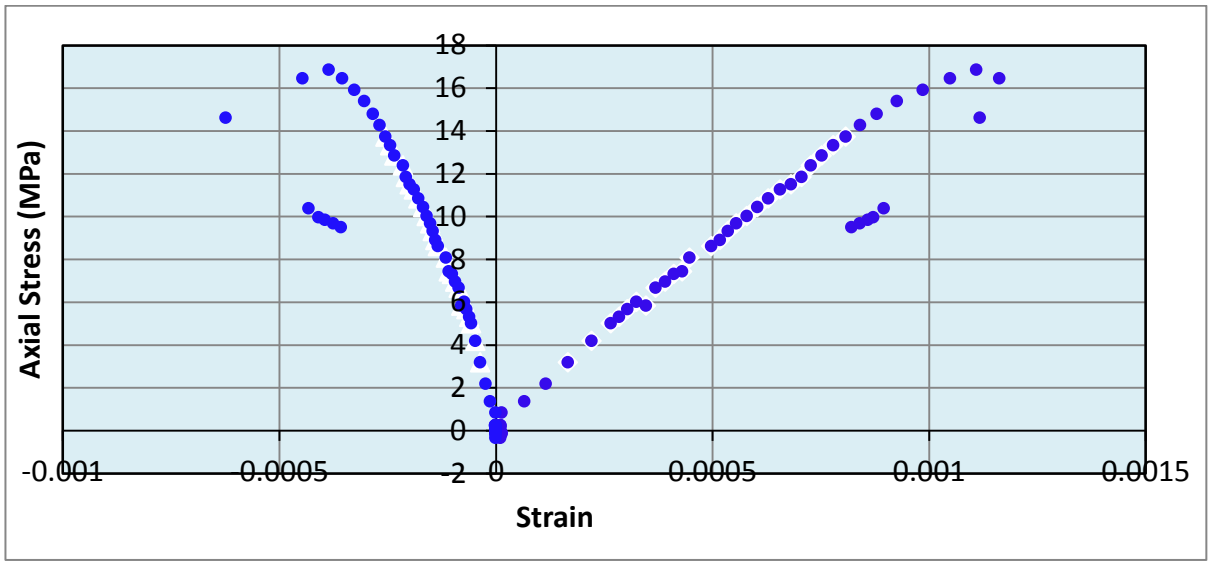

Figure B.3 Stress-strain curve for Pink Desert limestone sample (PD-U-2) before CO_2 sequestration.

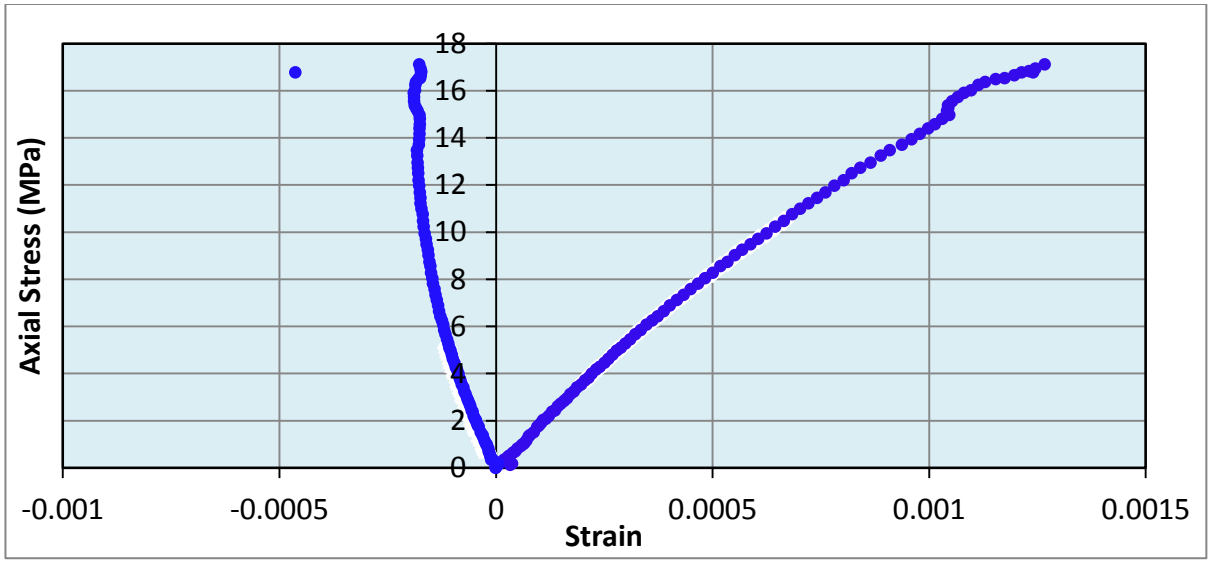

Figure B.4 Stress-strain curve for Pink Desert limestone sample (PD-U-1-A) after CO_2 sequestration (14 days).

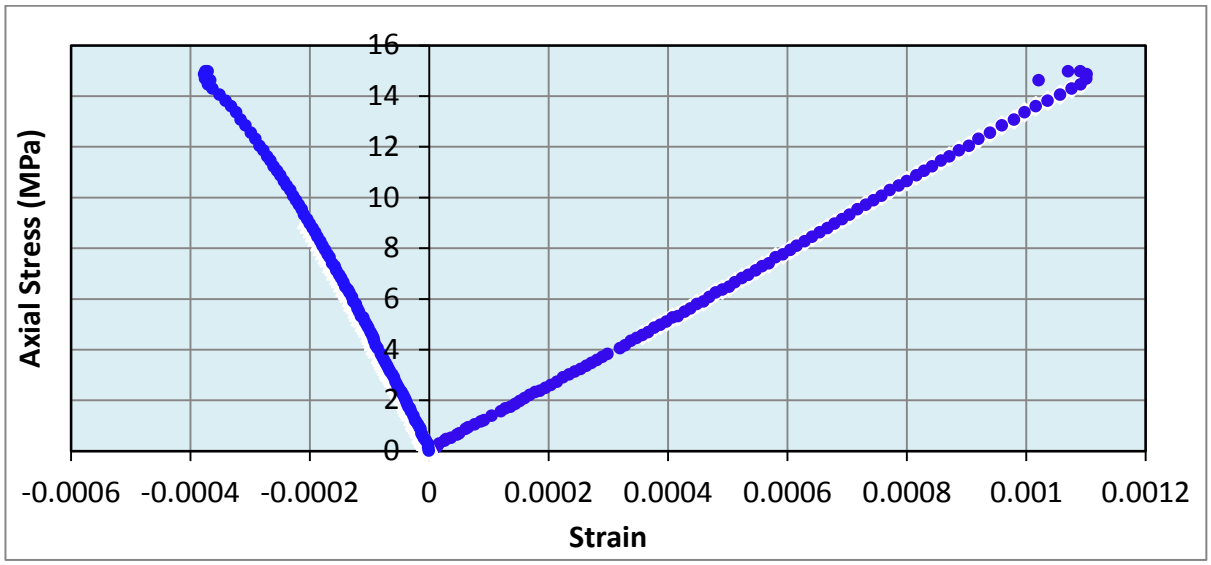

Figure B.5 Stress-strain curve for Pink Desert limestone sample (PD-U-2-A) after CO_2 sequestration (30 days).

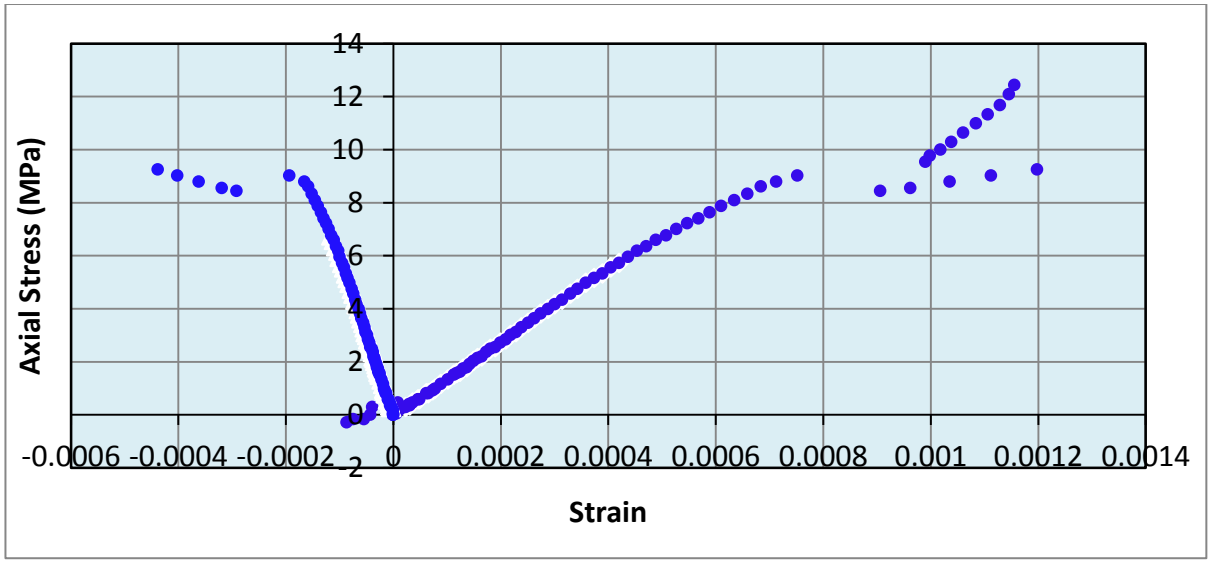

Figure B.6 Stress-strain curve for Pink Desert limestone sample (PD-U-3-B) after CO_2 sequestration (90 days).

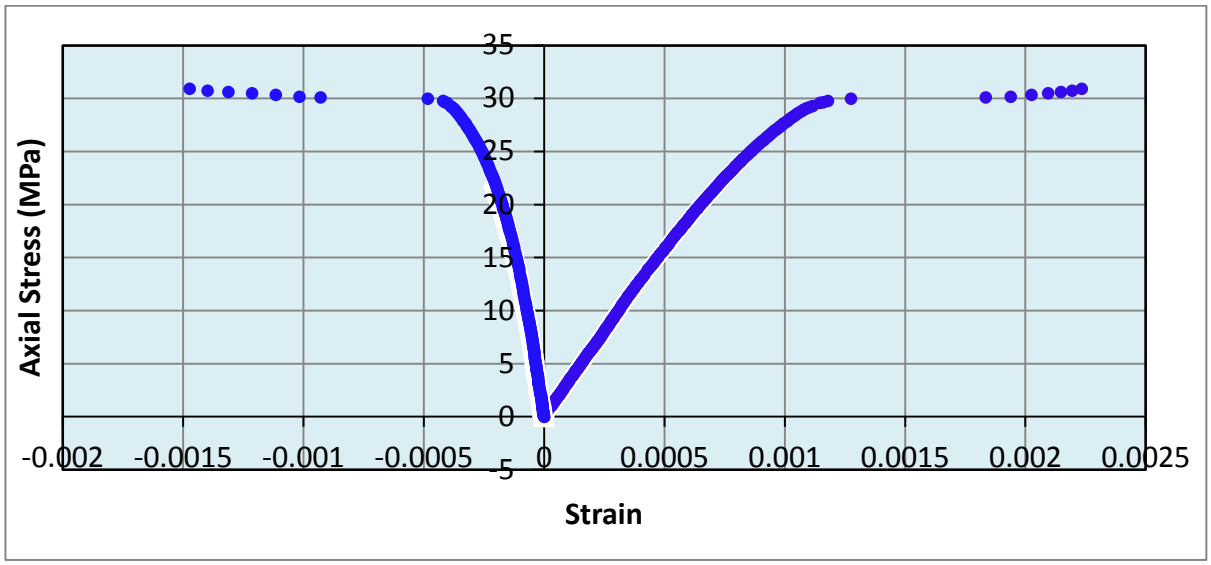

Figure B.7 Stress-strain curve for Khuff limestone sample (KH-U-1-B) before CO_2 sequestration.

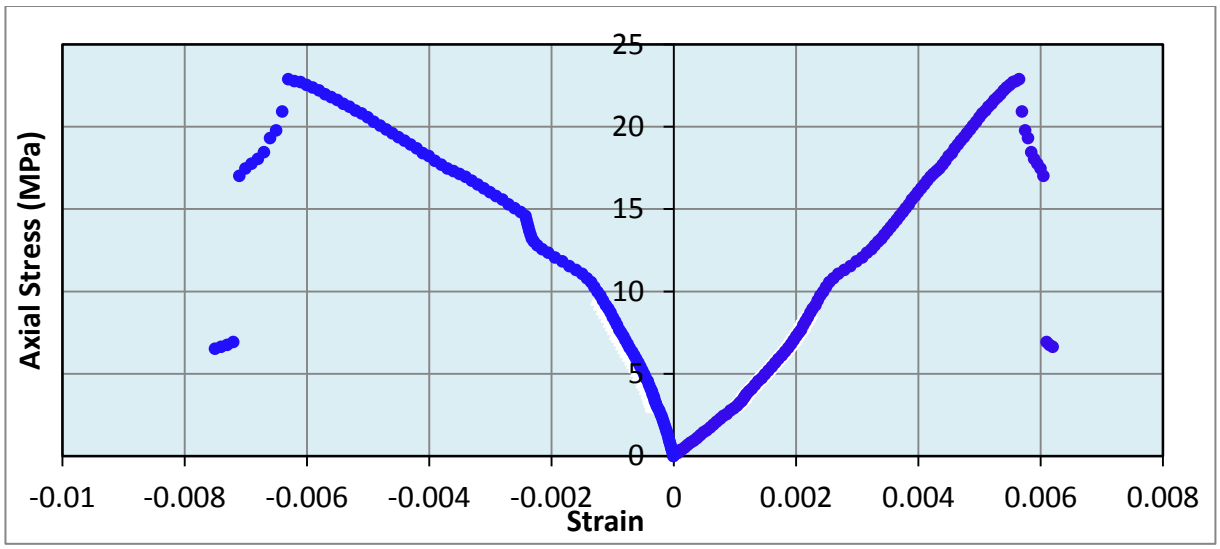

Figure B.8 Stress-strain curve for Khuff limestone sample (KH-U-1-A) after CO_2 sequestration (90 days)

APPENDIX-C (XRD RESULTS)

Quantitative analysis results (WPPF) for Indiana limestone sample before CO_2 sequestration.

Table C.1 Qualitative analysis results.

Phase Name	Formula	Figure of Merit
Calcite	$Ca\ CO^3$	0.806
Quartz Low HP, syn	$Si\ O_2$	1.423

Table C.2 Weight ratio.

Phase name	Content (%)
Calcite	100(3)
Quartz low HP, syn	0.36(15)

Table C.3 Peak list.

No.	2-theta(deg)	d(ang.)	Height(cps)	FWHM(deg)	Int.I(cps deg)	Int. W(deg)	Size (ang.)
1	23.217(9)	3.8280(14)	199(15)	0.14(2)	53.8(13)	0.27(3)	600(88)
2	26.798(18)	3.324(2)	47(7)	0.19(2)	14.7(11)	0.31(7)	460(59)
3	29.614(5)	3.0141(5)	10375(107)	0.141(4)	1942(21)	0.187(4)	610(16)
4	31.67(4)	2.823(3)	109(11)	0.16(4)	29.5(18)	0.27(4)	525(129)
5	36.201(8)	2.4793(5)	326(19)	0.156(8)	71.3(12)	0.219(16)	559(30)
6	39.632(7)	2.2722(4)	441(22)	0.181(6)	102.7(14)	0.233(15)	488(17)
7	43.400(7)	2.0832(3)	458(23)	0.164(7)	100.7(16)	0.220(14)	543(24)
8	47.772(13)	1.9023(5)	703(28)	0.19(2)	212(6)	0.30(2)	483(60)
9	48.710(7)	1.8679(3)	549(25)	0.181(8)	135.0(19)	0.246(15)	502(21)
10	56.70(2)	1.6221(5)	71(9)	0.20(3)	18.9(10)	0.27(5)	475(62)
11	57.529(15)	1.6007(4)	223(16)	0.172(18)	56.1(19)	0.25(3)	551(56)
12	60.851(14)	1.5210(3)	232(16)	0.17(2)	60(4)	0.26(3)	554(65)
13	61.147(9)	1.5144(2)	308(18)	0.141(17)	68(4)	0.22(3)	685(83)
14	63.175(17)	1.4706(4)	46(7)	0.194(17)	11.9(5)	0.26(5)	502(44)
15	64.814(8)	1.43727(15)	149(13)	0.184(9)	35.4(8)	0.24(3)	536(25)
16	65.804(10)	1.41804(19)	103(11)	0.189(11)	27.0(7)	0.26(3)	522(30)
17	69.39(2)	1.3532(4)	35(6)	0.19(2)	8.4(7)	0.24(6)	528(65)
18	70.37(2)	1.3368(4)	33(6)	0.31(3)	12.6(8)	0.39(10)	331(31)
19	73.05(2)	1.2942(3)	59(8)	0.29(2)	18.2(11)	0.31(6)	359(25)
20	73.84(7)	1.2824(10)	16(4)	0.36(7)	6.1(6)	0.38(14)	292(57)
21	76.44(3)	1.2451(4)	21(5)	0.30(4)	9.5(7)	0.46(14)	353(47)
22	77.353(8)	1.23260(11)	49(7)	0.187(14)	12.7(9)	0.26(6)	568(42)

Quantitative analysis results (WPPF) for Indiana limestone sample after CO_2 sequestration.

Table C.4 Qualitative analysis results.

Phase Name	Formula	Figure of Merit
Calcite	Ca CO^3	0.390

Table C.5 Weight ratio.

Phase Name	Content (%)
Calcite	100(2)

Table C.6 Peak list.

No.	2-theta(deg)	d (ang.)	Height(cps)	FWHM(deg)	Int.I(cps deg)	Int. W(deg)	Size (ang.)
1	17.3(3)	5.13(9)	5(2)	4.5(9)	23(3)	5(3)	19(4)
2	23.15(3)	3.839(4)	61(8)	0.27(2)	18.6(16)	0.31(7)	315(25)
3	29.473(8)	3.0282(8)	851(31)	0.232(13)	307(8)	0.36(2)	369(21)
4	36.07(2)	2.4879(13)	62(8)	0.392(15)	27.6(10)	0.44(8)	223(8)
5	39.449(18)	2.2823(10)	109(11)	0.357(14)	46.3(13)	0.42(5)	247(10)
6	43.24(2)	2.0907(9)	97(10)	0.385(15)	42.9(13)	0.44(6)	232(9)
7	47.246(8)	1.9223(3)	142(13)	0.090(8)	15.5(17)	0.11(2)	1004(90)
8	47.56(2)	1.9104(9)	99(10)	0.60(3)	72(2)	0.73(10)	152(8)
9	48.457(15)	1.8770(6)	128(12)	0.435(12)	64.0(15)	0.50(6)	209(6)
10	56.72(3)	1.6216(9)	25(5)	0.27(5)	8.7(10)	0.35(12)	343(67)
11	57.50(3)	1.6014(8)	46(7)	0.36(5)	22.2(16)	0.48(11)	261(33)
12	60.74(5)	1.5235(11)	39(7)	0.51(6)	21.4(18)	0.55(14)	188(21)
13	61.62(4)	1.5038(8)	47(7)	0.36(5)	18.1(17)	0.38(9)	270(35)
14	63.21(3)	1.4699(7)	8(3)	0.50(10)	4.5(9)	0.5(3)	196(39)
15	64.654(10)	1.4405(2)	37(6)	0.40(3)	15.7(12)	0.43(11)	246(19)
16	65.66(8)	1.4209(16)	13(4)	0.50(8)	6.9(7)	0.5(2)	196(30)
17	70.28(3)	1.3383(4)	30(6)	0.29(4)	11.6(11)	0.38(11)	349(47)
18	73.03(7)	1.2945(11)	13(4)	0.41(9)	6.8(10)	0.5(2)	251(55)
19	77.43(7)	1.2315(9)	11(3)	0.43(11)	6.7(9)	0.6(3)	245(62)

Quantitative analysis results (WPPF) for Pink Desert limestone sample before CO_2 sequestration.

Table C.7 Qualitative analysis results.

Phase Name	Formula	Figure of Merit
Calcite	Ca CO^3	0.966

Table C.8 Weight ratio.

Phase Name	Content (%)
Calcite	100.0(18)

Table C.9 Peak list.

No.	2-theta(deg)	d(ang.)	Height(cps)	FWHM(deg)	Int.I(cps deg)	Int. W(deg)	Size (ang.)
1	23.279(6)	3.8179(10)	444(22)	0.132(5)	78.0(12)	0.176(12)	642(24)
2	29.655(3)	3.0100(3)	5811(80)	0.125(3)	952(8)	0.164(4)	684(15)
3	31.695(11)	2.8207(10)	142(13)	0.106(15)	21.6(9)	0.15(2)	813(118)
4	36.250(4)	2.4760(3)	527(24)	0.135(4)	88.8(11)	0.169(10)	649(18)
5	39.704(3)	2.26827(19)	899(32)	0.126(4)	148.9(18)	0.166(8)	698(21)
6	43.447(4)	2.08110(16)	886(31)	0.130(4)	145(2)	0.164(8)	684(20)
7	47.395(5)	1.9166(2)	257(17)	0.139(8)	48.8(14)	0.190(18)	650(39)
8	47.772(3)	1.90231(10)	959(33)	0.129(3)	167(2)	0.174(8)	701(17)
9	48.769(4)	1.86574(13)	902(32)	0.138(4)	160(2)	0.177(9)	662(19)
10	57.603(11)	1.5988(3)	427(22)	0.139(11)	79(3)	0.185(17)	680(55)
11	60.880(5)	1.52037(12)	242(16)	0.147(5)	40.3(13)	0.166(17)	653(24)
12	61.220(8)	1.51275(18)	136(12)	0.161(10)	24.9(10)	0.18(2)	598(37)
13	61.578(11)	1.5048(3)	87(10)	0.177(14)	17.3(8)	0.20(3)	545(42)
14	64.874(6)	1.43609(11)	279(18)	0.144(5)	52.0(11)	0.186(16)	683(26)

Quantitative analysis results (WPPF) for Pink Desert limestone sample after CO_2 sequestration.

Table C.10 Qualitative analysis results.

Phase Name	Formula	Figure of Merit
Calcite	Ca CO^3	0.332

Table C.11 Weight ratio.

Phase Name	Content (%)
Calcite	100.0(13)

Table C.12 Peak list.

No.	2-theta(deg)	d(ang.)	Height(cps)	FWHM(deg)	Int.I(cps deg)	Int. W(deg)	Size (ang.)
1	23.150(9)	3.8389(15)	220(16)	0.154(7)	46.2(9)	0.210(19)	548(24)
2	29.534(5)	3.0221(5)	3340(61)	0.142(4)	624(7)	0.187(6)	606(17)
3	31.570(12)	2.8316(11)	126(12)	0.105(19)	19.0(11)	0.15(2)	818(148)
4	36.132(5)	2.4839(4)	420(22)	0.137(5)	75.8(11)	0.180(12)	639(24)
5	39.580(6)	2.2751(3)	560(25)	0.147(6)	106.0(17)	0.189(11)	602(25)
6	43.338(5)	2.0861(2)	557(25)	0.133(5)	95.8(17)	0.172(11)	670(27)
7	47.283(6)	1.9209(2)	209(15)	0.147(10)	43.3(15)	0.21(2)	618(43)
8	47.662(4)	1.90644(14)	595(26)	0.142(5)	118.1(18)	0.198(12)	641(21)
9	48.651(4)	1.86999(14)	607(26)	0.144(4)	117.1(14)	0.193(11)	630(19)
10	56.676(9)	1.6228(2)	122(12)	0.134(10)	24.0(8)	0.20(3)	704(54)
11	57.502(5)	1.60141(14)	346(20)	0.141(5)	65.5(12)	0.190(14)	671(26)
12	58.21(2)	1.5837(6)	38(6)	0.14(3)	6.5(8)	0.17(5)	696(132)
13	60.774(8)	1.52278(18)	167(14)	0.168(10)	34.1(15)	0.20(3)	572(33)
14	61.107(11)	1.5153(2)	93(10)	0.163(15)	18.4(12)	0.20(3)	591(53)
15	61.476(13)	1.5071(3)	74(9)	0.186(18)	16.7(10)	0.23(4)	518(50)
16	63.206(14)	1.4699(3)	59(8)	0.188(15)	13.7(7)	0.23(4)	517(41)
17	64.768(8)	1.43818(15)	183(14)	0.160(8)	39.3(9)	0.22(2)	613(31)
18	65.727(11)	1.4195(2)	121(12)	0.207(12)	29.6(9)	0.25(3)	477(28)
19	69.29(2)	1.3549(4)	39(7)	0.14(2)	7.5(7)	0.19(5)	736(129)
20	70.414(18)	1.3361(3)	53(8)	0.20(2)	13.1(8)	0.25(5)	497(51)
21	73.01(2)	1.2948(4)	83(10)	0.17(3)	21.5(12)	0.26(4)	606(89)
22	76.43(3)	1.2452(4)	31(6)	0.18(2)	6.3(7)	0.20(6)	600(81)
23	77.265(14)	1.23379(18)	65(9)	0.170(12)	14.6(6)	0.22(4)	624(45)

Quantitative analysis results (WPPF) for Khuff limestone sample before CO_2 sequestration

Table C.13 Qualitative analysis results.

Phase Name	Formula	Figure of Merit
Calcite	$Ca\ C\ O^3$	0.444

Table C.14 Weight ratio.

Phase Name	Content (%)
Calcite	100.0(15)

Table C.15 Peak list.

No.	2-theta(deg)	d(ang.)	Height(cps)	FWHM(deg)	Int.I(cps deg)	Int. W(deg)	Size (ang.)
1	23.181(8)	3.8339(13)	250(17)	0.153(6)	50.6(9)	0.202(17)	554(21)
2	29.550(4)	3.0204(4)	3522(63)	0.130(4)	621(6)	0.176(5)	659(20)
3	31.56(3)	2.833(3)	35(6)	0.15(4)	7.1(9)	0.20(6)	565(158)
4	36.148(5)	2.4828(3)	518(24)	0.128(5)	85.7(13)	0.166(10)	683(27)
5	39.588(6)	2.2746(3)	614(26)	0.143(6)	111.0(19)	0.181(11)	617(25)
6	43.330(4)	2.0865(2)	716(28)	0.113(5)	101(2)	0.141(8)	790(33)
7	47.299(8)	1.9202(3)	176(14)	0.142(12)	34.6(15)	0.20(2)	638(55)
8	47.667(4)	1.90625(16)	655(27)	0.132(5)	118(2)	0.180(11)	687(26)
9	48.654(5)	1.86987(18)	789(30)	0.126(5)	130(2)	0.165(9)	722(29)
10	56.70(2)	1.6223(6)	111(11)	0.129(17)	19.1(9)	0.17(3)	733(97)
11	57.495(6)	1.60158(16)	321(19)	0.152(7)	62.2(14)	0.194(16)	624(28)
12	58.157(16)	1.5849(4)	36(6)	0.13(2)	6.0(6)	0.17(5)	729(110)
13	60.796(12)	1.5223(3)	225(16)	0.130(14)	43(3)	0.19(3)	738(82)
14	61.080(12)	1.5159(3)	199(15)	0.14(2)	45(3)	0.23(3)	680(98)
15	63.166(14)	1.4708(3)	69(9)	0.161(16)	15.7(7)	0.23(4)	604(60)
16	64.417(17)	1.4452(3)	13(4)	0.17(3)	2.6(4)	0.19(8)	577(95)
17	64.778(6)	1.43799(13)	134(12)	0.146(6)	24.0(8)	0.18(2)	672(28)
18	65.688(18)	1.4203(3)	58(8)	0.182(18)	13.3(7)	0.23(4)	543(54)
19	69.328(16)	1.3543(3)	58(8)	0.10(2)	9.1(8)	0.16(4)	961(182)
20	70.373(11)	1.33673(18)	40(7)	0.222(19)	9.7(6)	0.24(5)	458(39)
21	73.033(9)	1.29448(14)	59(8)	0.176(14)	13.8(7)	0.23(4)	587(46)
22	73.79(3)	1.2831(4)	18(5)	0.21(3)	4.1(5)	0.22(8)	495(70)
23	76.393(19)	1.2457(3)	26(5)	0.178(17)	5.0(5)	0.19(6)	592(56)
24	77.248(7)	1.23402(10)	42(7)	0.181(12)	9.5(4)	0.23(5)	588(38)

Quantitative analysis results (WPPF) for Khuff limestone sample after CO_2 sequestration.

Table C.16 Qualitative analysis results.

Phase Name	Formula	Figure of Merit
Calcite	Ca C O^3	0.493

Table C.17 Weight ratio.

Phase Name	Content (%)
Calcite	Ca CO^3

Table C.18 Peak list.

No.	2-theta(deg)	d(ang.)	Height(cps)	FWHM(deg)	Int.I(cps deg)	Int. W(deg)	Size (ang.)
1	23.105(8)	3.8463(13)	190(15)	0.136(10)	37.9(9)	0.20(2)	622(46)
2	29.519(5)	3.0236(5)	3704(64)	0.117(5)	578(9)	0.156(5)	732(31)
3	31.57(3)	2.832(2)	38(6)	0.14(3)	6.0(9)	0.16(5)	633(147)
4	36.107(4)	2.4855(3)	479(23)	0.132(4)	77.9(11)	0.163(10)	662(20)
5	39.555(4)	2.2765(2)	674(27)	0.127(5)	110.1(17)	0.163(9)	692(25)
6	43.307(6)	2.0875(3)	669(27)	0.128(6)	104(2)	0.156(10)	697(31)
7	47.243(8)	1.9224(3)	172(14)	0.132(11)	30.7(12)	0.18(2)	685(56)
8	47.619(6)	1.9081(2)	357(20)	0.145(7)	69.2(16)	0.193(15)	627(32)
9	48.619(5)	1.87114(16)	813(30)	0.127(5)	128(2)	0.158(9)	718(26)
10	56.646(7)	1.62355(17)	204(15)	0.125(7)	33.4(10)	0.164(17)	751(39)
11	57.479(8)	1.6020(2)	303(18)	0.137(9)	55.4(17)	0.183(17)	689(43)
12	60.772(6)	1.52283(14)	230(16)	0.141(6)	39.9(15)	0.173(19)	681(31)
13	61.068(15)	1.5162(3)	66(9)	0.16(2)	12.8(10)	0.19(4)	596(77)
14	61.450(12)	1.5077(3)	68(9)	0.150(15)	12.2(9)	0.18(4)	642(63)
15	63.143(14)	1.4712(3)	65(8)	0.152(13)	12.3(7)	0.19(4)	640(56)
16	64.762(5)	1.43830(10)	386(21)	0.145(5)	66.1(15)	0.171(13)	676(21)
17	65.697(5)	1.42008(10)	238(16)	0.134(4)	38.3(9)	0.161(15)	738(25)
18	69.30(3)	1.3549(4)	34(6)	0.16(3)	7.8(6)	0.23(6)	633(105)
19	70.352(15)	1.3371(2)	53(8)	0.178(14)	10.2(7)	0.19(4)	571(45)
20	72.98(2)	1.2953(3)	63(8)	0.17(2)	15.5(9)	0.24(5)	610(77)
21	76.350(10)	1.24628(14)	44(7)	0.159(14)	9.0(6)	0.21(5)	663(60)
22	77.231(5)	1.23424(6)	71(9)	0.166(7)	13.5(5)	0.19(3)	638(26)

VITAE

Name:	Wahbi Abdul Qader Al-Ameri
Nationality:	Yemeni
Date of Birth:	9/23/1983
Email:	wahbi737@gmail.com
Mobile:	00967712596537, 00966550454286
Address:	Tarbh Village, Seyion City, Hadhramout Governorate, Republic of Yemen
Academic Background:	M.S in Petroleum Engineering, December 2014 King Fahd University of Petroleum and Minerals Dhahran, Saudi Arabia B.S in Petroleum Engineering, July 2008 Hadhramout University for Science and Technology, Hadhramout, Republic of Yemen

Publications:

AL-Ameri, W., Abdulraheem, A., Mahmoud, M., Abdullatif, O., and Adebayo, A. 2014. Effect of CO_2 Sequestration Period on the Mechanical Properties of Carbonate Aquifers. Paper SPE 171702-MS presented at the Abu Dhabi International Petroleum Exhibition and Conference held in Abu Dhabi, UAE, 10–13 November 2014.

AL-Ameri, W., Abdulraheem, A., Mahmoud, M., Abdullatif, O., and Adebayo, A. 2014. Aquifer Selection for CO_2 Sequestration Based on Mechanical Properties Evaluation. Paper SPE 172526-MS prepared for presentation at the SPE Middle East Oil & Gas Show and Conference held in Manama, Bahrain, 8–11 March 2015.